UNIVERSITY OF LONDON THESIS

Degree PhD Year 2007 Name of Author GERONTAS, Spyridon

Bioreactor design for the controlled formation of engineered tissues

Thesis submitted for the degree of

Doctor of Philosophy
in
Biochemical Engineering

by
Spyridon Gerontas

The Advanced Centre for Biochemical Engineering
Department of Biochemical Engineering
University College London

September 2007

ProQuest LLC
789 East Eisenhower Parkway
P.O. Box 1346
Ann Arbor, MI 48106-1346

ACKNOWLEDGEMENTS

I would like to thank Professor Michael Hoare for his exceptional supervision. Many thanks go to Dr Suzanne Farid for quick and useful advices.

Special thanks to Professor Peter Dunnill, Dr Christopher Mason and Dr Farlan Veraitch for advice on tissue engineering.

I would like to thank my friends and colleagues in the ReMeBio team and in the department for support. Specifically, I would like to thank Julia, Garr, Alfred, Leda, Ioannis, Matt, Ju Wei, Carol, Charo, Meg, Minal, Emma, Jordan, Alex, Emily, Paul, Evi, Lucy, Rezwan, Jaspreet, Ed, Helen, Julio, Peter, Samir, Sally, Wellae, Alex B. and Garreth.

I also want to thank my friends in London for the necessary entertainment and support. In particular I would like to thank Charo, Evi, Ioanna and Thanasis.

Finally, I would like to thank my parents and my brother for being always close to me.

ABSTRACT

The availability of large numbers of engineered organs would offer significant benefits to the clinical management of surgery. Tissue engineering offers the potential of providing tissues that can mimic the morphology, function and physiologic environment of native ones. Cells could grow *in vitro* within a biodegradable polymer to construct tissue for implantation. However no generic bioreactor design currently exists. There is now a need to establish a robust process for the production of engineered tissues using autologous cells. A key challenge will be the prediction of the supply of nutrients and removal of metabolites.

Models of transport phenomena were developed in order to predict the fluid flow and mass transfer requirements of a prototype bioreactor for the formation of engineered tissues. These models were solved to generate windows of operation which relate key operating parameters with the feasibility of tissue preparation. Examples highlight how the windows of operation can be used to visualize rapidly the region of operating conditions that satisfy the design constraints.

The impact of the cell concentration, tube geometry, alginate diffusivity, substrate and metabolite concentration levels, feed and recycle rate on the design of the bioreactor is illustrated. The result of this analysis determines the best configuration of the bioreactor which can meet the cellular transport requirements as well as being reliable in performance whist seeking to reduce the amount of valuable nutrients to be used.

Micro scale experiments were designed in order to evaluate from measurements, effective diffusivities of substrates and metabolites in alginate matrices as well as substrate consumption and metabolite production rates in matrices with immobilized growing cells. The oxygen diffusivity and oxygen uptake rate of alginate immobilized neonatal fibroblasts were evaluated using integrated oxygen sensor spots. Additionally, alginate cylindrical constructs with immobilized neonatal fibroblasts were prepared in transwells in order to

evaluate the effective diffusivities of glucose and lactate as well as the glucose consumption and lactate production rate.

The advantage of such micro scale experiments was that greater data sets could be generated with the small number of cells available but in a way which predicts the larger scale. The database which was created was used to construct the windows of operation to give quantitative solutions of how engineered tissues may be prepared and to visualize process operability in a more explicit way.

TABLE OF CONTENTS

LIST OF FIGURES

Chapter 2

Chapter 3

Chapter 4

Chapter 5

Chapter 6

List of Tables

Chapter 3

Chapter 4

Chapter 1

Introduction

One of the most common, and costly problems confronted by the healthcare providers of today, is treating patients who have suffered from the loss or failure of an organ or tissue. Current solutions to this problem include medication, transplantation of organs, surgical reconstruction, and use of mechanical devices. None of these solutions is ideal. For example, organ and tissue transplantation is characterized by a number of limitations. Firstly, there is a large mismatch between the number of donors and waiting list numbers. Additionally, transplantation recipients are obliged to follow lifelong immunosuppression regimens with unwanted side effects at increased risks of infection and tumour development. Transplant surgery in general is hampered by both a lack of available donor tissue and donor morbidity. Finally, the use of mechanical devices or artificial organs is associated with infection, thromboembolism and finite durability. The field of tissue engineering emerged as an alternative way to face up to the problem of replacing a damaged tissue with living tissue that is "designed and constructed to meet the needs of each individual patient" (Fuchs, 2001). However no generic bioreactor design currently exists upon which a robust process for the production of engineered tissues will be established. A key challenge will be the prediction of the supply of nutrients and removal of metabolites. This thesis focuses on integrating transport phenomena models with scale down experiments so as to specify the design constraints and optimal operating conditions required to successfully produce artificial vascular tissues.

This introductory chapter provides an overview of tissue engineering. Its progress in restoring function in several tissue types is analyzed. Emphasis is given on the vascular tissue engineering as the thesis objective to design a bioreactor for artificial arteries. The significance of scaffolds, cells sources, oxygen, substrates, mechanical stimulation and bioreactor design in tissue engineering is presented. Finally, the aims and organisation of the thesis are presented.

1.1 Tissue engineering principles

1.1.1 Basic principles

Tissue engineering is "an interdisciplinary field that applies the principles and methods of engineering and the life sciences toward the development of biological substitutes that restore, maintain, or improve tissue function" (Fuchs, 2001; Nasseri et al., 2001). The goal of tissue engineering is to "restore function through the delivery of living elements which become integrated into the patient" (Nasseri et al., 2001). To render this goal realistic, cell biologists, engineers, material scientists, mathematicians, genetists, and clinicians have to cooperate and combine their knowledge. The first tissue engineering attempts were made in the early 1980s. Chick et al. (1986) managed to control glucose levels in patients with diabetes by using encapsulated pancreatic islet cells in semi permeable membranes. Yannas et al. (1980) designed a collagen, glucosaminoglysan scaffold, which aided in regeneration of dermis for burns patients. Bell et al. (1983) added fibroblasts to a contracted collagen gel to replace skin. Lately, the construction of vascular-engineered tissue by seeded cells in 3D, porous, biodegradable, synthetic scaffolds is a reality and offers promise for the future (Nasseri et al., 2001).

Tissue engineering is based on the three basic components of biologic tissues, namely: the cells, the extracellular matrix (ECM-made up of a complex of cell secretions immobilized in spaces continuous with cells) and signalling systems (biological communication mechanisms which act through differential activation of genes or cascades of genes, whose secreted products are responsible). Scaffolds may be fabricated from both natural and synthetic polymers which may or may be not biodegradable. Construct is a combination of scaffold and cells (Garner, 2004; Lanza et al., 2000).

Several attempts at making constructs for a broad range of tissues have been reported in the literature. These range from skin to blood vessels to liver tissue and are elaborated upon further in the following section.

1.1.2 Progress of tissue engineering in restoring function in several tissue types

Skin was the first engineered tissue to receive FDA approval for clinical application. Today, tissue-engineered skin products are made of ECM components, cells, or a combination of cells and matrices. They are not a true skin replacement since they are not based on the patient's own tissue. In reality, they act as "super bandages" which promote wound healing and, over time, they are thought to be replaced by the recipient's own tissue (Lalan et al., 2001). Currently one of the most successful tissue-engineered skin products is Apligraf marketed by Organogenesis Inc. (Canton Massachusetts, USA). It is approved for the treatment of venous leg ulcers and diabetic foot ulcers. Like human skin, Apligraf has two primary layers, a dermis and an epidermis. The epidermal layer is composed of human keratinocyte cells that form an outer protective layer. The dermal layer lies beneath the epidermis and is made up of human fibroblast cells. While matrix proteins and cytokines found in human skin are present in Apligraf, Apligraf does not contain Langerhans' cells, melanocytes, macrophages, lymphocytes, white blood cells, blood vessels, hair follicles or sweat glands. In a study of all patients with venous ulcers of greater than one month in duration (n=240), more patients achieved complete wound closure by 24 weeks with Apligraf plus compression therapy (57%) than with the previous preferred treatment using compression bandage therapy alone (40%). The median time to wound closure was 65 days for diabetic foot ulcers treated with Apligraf versus 90 days for ulcers treated with conventional therapy (debridement plus saline dressings) (Lalan et al., 2001).

Tissue engineering techniques have produced new cartilage from autologous isolated cartilage cells (chondrocytes). Chondrocyte-seeded polyglycolic acid tubes or meshes have been used for the treatment of hydrocephalus or to close full-thickness cranial defects. A commercial process to grow chondrocytes for use in treating damaged articular cartilage of knee (not associated with ostearthritis) has been employed by Genzyme Biosurgery. The procedure is called Autologous Chondrocyte Implantation and the autologous cultured chondrocytes products are called Carticel (Lalan et al., 2001).

Vascular tissue engineering is focused on small and medium blood vessels (< 6mm inner diameter). Each year over 1 million surgical procedures require grafts of less than 4 mm diameter. Current treatment includes replacing a blocked blood vessel with autologous vessel harvested from elsewhere in the patient but this is far from ideal. The use of synthetic grafts such as ePTFE (expanded polytetrafluoroethylene; woven form of polytetrafluoroethylene that creates a mesh-like structure) and Dacron is unfortunately unsatisfactory (Lalan et al., 2001). Vascular tissue engineering can be loosely categorized in three categories. These include using cells seeded in non-biodegradable scaffolds, using cells seeded in biodegradable scaffolds and using smooth muscle cells and fibroblasts seeded to form a monolayer which is rolled around a mandrel to form tissue layers in a tubular wall (Ratcliffe et al., 2000; Teebken and Haverich, 2002). These approaches are discussed in more detail in section 1.5.

For peripheral nerve repair research synthetic nerve guidance is being used. Tubular nerve guidance conduits have been created using a polyglycolic acid (PGA) scaffold and cultured Schwann cells (cells which function as physical support for neurons) possessing the macroarchitecture of a peripheral nerve. Also, nerve regeneration conduits have being created using material originally designed for drug delivery applications. In an animal model, the presence of inosine (believed to promote axomal extension after neural injury) resulted in neural regeneration whose histological features suggested possible superior long-term movement control (Lalan et al., 2001; Nasseri et al., 2001).

Tissue engineering of the liver is based on hepatocyte transplantation using polymer devices to encapsulate the cells, but the problem of insufficient engraftment and survival of an adequate transplanted hepatocyte mass in the polymer scaffold has not yet been solved. However, recent results suggest the use of a co-culture of small hepatocytes (considered as progenitor cells) with nonparenchymal cells (parenchymal cells are these cells which are specific to an organ and are contained in and supported by the connective tissue) can lead to the fabrication of liver tissue on 3-dimensional polymer scaffolds producing a liver-like structure (Nasseri et al., 2001).

A potential treatment of patients with dysfunctional intestines is based on tissue engineered intestinal transplantation, where intestinal progenitor crypt cells are seeded onto sheets of nonwoven PGA, which are in turn wrapped around a silastic stent (expandable wire form or perforated tube made of silastic which is a flexible, inert silicone elastomer). Following transplantation in mice stratified epithelium 5-7 cell layers thick was grown in two weeks. However, this method led to fetal gut being produced which is different from the adult gut required by the patient (Nasseri et al., 2001).

1.2 Biomaterial scaffolds

1.2.1 Introduction

Biomaterials play the role of an artificial ECM which is the material that surrounds cells in tissue and provides space for new tissue formation. The biomaterials serve as scaffolds to provide cells with a suitable growth environment, optimal oxygen levels, effective nutrient transport and mechanical integrity as well as to guide differentiation and vascularisation. Ideally, the scaffold's degradation rate must be synchronized with the deposition of ECM produced by the cells in order to form 3D structures that will be a close mimic of the native tissue architecture. However, the current fabrication methods cannot provide engineered tissues which are larger than a few hundreds of micrometers due to oxygen diffusion limitation (Khademhosseini et al., 2006).

There are two approaches to make a biomaterial to promote specific cellular responses and direct new tissue formation mediated by specific interactions. The first approach is to construct biomaterials which incorporate soluble bioactive molecules such as growth factors and plasmid DNA into biomaterial carriers so that the bioactive molecule can diffuse out and modulate tissue formation. The other approach is the chemical or physical modification of the biomaterial by incorporating cell-binding peptides. Cell-binding peptides include a native long chain of ECM proteins as well as peptide sequences derived from

ECM proteins which can incur specific interactions with cell receptors (Augst et al., 2006; Shin et al., 2003).

Materials like glass and ceramics have been used as scaffolds to engineer artificial bone. Their strong mechanical properties are an asset in bone engineering. In contrast, biodegradable polymers, either synthetic or biological, have a widespread usage for cardiac, liver skin and nerve engineering (Park et al., 2007).

Commonly used and FDA-approved hydrolytically biodegradable synthetic polymers are homopolymers and copolymers of poly(L-lactic acid), poly(glyconic acid) and poly(lactide-co-glycolide) (PLA, PGA, PLGA) (Atala, 2002; Park et al., 2007). Their biodegradation can vary from days to years and is a function of their molecular weights and co-polymer ratio. They have been used to engineer artificial cartilage (Freed et al., 1994; Vacanti et al., 1991), cardiac muscle (Bursac et al., 1999; Caspi et al., 2007; Levenberg et al., 2003) blood arteries (Niklason et al., 1999; Shin'oka et al., 1998), bladder (Atala, 2006) and ligament (Lu et al., 2005). However, their poor cell attachment properties, their non-uniform degradation rate *in vivo* and their hydrophobic nature which made cell entrapment a challenging task has led the interest in biological polymers (Park et al., 2007).

Biological polymers which have been used extensively in tissue engineering applications include alginate, collagen, hyaluronic acid and self-assembling peptides. Their degradation times vary from days to years without by-product accumulation. They are highly hydrated (above 90%) and they promote cell adhesion, proliferation and differentiation. Chemical or physical modifications of the biological polymers offer control over the physical and chemical signals to the cells (Park et al., 2007). These polymers and their applications are discussed in more detail in the following section.

1.2.2 Alginate

Alginate is a common term for a family of unbranched polymers. It consists of 1,4-linked β-D-mannuronic (M) and α-L-guluronic acid (G) residues and is derived from brown seaweed and bacteria. The monomers are distributed sequentially in repeating or alternating blocks in varying proportions, sequence and molecular weight (Drury and Mooney, 2003; Smidsrød and Skjåk-Braek, 1990). The monomers are arranged in a pattern of blocks along the chain, with homopolymeric regions (termed M and G blocks) interspersed with regions of alternating structure (MG blocks) (Smidsrød and Skjåk-Braek, 1990). The amount and distribution of the monomers depends on the species, age and location of the seaweed.

Alginate gelation occurs when divalent or multivalent cations (usually Ca^{2+}) interact ionically with blocks of guluronic residues between two different chains resulting in a three-dimensional network. The model that best describes this interaction is the "egg-box model" (Grant et al., 1973). The alginate chains of the gel are orientated preferentially perpendicular to the direction of gel growth. When the alginate solution and the salt solution are brought into contact, an amorphous gel layer is formed. Capillary formation requires this layer to reach a thickness of several micrometers. The diameter of the capillaries usually varies between about 5-300 μm, depending on the guluronic acid content of the alginate and the concentrations of salt solution and alginate solution. After some time of gel growth, the capillary comes to an end although gel growth goes on. Capillary formation does not take place at very small concentrations of the crosslinking cation, nor at very large alginate concentration in solution (larger than 5% w/v) (Sabra et al., 2001). The gel formation time is increased by decreasing temperature (calcium diffusion rate is reduced) and increasing phosphate concentration (phosphate binds with calcium ions reducing the number of ions available for crosslinking) (Drury et al., 2004).

The compression modulus of non-modified alginate gels ranges from 1 to 1000 kPa and the shear modulus ranges from 0.02 to 40 kPa. Their stiffness is a function of the MG block ratio and the stoichiometry of the reaction. Alginate

gels with a high G content are stronger mechanically than high M alginate gels (Constantinidis, 1999; Drury et al., 2004). Alginate hydrogels do not specifically degrade but undergo slow uncontrolled dissolution. Their strength increases by increasing calcium concentration and it stabilizes at the calcium concentration of 0.02 M (Drury et al., 2004; Smidsrød and Haug, 1972). Alginate gels do not specifically degrade in culture medium but undergo slow uncontrolled dissolution. The alginate gel loses mechanical strength over time due to loss of crosslinking from competition between the calcium and the sodium ions and it swells with a decrease in its solid volume fraction (Drury et al., 2004; LeRoux et al., 1999).

Cells immobilized in the alginate gel can be recovered by reversing the alginate gel formation. This can be achieved by placing the alginate gel in solutions rich in monodivalent ions or chelators of divalent ions (sodium citrate, EDTA). The monovalent ions and the chelators dissociate the alginate matrix by reacting with its divalent ions (Lee et al., 1991; Martinsen, 1989).

Cells do not naturally attach to alginate (Rowley et al., 1999). The fibronectin derived adhesion peptide arginine glycine aspartic acid (RGD) and its subtypes have been coupled to alginate to promote adhesion. Rowley et al. (1999) have demonstrated that myoblasts can adhere, proliferate and fuse to RGD coupled alginate (Rowley et al., 1999). They showed that the myoblast phenotype can be controlled by manipulating the RGD concentration and composition of the gel. The same group uses models to predict the organization of the peptides and the changes in clustering of the cell receptors. Additionally, it has been shown that the presence of RGD peptide in alginate does not affect its mechanical properties (Drury et al., 2004).

Alginate has been used to engineer artificial cartilage (Drury et al., 2203). It has been mixed with chrondrocytes and either injected into the site of interest (Atala et al., 1994; Bent et al., 2001; Paige et al., 1995) or moulded and then implanted (Chang et al., 2001). It has been demonstrated that chrondrocytes immobilized in alginate constructs were viable producing ECM proteins as early as four weeks after implantation (Atala et al., 1994; Chang et al., 2001).

1.2.3 Collagen

Collagen is the most abundant protein in mammalian tissues and the main component of the ECM of the connective tissue. There are 19 types of collagen with the same triple-helix structure. This structure is composed of three polypeptide chains, which wrap around one another. The strands are held by hydrogen and covalent bonds. Stable fibres can be formed by self-aggregation of collagen, by introduction of chemical crosslinkers (glutaraldehyde, formaldehyde, carbodiimide chemistry), by crosslinking with physical treatments (UV irradiation, freeze-drying, heating) and by blending with other polymers (hydroxyapetite, PLA, PLGA, chitosan, PEO) (Drury and Mooney, 2003). Physically formed collagen gels have an overall porosity of 90 % with pore size in the range of 100-150 μm (Park et al., 2007). Additionally, they are thermally reversible, they promote adhesion and proliferation as well as being degradable by cell action (Drury and Mooney, 2003).

The type of the collagen of the construct has an effect on the metabolism of the immobilized cells. Cells immobilized in collagen type II showed greater chondrogenic activity than cells immobilized in type I collagen. On the contrary mesenchymal stem cells (MSCs) immobilized in collagen type I showed better biomechanical properties *in vivo* than MSCs immobilized in type II collagen (Fedorovich et al., 2007).

Weinberg and Bell (1986) used collagen to mimic the adventitial and medial layers of native artery using culture derived collagen / fibroblast gel sheets and a similar collagen / smooth muscle cell (SMC) sheet wrapped over each other to form a tubular construct. However, owing to the inherent physical weakness of the collagen gel and limited ECM deposition by cultured SMC, the mechanics of these grafts were insufficient for implantation (Weinberg and Bell, 1986; Garner, 2003). Additionally, collagen gels have been used to entrap MSCs, chrondrocytes and osteoblasts which maintain their differentiated phenotype and produced ECM. However, their low mechanical strength scaffolds and the loss of shape and consistency through shrinkage have restricted its use for tissue engineering applications (Fedorovich et al., 2007).

1.2.4 Hyaluronic acid

Hyaluronic acid is a major component of the ECM. It is found in developing embryonic mesenchymal tissues, in the synovial fluid of the joints and it is prevalent during wound healing (Caplan, 2000; Drury and Mooney, 2003). It is a linear polysaccharide composed of a repeating disaccharide and (1-4)-linked β-D-glucuronic acid and N-acetyl-β-D-glucosamine units. Specifically, it can be produced by crosslinking with hydrazide derivatives, by esterification and by annealing (Drury and Mooney, 2003). It can be modified chemically and physically into different physical forms including fibres, strands, ropes, films, woven and no-woven materials, sheets and sponges (Carlan, 2000). It is degraded naturally by hyaluronidase allowing the immobilized cells to control its presence in a localized manner (Drury and Mooney, 2003).

The hyaluronic acid is known for its dual functionality which is attributed to the effect of its molecular weight on its degradation rate. Analytically, hyaluronic acid with low molecular weight (below 35 kDa) breaks down in 7 to 10 days whereas high molecular weight hyaluronic acid (200-400 kDa) breaks down in 8 to 10 weeks. It has been demonstrated that hyaluronic acid with a high molecular weight has chrondrogenic abilities and hyaluronic acid with low molecular weight has angiogenic abilities (Alison and Grande-Allen, 2004; Caplan, 2000). High molecular weight hyaluronic acid is commercialized under the name Hyaff-11 and low molecular weight hyaluronic acid under the name ACP (Caplan, 2000).

Hyaluronic acid on its own does not posses all the properties of ECM. It has been combined with collagen and gelatine and crosslinked with RGD peptide (carbodiimide chemistry) in order to improve cell attachment and proliferation (Alison and Grande-Allen, 2006; Duflo et al., 2006). Modified and non-modified hyaluronic acids have been used mainly to engineer artificial cartilage, bone and ligament. However, their weak mechanical strength (even with the modifications) and the presence of impurities compromise their use (Fedorovich al, 2007).

1.2.5 Self-assembling peptide nanofiber scaffold

Self-assembling peptide nanofiber scaffolds (SAPNS) are synthetic biological materials which are formed through the ionic assembly of positive and negative 8 to 16-residue peptide (≈ 2.5-5 nm in length) by changing to neutral pH or by adding physiological concentrations of salt solutions. The gelation leads to a hydrogel of interwoven nanofibers with a diameter in the range of 10 nm and with a water content greater than 99% w/v (Ellis-Behnke et al., 2006; Holmes et al., 2000; Zhang et al., 1995). These environments not only allow attachments between cells and the basal membrane, but also allow access to oxygen, hormones and nutrients, as well as removal of waste products (Gelain et al., 2006). Immobilized cells can be recovered in a three-stage process which involves mechanical disruption, centrifugation and suspension in trypsin / EDTA (5-10 min) (Garreta et al., 2006).

The nanofibers of the SAPNS are 3 orders of magnitude thinner than other biopolymer microfibers. They are of a scale similar to native ECM providing a better *in vitro* mimic of the *in vivo* cell growth environment (Ellis-Behnke et al., 2006). It degrades to L-amino acids which could be used potentially by nearby cells for growth and repair (Ellis-Behnke et al., 2006). It has been reported that *in vivo* most of it is excreted in the urine in 3-4 weeks. It is free of biological and chemical components as it is chemically defined (Ellis-Behnke et al., 2006). Additionally, it does not initiate inflammatory response when implanted in the human body (Ellis-Behnke et al., 2006).

SAPNS support proliferation, differentiation, migration and ECM production (Kisiday et al., 2002; Garreta et al., 2006; Zhang, 2003). Lately, Ellis-Behnke et al. (2006) showed that SAPNS promote the closing of neural tissue gaps enabling axon regrowth. They believe that this is attributed either to cell migration into the lesion area which creates a growth permissive environment or to a contractile process that brings the two lesions of the gap together.

1.3 Cell sources used in tissue engineering

1.3.1. Introduction

The ideal cell for tissue engineering applications should possess characteristics such as the ability to proliferate rapidly *in vitro*; be easily obtainable via biopsy; able to differentiate to a variety of tissue-specific cell lines; and to be acceptable from the recipient's immune system without the need of immunosuppression therapy (Nasseri et al., 2001).

Currently, cells used in tissue engineering are allogeneic, xenogeneic, or autologous and they can be used as primary culture, as expanded *in vitro* and as cryopreserved (Lalan et al., 2001). Autologous cells are derived from a patient's own cells thus harvest or donation in advance of need coupled with *in vitro* culture is required. However, there is no danger of immunogenicity / rejection and transmission of disease (Garner, 2004). Allogeneic cells are derived from an individual of the same species other than the recipient and xenogeneic cells are derived from a species different than the recipient. Allogeneic and xenogeneic cells are transplanted in an encapsulated fashion in order to avoid contact with the recipient's immune system. Additionally, they have the advantage of constructs being prepared in advance of need (Garner, 2004; Nasseri et al., 2001). Nevertheless, a therapy based on the use of these cell sources does pose the risk of transmission of a disease from the donor to the host as well as of the rejection of the transplant (Nasseri et al., 2001).

Some tissue-specific cell types proliferate rapidly *in vitro* but others, like cardiac muscle cells and hypatocytes, proliferate slowly or not all making their expansion difficult. Additionally, they can divide only a finite number of times (depending the age of donor) which limits their supply and they may accumulate genetic changes over time (Evans et al., 2006; Kuo and Tuan, 2003; Nasseri et al., 2001). Therefore, research in tissue engineering has shifted from the use of tissue-specific cells to the use of adult and embryonic stem cells as therapeutic agents, which are discussed in more detail in the following sub-sections.

1.3.2 Adult stem cells

Adult stem cells are multipotent stem cells (can produce many cell types) which have been found in many tissues including bone marrow, peripheral blood, adipose tissue and umbilical cord (Evans et al., 2006; Huang et al., 2007; Riha et al., 2005). The benefits of using adult stem cells include immuno-compatibilty of autologous cells, ease of inducing differentiation, and availability (Barrilleaux et al., 2006).

Adult stem cells have the ability to regenerate damaged tissue *in vivo* throughout an entire human lifetime but they have limited proliferative capacity *ex vivo*. Research is underway in order to replicate the stem cell micro-environment or "niche" in order to enhance their regenerative potential (Huang, et al., 2007).

The most widely studied stem cells in tissue engineering are the mesenchymal stem cells (MSCs). MSCs reside mainly in the stroma of bone marrow (Evans et al., 2006; Riha et al., 2005). They were first identified by Friedenstein et al., (1966) and they represent 0.01% of the total cell population in the bone marrow (Evans et al., 2006). Isolation has been reported from umbilical cord vein, adult fat, muscle, brain, synovial membrane tracebular bone and blood (Riha et al., 2005). MSCs can form bone, cartilage, tendon, muscle fat, neural tissue and hematopoietic supporting stroma by selecting the appropriate culture conditions (Kopen et al., 1999; Kuznetsov et al., 1997; Mauney et al., 2005; Pittinger et al., 1999; Prockop, 1997).

After aspiration, marrow cells are cultured in Dulbecco's modified Eagle's medium with 10% fetal bovine serum. Following removal of the nonadherent cells, adherent MSCs can be passaged and differentiated. When MSCs are attached to a plastic surface they resemble morphologically cells of the connective tissue. Phinney et al. (1999) have reported though that 10-20% of those cells showing plastic-adherent ability are actually MSCs. Therefore, cells derived from bone marrow with plastic-adherent ability are referred to as marrow stromal cells (Evans et al., 2006).

The concentration of MSCs and partially differentiated progenitor cells in bone marrow can be highly variable. There can be variation between donors or even between aspirates from the same donor (Muschler et al., 1997). Additionally, the younger the donor the higher will be the concentration of MSCs in the bone marrow (D' Ippolitto et al., 1999).

MSCs are defined by their behaviour and not by any molecules or structures they contain (Barrilleaux et al., 2006). There is no one specific cell marker which can be used to distinguish MSCs from their closest differentiated neighbours. This suggests that MSCs are adjacent to non-stem cells and that the maintenance of their stem cell properties may depend on adhesion to non-stem cells (Barrilleaux et al., 2006).

Cell surface markers are used to isolate and characterize MSCs using flow-activated cell sorting (Huang et al., 2007). The expression of cell surface markers like STRO-1 (a stromal cell surface antigen), CD29 (integrin β_1), CD44 (receptor for hyaluronic acid and matrix proteins), CD105 (endoglin, receptor for transforming growth factor β (TGF-β) and CD166 (cell adhesion molecule) has been related to a MSC phenotype. These markers though are also expressed by cells which are not MSCs. However, MSCs can be distinguished from these other cell types since MSCs do not express the following markers: CD14, CD34, CD45, HLA-DR (hematopoietic stem cell markers), CD11a (lymphocyte function-associated antigen), CD31 (platelet endothelial cell adhesion molecule) and integrins α_4 (hematopoietic stem cells) and β_2 (T-lymphocytes) which are not related with a MSC phenotype (Barrilleaux et al., 2006; Huang et al., 2007; Riha et al., 2006).

Studies have shown that there are marrow cells which co-purify with MSCs and they can be expanded for more than 80 population doublings (Jiang et al., 2002; Oswald et al., 2004). These cells have been termed multipotent adult progenitor cells (MAPCs). It has been shown that MAPCs can differentiate not only into mesenchymal lineage cells but also endothelium and endoderm (Jiang et al., 2002). Their existence though is still debatable (Riha et al., 2005; Rouffose et al., 2004).

1.3.3 Embryonic stem cells

Human embryonic stem cells (hESCs) are pluripotent stem cells which are derived from the inner cell mass of reimplantation embryo. As a result of their pluripotency they possess the ability to form derivatives of all three embryonic germ layers while remaining stable karyotypically and phenotypically (Thomson et al., 1998). Their enhanced telomere activity makes them capable of unlimited undifferentiated proliferation *in vitro*. They express Oct-3/4 (transcription factor), Nanog (homodomain protein), SSEA-3/4 (surface marker) and TRA 1-60/1-81 (surface marker) markers and in addition they possess enzyme activities for alkaline phoshatase and telomerase (Baker et al., 1997; Mitsui et al., 2003; Thomson et al., 1998; Wobus et al., 1984).

Human ESCs are cultured in the presence of mouse embryonic fibroblasts (MEF) feeder cells in order to maintain their self-renewal without differentiation. In the absence of MEFs they form embryoid bodies (EBs) comprised of undifferentiated and differentiated cell types (Huang et al., 2007; Xu et al., 2001). The practice of using MEFs is challenging technically for large scale production of hESCs because it depends on routine availability of large numbers of MEFs requiring methods amenable to scale up (Xu et al., 2001). Additionally, this practice has raised concerns about the therapeutic potential of hESCs exposed to animal cells (Huang et al., 2007). The development of feeder-free culture systems is a way to alleviate the above difficulties. Specifically, the hESCs are cultured on Matrigel (murine basement membrane matrix extracted from Engelbreth-Holm-Swarm sarcoma) in MEF-conditioned culture medium (Xu et al., 2001).

It has been demonstrated that hESCs can differentiate into contractile cardiomyocytes and vascular cell types in EBs (Kehat et al., 2004; Laflamme and Murry, 2005; Levenberg et al., 2002). However the therapeutic potential of ESCs is limited by the induced immunogenecity upon differentiation after ESC transplantation and by the risk of formation of teratomas after implantation (Cao et al., 2005; Huang et al., 2007; Henderson et al., 2002; Swijnenburg et al., 2005).

1.4 Non-invasive techniques for tissue engineering applications

The use of direct non-invasive methods is essential in tissue engineering applications for monitoring the interactions among cells, biomolecules, and the scaffolds that support them *in vitro* and *in vivo* without disrupting its integrity or damaging the cells. Direct non-invasive methods, which are used in tissue engineering, include nuclear magnetic resonance (NMR) and optical coherence tomography (OCT).

NMR detects the presence of compounds and determines their concentration through the exposure of the construct to magnetic fields. Analytically, the unpaired nuclei (nuclei that contain odd numbers of protons or neutrons) in a construct tend to align at an applied magnetic field at a specific frequency for a given nucleus due to their intrinsic magnetic moment and angular momentum. This alignment of nuclei produces a magnetisation (property of a material that describes to what extent it is affected by magnetic fields, and also determines the magnetic field that the material itself creates), which can be manipulated by an additional magnetic field orthogonal to main one. If the frequency of the additional magnetic field is at resonance with the magnetization, it will nutate (rock) it away from the alignment with the main field. This generates a radiofrequency signal that is detected by a sensitive antenna placed around the specimen (Burg et al., 2002).

NMR data are acquired in the form of a spectrum or an image (Constantinidis and Sambanis, 1999). The spatial resolution of NMR can reach 10 μm and it is not dependent on the opacity or thickness of the construct but on the intensity of the applied magnetic field (Burg et al., 2002; Jacobs and Cherry, 2001). Nuclei like ^{13}C, ^{19}P and ^{1}H can be detected but the higher sensitivity of ^{1}H nucleus makes ^{1}H-NMR spectroscopy more favourable to study changes in the concentrations of proton-containing metabolites at concentrations as low as 1 mM (Constantinidis and Sambanis, 1998).

Some of the applications of NMR in tissue engineering include the determination of cell number, the measurement of the permeability of

engineered meniscal constructs, the monitoring of changes in metabolic activity of entrapped cells and the study of alterations in cell volume and water exchange time on perfused cells (Stabler et al., 2005; Neves et al., 2006; Pfeuffer et al., 1998; Constantinidis et al., 1997).

OCT can produce cross-sectional images in biological systems by measuring the back-scattered / back-reflected intensity of light from structures in tissue (Fujimoto et al., 1995; Bagnanichi et al., 2007; Ko et al., 2006; Mason et al., 2004). It is as a technique analogous to radar except it uses near-infracted light instead of radio waves. The sufficient number of scattering objects (membranes, organelles, nuclei, etc.) in most biological tissues produce contrast in OCT images making tissue imaging possible (Ko et al., 2006). OCT can achieve spatial resolutions of 1 μm but the imaging depth is limited to 2-3 mm due to light scattering in most tissues (Fujimoto et al., 1995; Mason et al., 2004). A wide range of tissues can be accessed by catheter or by an endoscope (Fujimoto et al., 1995; Mason et al., 2004).

OCT has been used in tissue engineering to image constructs with immobilized mouse embryonic fibroblast, smooth muscle cells, endothelial, tendon, bone and neuronal cells (Bagnanichi et al., 2006; Mason et al., 2004; Morgan et al., 2006; O'Halloran Cardinal et al., 2006; Tan et al., 2004). Additionally, it has been combined with elastography to characterize biomechanical properties of biological tissue (Chan et al., 2004; Ko et al., 2006; Rogowska et al., 2004; Schitt, 1998).

1.5 Tissue engineering of blood vessels

1.5.1 Introduction

Having provided an overview of the overall status of tissue engineering efforts, the thesis will now focus on vascular tissue engineering in more detail. The role of the vascular system is to channel blood in a controlled manner around the entire human body. It consists of arteries, veins and capillaries with varying size, different mechanical properties and cellular content depending on their location and function. The arteries are relatively thick-walled, viscoelastic tubes which work at high pressure. The large arteries carry blood from the heart to smaller arteries which deliver the blood to the organs and tissues through a distribution of smaller arterioles and capillaries. Veins are thinner walled than arteries but they have a larger calibre. They operate at low pressure and return the blood to the heart. The wall structure of the blood vessels could be described by three distinct, well-defined, and well-developed layers. These three layers are reduced in the arterioles and they are almost absent in the capillaries. From innermost to outermost, these layers are the thinnest *tunica intima*, the thickest *tunica media* and the *tunica adventitia. Tunica intima* consists of *a* continuous lining (the vascular endothelium) of a single layer of simple squamous (thin, sheetlike) endothelial cells, resting on a thin subendothelial connective tissue bed of basement membrane and matrix molecules to form the subendothelium. This endothelium sheet works as a barrier to the plasma proteins and also secretes many vasoactive products. Its integrity protects the blood vessel from the development of atherosclerosis. It is separated from the next adjacent wall layer by a thick elastic tissue band called the *internal elastic lamina.* The thickest *tunica media* offers mechanical strength and contractile power. It is composed of a significant amount of smooth muscle cells arranged concentrically in radial layers, embedded in a matrix of circularly arranged elastic and collagen fibers. It is separated from the next adjacent wall layer by another thick elastic band called the *external elastic lamina.* Finally, the medium-sized *tunica adventitia* is an outer vascular sheath with no distinct outer border consisting entirely of fibroblasts, nerves and blood vessels (vasa vasorum), which carry blood to the

tunica media. It serves to add rigidity and strength to the blood vessel wall (Palsson et al., 2003; Ratcliffe, 2000).

The ECM surrounding the vascular cells is complex and combines to provide the biomechanical properties of the tissue (Wight, 1996). The molecular network consists primarily of collagen (primarily types I and III), elastin in the form of fibers, proteoglycans (including versican, decorin and biglycan, lumican and perlican), hyaluronan, glycoproteins (for example, laminin, fibronectin, thrombospondin and tenascin). The mechanical properties critical to blood vessel function include the tensile stiffness, elasticity, compressibility and viscoelasticity. The collagens provide the tensile stiffness, the elastin the elastic properties, whereas the proteoglycans contribute to the compressibility, and combined with the collagen and elastin they are responsible for the viscoelastic properties. This complex mixture of molecules and their organization provide the blood vessels with their properties that allow them to function throughout life (Ratcliffe, 2000).

1.5.2 A completely biological tissue-engineered human blood vessel

L' Heureux et al. (2005) have presented a tissue-engineered blood vessel by using cultured human cells without employing an artificial scaffold. They hypothesize that this way of fabricating a vessel has several advantages over scaffold-based approaches, which will result in increased overall patency. Firstly, its biological matrix can be remodelled by the body according to the need of the environment. Secondly, the absence of synthetic material will prevent foreign body reaction and allow complete graft integration. Their blood vessel appeared histologically identical to normal artery (L' Heureux, 2005).

L'Heureux et al. (2005) constructed a human tissue-engineered blood artery exclusively with fibroblasts. Their engineered arteries were composed of 3 components: a living adventitia, a decullarized internal membrane and an endothelium. Analytically, fibroblast sheets with a thickness of 43 mm were produced in 6 weeks. Their thickness increased at a rate of 5 mm per week

through 15 weeks. The internal membrane was assembled by wrapping the sheet around a Teflon-coated stainless steel temporary support tube for 3 revolutions. Following 10 weeks maturation, this tissue was dehydrated to form an acellular membrane for endothelial cell seeding. A secondary role of the membrane was to provide a barrier against cell migration in the lumen. The adventitia was formed in a similar manner by wrapping a living sheet of fibroblasts around the internal membrane. After a second maturation, the Teflon support was removed and the tube was seeded with endothelial cells in the lumen of the artificial artery. The vessel was then subjected to pulsatile flow for a 3-day preconditioning period.

The engineered arteries had an internal diameter of 4.2 mm and a wall thickness of 400 μm with mechanical properties similar to saphenous veins. A long-term implantation study was conducted in rats. After 225 days, the patency was 85%. Graft diameter remained stable, which indicates mechanical stability whereas cell and ECM organisation were similar to native arteries. There was no sign of aneurysm (localized dilation or ballooning of the blood vessel due to weakening of its wall), reendothelialisation of the internal membrane or formation of vasa vasorum (smaller blood vessels that supply the cells which are located at the outer wall of the main blood vessel) (L'Heureux et al., 2005).

1.5.3 Tissue engineered blood vessel from collagen and cultured cells

Weinberg and Bell (1986) have mimicked the adventitial and medial layers of native artery using culture derived collagen / adventitial fibroblast gel sheets and a similar collagen / bovine aortic SMC sheet wrapped over each other to form a tubular construct. These were then lined by anbovine aortic EC monolayer.

The middle layer of the blood vessel model, corresponding to the media of an artery, was prepared by casting culture medium, collagen, and SMCs together in an annular mold. The mixture jelled after a few minutes at 37°C and contracted within a few days to produce a tubular lattice around the central

mandrel. After 1 week, an open Dacron mesh sleeve was slipped over the lattice to provide additional mechanical support. The outer layer, corresponding to the adventitia, was cast around the first lattice with adventitial fibroblasts rather than SMCs. Two weeks later, when the outer layer was fully contracted, the tube was slipped off the mandrel with jeweller's forceps and either used for mechanical testing or lined with ECs. For the latter, the model was cannulated, a suspension of ECs was injected into the lumen, and the vessel was rotated around the longitudinal axis at 1 rpm for 1 week to distribute ECs uniformly on the luminal surface (Weinberg and Bell, 1986).

The model resembled a muscular artery, except for the Dacron mesh. Electron microscopy showed that the SMCs are well-differentiated bipolar cells containing bundles of filaments with dense bodies. They appeared to be secreting collagen into the extracellular space, thus contributing to the matrix. Examination revealed that the entire luminal surface was covered by ECs covered (92.1 ± 2.5% of the surface) (Weinberg and Bell, 1986).

The endothelial lining of the blood vessel model functioned like a normal endothelium in several respects, including producing von Willebrand factor and forming a permeability barrier for large molecules such as albumin. ECs release prostacyclin *in vivo*. This is a potent inhibitor of platelet aggregation and it is believed to prevent thrombosis (blood clotting in the lumen). The ability of the blood vessel model to withstand intraluminal pressure depended on several factors including the mesh, collagen concentration, initial cell concentration and time elapsed after casting. The burst strength of the model was proportional to the logarithm of the collagen concentration. The increase in strength with time was probably due to greater cross-linking of the collagen. The decrease in strength after long times may be caused by collagenase secreted by the SMCs and fibroblasts in the lattices. To maximize the burst strength, they optimized the above parameters and produced models with burst strength of 320 mmHg (42 kPa) (Weinberg and Bell, 1986).

Their model resembled the structure of a native blood vessel but there were substantial differences between them. Firstly, elastin, the principal connective

tissue protein besides collagen was absent. Secondly, the orientation of SMCs was longitudinal as the contraction of the lattice layers around the mandrel was radial rather than in the alternating left and right handed spirals of blood vessels. Finally, the densities of the SMCs were approximately 12-25% of those of a normal blood artery (Weinberg and Bell, 1986).

1.5.4 Cell and non-biodegradable scaffold

Ratcliffe et al. (2000) made use of polyurethane, a non-biodegrable scaffold, to provide the necessary mechanical properties needed for a blood vessel to function immediately after implantation. Specifically, polyurethane scaffolds with immobilized allogeneic SMCs were cultured *in vitro* and seeded on the luminal surface with ECs under fluid flow. The resultant constructs were substituted for the carotid arteries of dogs, and were found to remain patent and retain an endothelial lining for 4 weeks. Their mechanical properties were similar to native vessels in terms of elasticity, tensile stiffness, and failure strength. They had SMCs oriented circumferentially with an ECM containing collagen, elastin and proteoglycan, and they had an endothelial layer with the cells oriented parallel to the fluid flow and able to inhibit thrombosis. The use of a non-degradable material provided a method to prevent burst or rupture (Ratcliffe, 2000). However, such a system will not be remodelled into the host into a natural form and it has the potential to become infected (Germain et al., 2000; Ratcliffe, 2000).

1.5.5 Cell seeded in biodegradable polymer

Once cells are immobilized to a three-dimensional biodegradable polymer, the resulting tissue construct can be implanted *in vivo*, where the cells continue to grow and develop ECM. While the cellular structure and matrix develop, the polymer degrades, leaving only the engineered tissue without foreign material. Approaches for the development of a functional artery using biodegradable polymer can further be classified into these that adopt and these that do not pulsatile flow. These are discussed further in the following sub-sections.

1.5.5.1 Pulsatile Flow

Niklason et al. (1999) used a system composed of bioreactors containing engineered vessels assembled in a parallel flow system. In initial experiments, a suspension of SMCs isolated from the medial layer of bovine aorta was pipetted onto tubular biodegradable polyglyconic acid (PGA) scaffolds that were secured in bioreactors. The surface of the PGA scaffolds was modified chemically with sodium hydroxide, which caused ester hydrolysis on the surface of the fibres, leading to increased hydrophilicity, increased adsorption of serum proteins, and improved SMC attachment. After an initial SMC seeding period of 30 min, the bioreactors were filled with medium and the SMCs were cultured under conditions of pulsatile radial stress for 8 weeks. Control vessels were cultured without pulsatile radial stress under otherwise identical conditions (Niklason et al., 1999).

After 8 weeks of culture, the gross appearance of the vessels was identical to that of native arteries except the wall thickness was considerably bigger. Histological examination of pulsed vessels revealed that SMCs migrated inward to envelop PGA fragments in the vessel wall; resulting in a smooth luminal surface onto which bovine aortic ECs could easily be seeded. In contrast, nonpulsed controls exhibited no such inward SMC migration through the polymer scaffold and possessed an uneven layer of polymer fragments in the vessel lumen. Thus, vessels cultured under pulsatile conditions had a histological appearance more similar to that of native arteries.

The mechanical properties of native arteries rely on contractile SMCs, collagen and elastin. Models of the wall mechanics of muscular arteries have shown that structured bundles of collagen fibers contribute most of the incremental elastic modulus at intraluminal pressures above 100 to 200 mmHg (130-260 kPa). Due to fact that the mechanical properties of vessel derive from the SMCs and their ECM they optimize its production by supplementing in the culture ascorbic acid, copper ion and amino acids (Niklason et al., 1999).

Pulsatile culture conditions did not significantly affect SMCs density although these SMCs densities were higher than those reported in systems where collagen gels were used as matrix. The difference in calculated cell density between engineered and native vessels may be due to the volume occupied by the polymer fragments in the engineered vessel wall. The SMCs of vessels cultured under pulsatile conditions stained more intensely for myosin heavy chains, a late marker in SMCs development as compared with nonpulsed vessels. The application of pulsatile stress did not increase the mitotic rate in dense cellular areas. However, the percent of stained SMCs in the polymer scaffold regions of endothelialized vessels was decreased to 0.5 ± 0.7%, as compared with vessels that did not contain ECs. This result was consistent with the expected inhibition of replication of SMCs by confluent ECs and would decrease the likelihood of hyperplasia of SMCs and vessel stenosis (narrowing) after implantation (Niklason et al., 1999).

1.5.5.2 No pulsatile flow

Shin'oka et al. (1998) examined the feasibility of a tissue engineering approach to constructing tissue-engineered "living" pulmonary artery. Ovine or vein segments were harvested from 20-day old lambs, separated into individual cells, expanded in tissue culture and seeded onto synthetic biodegradable (polyglactin / polyglyconic acid) tubular scaffolds (20 mm long x 15 mm diameter). After 7 days of *in vitro* culture, the autologous cell / polymer vascular constructs were used to replace a 2 cm segment of pulmonary artery in lambs. One other control animal received an acellular polymer tube sealed with fibrin glue without autologous cells (Shin'oka et al., 1998).

Two weeks after implantation, echocardiography showed patent conduits. Thrombus formation was identified in the control animal causing narrowing of the artery. After 10 to 12 weeks, tissue engineered conduits showed no evidence of thrombus formation or calcification. In addition, the high-density material in the conduit wall had disappeared. The gross appearance of the tissue-engineered conduits resembled the native pulmonary artery although

they were somewhat thinner. The specimens from the animals showed disappearance of PGA polymer and the tissue-engineered conduit had the same structure as the native artery (Shin'oka et al., 1998).

Levelberg et al. (2003) engineered tissue-like constructs derived from human embryonic stem cells (hESCs) by using polymer scaffolds. They created a series of 3D culture conditions using biodegradable scaffolds and Matrigel (protein mixture extracted from Engelbreth-Holm-Swarm (EHS) mouse sarcoma) and they evaluated attachment and 2-week survival of differentiating human embryonic stem cells by using two methods of seeding. The first one is by seeding the cells onto the scaffold with Matrigel and the second one by coating the scaffold with fibronectin (Levenberg et al., 2003). Comparison of vessel-like structures in the scaffolds in the presence and absence of Matrigel indicated that Matrigel was not required, as samples seeded on fibronectin-coated scaffolds resulted in higher levels of endothelial differentiation and vascularization. The differences might be caused by effects of fibronectin or growth factors still present in the Matrigel after growth factor reduction (Levenberg et al., 2003).

1.6 Control of cell metabolism

1.6.1 Oxygen

Oxygen plays a significant role in the cell metabolic behaviour. Mammalian cells require oxygen for energy production through adenonosine triphosphotate (ATP). Energy production through aerobic metabolic pathways yields 38 ATP moles per mole of glucose whereas through anaerobic metabolic pathways yields only 2 ATP moles per mole of glucose. The proximity of a cell to an environment rich of oxygen regulates the dominant mechanism of energy production. For example, chrondrocytes being in a low oxygen environment (1-6% tension) follow primarily anaebobic metabolic pathways in order to produce energy (Malda et al., 2007).

Oxygen not only acts as substrate but also influences cell-fate processes. Ezashi et al. (2005) suggest that the maintenance of hES cells under low oxygen tension of the order of 1-4% should be preferred against 21% if differentiation need to be avoided. Additionally, oxygen tension has been reported to control differentiation in bone marrow. Under 5% O_2 the cells are maintained in an early progenitor stage whereas under 21% O_2 the production of mature phenotypes is enhanced (Hevehan et al., 2000; Mostafa et al., 2000). Low oxygen conditions which mimic the *in vivo* cartilage environment promote collagen type II and GAG instead of collagen type I which is enhanced at ambient oxygen tension (Malda et al., 2004, Murphy and Sambanis, 2001). Human dermal fibroblasts regulate mRNA-VEGF expression under 2% O_2 (Steinbrech et al., 1999). Studies of the effect of oxygen tension on cell proliferation have given contrasting results. Examples include studies of Malda et al. (2004) and Murphy and Sambanis (2001) on chrondrocytes where reduced oxygen tension had no effect on proliferation. On the contrary, Grayson et al. (2005) reported that the proliferation of human mesenchymal stem cells is enhanced under low oxygen tension.

There is a wide variation in oxygen levels in tissues. For example in newborn embryos it is 1.5-5.3%, in bone marrow 5-7%, in lungs ~16%, in arteries ~14% and in veins ~8% (Ezashi et al. 2005; Mostafa et al., 2000). Additionally, there is a variation in oxygen consumption with the cell type (hematopoietic stem cells, $0.047\text{-}0.330\times10^{-18}$ mol $cell^{-1}$ s^{-1}; fibroblasts, $0.4\text{-}0.7\times10^{-18}$ mol $cell^{-1}$ s^{-1}; granulocytes and monocytes, $0.06\text{-}1.80\times10^{-18}$ mol $cell^{-1}$ s^{-1}; hypatocytes 0.038×10^{-18} mol $cell^{-1}$ s^{-1}; chondrocytes, $0.2\text{-}0.4\times10^{-18}$ mol $cell^{-1}$ s^{-1}; cardiomyocytes, 0.25×10^{-18} mol $cell^{-1}$ s^{-1}) (Foy et al., 1992; Grayson et al., 2005; Lewis et al., 2005; Malda et al., 2004; Muschler et al., 2004; Radisic et al., 2005; Zhao et al., 2005).

There is a recent understanding of the way mammalian cells sense and respond to low oxygen levels (hypoxia). Analytically, oxygen interacts with a heterodimeric basic helix-loop-helix protein the hypoxic-inducible factor 1 (HIF-1α) independently of the mitochondric respiration causing its inactivation. HIF-1α is activated after the dissociation of the oxygen followed by a decrease in its

level. Consequently, this leads to the activation of various genes. For example HIF-1 activates glycolytic genes and stimulates the conversion of glucose to pyruvate and consequently to lactate (Kim, 2006; Malda et al., 2007). Studies of Jiang et al. (1996) have shown that the HIF-1α expression in HELA cells varies exponentially over a physiologically range of oxygen tension. They also calculated the half-maximal response or the 50% inhibitory concentration of catalytic function to occur at 1.5-2% with the maximal response at 0.5%. They also concluded that above 6% O_2 the levels were constant.

In vivo, oxygen diffuses from the lumen of a capillary to a cell membrane with the maximum diffusion distance to be in the order of 40-200μm. This distance is characteristic of the oxygen requirements because a balance between delivery and consumption has to be maintained. Up to now tissue engineered constructs are avascular so when they are transplanted in the human body the cells are competing for oxygen. Studies that describe the interaction between the oxygen profile and cell distribution have shown significantly higher cell density in the peripheral layers than in the interior of the construct as well as uneven ECM distribution (Dunn et al., 2006; Lewis et al., 2005; Malda et al., 2004; Martin et al., 1999, Wendt et al., 2006). It has been concluded that the critical variables are the oxygen concentration at the surface of the construct, its size and geometry, the metabolic state of the cell and the cell density (Foy et al., 1992; Malda et al., 2004; Radisic et al., 2005; Zhao et al., 2005).

In order to avoid having significant variations in oxygen concentration within the construct, the size of the construct has either not to overcome the maximum *in vivo* distance of the cells from the vessels or the construct has to be seeded with less cells assuming though that its integration in the human body will not be affected (Muschler et al., 2004). Alternatively, the construction of scaffolds which will include interconnected pores formed by laser drilling or 3D printing techniques will enhance the oxygen transfer into the construct (Malda et al., 2007). Additionally, the construction of biomaterials with controlled-release capabilities of angiogenic signals can stimulate angiogenesis enhancing the oxygenation of the construct (Malda et al., 2007)

1.6.2 Substrates and metabolites

In mammalian cells the main carbon and energy source is glucose and the main nitrogen source is glutamine. Glucose is metabolized mainly through the glycolysis (anaerobically) to form lactate but also through oxidative phosphorilization (aerobically) to form CO_2. When lactate is produced only 2 moles of ATP are obtained in comparison with 36 moles of ATP through oxidative phosphorilization. Lactate is produced in order to maintain the oxidative state of the cell but its accumulation causes inhibition to cell proliferation especially when it is accompanied by a decrease in pH. Patel et al. (2000) noted that the inhibition in the proliferation of peripheral blood mononuclear cells was around 60% when the lactate concentration was increased to 25 mM and the pH decreased from 7.2 to 6.9. This inhibition though was around 25% when the pH was maintained relatively constant (7.1-7.3) and the lactate was allowed to reach 30 mM.

Glutamine is metabolized through glutanimolysis to ammonia and glutamate. Glutamate is further metabolized to a-ketoglutarate then degraded in the TCA cycle. Ammonia is also formed from the first order spontaneous degradation of glutamine. The pH has a strong influence on the decomposition rate and the half-life of glutamine. On the contrary, serum concentration has no noticeable effect unless it contains glutaminase. A typical Iscove's medium culture without pH control can be initiated at pH 7.2 and end up at pH 6.8 causing a change in the decomposition rate by a factor of 2.5. If the chemical decomposition of glutamine is neglected, it will be calculated with a 200-300% error leading to false conclusions (Ozturk and Palsson, 1990).

A concentration between 2 and 10 mM has been reported to reduce cell proliferation rate and final cell concentration with the mechanisms of its toxicity to remain unclear (Patel et al., 2000; Schneider et al., 1996). Different effects on metabolic pathways have been reported like reduction of the sialylation of granulocyte colony-stimulating factor (G-CSF) in recombinant CHO cells, increase in the intercellular pool of UDP-acytylglucosamine and UDP-acetylgalactosamine in several mammalian cell lines and cell apotopisis in

hybridomas (Maranga and Goochee, 2005). Due to this low limit a few strategies have been associated to reduce its formation. The two basic strategies are the optimization of the fresh medium feeding strategy and the use of glutamine based dipeptides such as L-alanine-L-glutamine. The latter is split up gradually by cellular released aminopeptidases to give alanine and glutamine. This gradual release resembles the continuous addition of glutamine in fed-batch cultures operated to maintain its concentration low (Christie and Butler, 1994).

Under oxygen excess, the stoichiometric ratio of glucose to lactate and glucose to glutamine is relatively constant on the order of 0.7-1.5 mol mol^{-1} (Xie and Wang, 1993) and 0.2-0.5 mol mol^{-1} respectively (Zeng et al., 1998). Additionally studies from Xie and Wang (1993) have shown that 80% of glutamine is metabolized to ammonia. Typical consumption rates for glucose and glutamine has been reported to be on the order of 2.8-13.8x10^{-18} mol $cell^{-1}$ s^{-1} (Palsson and Bhatia, 2003). It has been reported though that those values are lowered considerably when the glucose and glutamine concentration are around 0.25 mM without causing any alteration in the cell proliferation rate. Glucose is used in a more efficient way reducing the produced amount of lactate and ammonia. Above these concentrations, the stoichiometric ratios are relatively constant and independent of the cell type (Gambhir et al., 2003; Zeng et al., 1998). This desirable metabolic shift has not been recently exploited for mammalian cells therefore it is not yet well understood how it affects cell-fate processes.

1.6.3 Mechanical stimulation

Application of mechanical stimulation to cells immobilized in a scaffold has been shown to increase their biosynthetic activity improving and accelerating tissue regeneration *in vitro* (Martin et al., 2004). A complete simulation of the *in vivo* environment has not yet been achieved but a variety of effects of mechanical stress in cell shape, proliferation, differentiation, synthesis and secretion of proteins, mechanical stiffness and intracellular signalling have been studied. Additionally, this has been extended to the level of gene expression and

messenger RNA regulation (Ziegler and Nerem, 1994). The types of mechanical stimulation which have been used are cyclic tensile and shear strain, static and dynamic compression, pulsatile radial stress, fluid shear stress and hydrodynamic pressure.

Analytically, Kim et al. (1999) observed that engineered smooth muscle cells subjected to cyclic tensile strain for 20 weeks has 12 fold and 34 fold increase in tensile strength and Young's modulus respectively compared to controls. Additionally, they noticed a significant increase in cell alignment in the direction perpendicular to the cyclic strain in stimulated tissues. Similar results about vascular smooth muscle cells have been reported by O'Callaghan and Williams (2000) and Selictar et al. (2003). Studies have also demonstrated that mesenchymal stromal cell either in monolayer or 3D culture follow osteogenic differentiation under either chemical or combined chemical and cyclic tensile strain stimulation (Bruder et al., 1997; Halvorsen et al., 2001; Jaiswal et al., 2000; Jagodzinski et al., 2004; Simmons et al., 2003, Sumanasinghe et al., 2006).

Dynamic compression using frequencies ranges from 0.01 Hz to 3 Hz of articular cartilage constructs enhanced their mechanical properties. (Bonassar et al., 2001; Buschman et al., 1995; Lee et al., 2000; Sah et al., 1989). Static loading instead resulted in a decrease of matrix biosynthesis (Buschman et al., 1995; Davisson et al., 2002; Lee and Bader, 1997). A further improvement of the mechanical properties was achieved with the synergistic use of chemical stimulation (transforming growth factor TGF-β1, insulin-like growth factor IGF-1 and dihydropyridine agonist Bay K8644) and dynamic loading (Mauck et al., 2003; Wood et al., 2006).

Static and cyclic hydrostatic pressure culturing has been shown to improve matrix synthesis. Its effect is defined by its duration, magnitude and frequency. Specifically, Hall et al. (1991) observed an increase in GAG production as a result of a short 20 s stimulus in the range of 7.5 to 20 MPa followed by 2 h in static culture in bovine explants but pressure from 2.5 to 10 MPa with the same 20 s / 2 h culture had the opposite result. Additionally, when pressures were

applied for the full two hours the production of collagen and GAG increased but was followed by a decrease in cellular production. Parkkinen et al. (1993) tested bovine cartilage extracts with 5 MPa under cyclic hydrostatic loading at 0.0167, 0.05, 0.25 and 0.5 Hz but achieved increased GAG production in bovine cartilage extracts only at a frequency of 0.5 Hz. Smith et al. (1995) have demonstrated the duration of loading as a regulatory factor of matrix production. They used a monolayer culture of adult bovine cells under 10 MPa peak pressure at 1 Hz for 2, 4, 8, 12 and 24 h observing increased collagen production for the 4 h cyclic loading.

Shear stimulation either as fluid shear or direct shear has been demonstrated to induce ECM production. Shear produced by flow entering on one side of a construct with immobilized cells and exerting on the other has increased proliferation rates, GAG and collagen production. The mechanical properties though of those constructs have not been examined (Davisson et al., 2002; Pazzano et al., 2000). Concerning the direct shear loading, Jin et al. (2002) concluded that dynamic tissue shear above 1.5% strain amplitude significantly stimulated protein and proteoglycan synthesis, by maximum values of 35 and 25%, respectively, over statically held control specimens. Additionally, the combined stimulatory action of IGF-I and dynamic tissue shear deformation was greater than that of either stimulus alone.

Pulsatile radial stress has been tested successfully as a way of mechanical conditioning to tissue engineer valves and small calliper vascular grafts (Dumont et al., 2002; Elizondo et al., 1999; Hoerstrup et al., 2000; Jockenhoevel et al., 2002; Niklason et al., 1999; Sodian et al., 2000; Williams et al., 2004; Wolfinbarger et al., 2002). The most representative study is the one of Niklason et al. (1999) where bovine smooth muscle cells immobilized in tubular biodegradable polyglycolic acid (PGA) scaffolds were cultured under conditions of pulsatile radial stress for eight weeks (165 beats per minute, 5% radial strain). Following seeding of endothelial cells onto the luminal surface, the artificial arteries were implanted into pigs and remained patent for four weeks. Their rupture strength was around 2000 mmHg (263 kPa), their suture retention strength was 90 g, their collagen content was around 50% and their final cell

density $1.19x10^8$ cells mL^{-1}. The values of cell density and suture retention strength were 3 times lower and the value of wall thickness was 30% higher than the physiological ones. The rupture strength and the collagen content had physiological values.

1.6.4 Bioreactors for tissue engineering

1.6.4.1 Introduction

Bioreactors are defined generally as a cell culture system in which biological or biochemical process take place under controlled environmental and operating conditions (Martin et al., 2004). In tissue engineering a bioreactor should be designed to establish uniform concentrations of cells in biomaterial scaffolds, to control the conditions of culture medium in terms of pH, temperature, dissolved gas concentration, nutrients, metabolites and regulatory molecules and provide relevant physical signals in terms of fluid flow, hydrostatic pressure and mechanical / electrical stimulation (Vunjak-Novakovic et al., 2006). Each of those variables can be studied individually to understand its influence on the properties of the engineered tissue (Bilodeau and Mantovanni, 2006). Mathematical models can be used to rationalize data and predict the bioreactor's behaviour under different operating conditions (Chung et al., 2006; Ma et al., 2007; Malda et al., 2004; McGuigan and Sefton, 2007; Radisic et al., 2005; Sengers et al., 2005; Ye et al., 2006; Zhao et al., 2007). The models can be used to predict the development of engineered tissue with time and to enable timely planning of the surgery from acquired on-line data (Martin et al., 2004).

Furthermore, the bioreactor should be integrated into a manufacturing system which will include cell seeding, cell growth, freezing, shipping and storage of tissue-engineered products in order to maintain sterility, reduce labour and eliminate the need for sterile repacking (Neughton, 2002). Additionally, the automated operation of the bioreactor is crucial for controlled, reproducible basic studies and for future routine manufacturing of tissues for clinical

application. A detailed description of representative bioreactors for tissue engineering is given below.

1.6.4.2 Dishes-flasks-roller bottles-microplates

Tissue culture flasks, petri dishes, roller bottles and microplates have been developed mainly for the monolayer culture of adherent cells. The mass transfer of nutrients and metabolites in these systems is based on molecular diffusion which is adequate for the 10 μm thickness tissue under construction. They are easy to use, disposable and low-cost. Nevertheless, they require individual manual handling which limits their use in large numbers. This can be overcome to some extent with the use of sophisticated robotics.

These culture systems have been also used to study the performance of three-dimensional cell cultures (Glicklis et al., 2000; Malda et al., 2004; Radisic et al., 2005) and specifically to measure diffusional gradients of oxygen, distribution of cell viability and ECM. The results of these studies demonstrated a decrease in cell numbers and a lack of homogeneity of cell and matrix distribution with greater values for these parameters close to the surface of the construct. Measurement of the oxygen profile and of the ratio of lactate produced to glucose consumed indicated oxygen depletion at depths beneath 100-200 μm and anaerobic metabolism. When constructs were exposed to medium flow the oxygen concentration in the construct interior was higher and the cell distribution more homogenous. This effect is attributed to the decrease of the thickness of the mass transport boundary layer around the construct.

The first generation bioreactors which alleviated the diffusion limitation by continuous stirring were the spinner flasks. A spinner flask is a simple cylindrical glass container with two to four needles being inserted into its cap, holding the tissue constructs in fixed positions. Each needle is holding three constructs separated by small silicone spacers. The cells immobilized in these constructs are grown in a mixed environment provided by a magnetic stirrer. The mass transfer of nutrients and metabolites is based on turbulent convection. The

shear stress is not constant along the surface of the construct and it has a maximum value close to the stirrer of the flask. The morphology and the biochemical composition of the construct are a function of the mass transfer rate and hydrodynamics of the bioreactor. However, their responses cannot be predicted due to incomplete understanding of the mechanism involved.

Such bioreactors have been used mainly for preparation *in vitro* chrondrogenesis. Studies from Freed et al. (1993) and Vunjak-Novakovic et al. (1999) have shown that scaffolds cultured in stirrer flasks weighed twice those cultured in mixed dishes and contained 2.5 times more GAG and collagen. However close to the surface of the construct 300 μm capsules of elongated cells were formed with high collagen content but little GAG. The authors attributed this effect to the turbulent flow on cells immobilized close to the surface of the construct. Spinner flasks have been used lately for the large scale expansion and differentiation of murine embryonic stem cells as aggregates. The level of cell aggregation and differentiation was effectively controlled by adjusting shear forces and inoculation density, achieving a 31-fold expansion in five days (Cormier et al., 2006).

1.6.4.3 Perfusion bioreactors

A perfusion bioreactor for tissue engineering applications uses a pulsatile pump to deliver fresh nutrients to the cells, which are immobilized in a scaffold (Martin et al., 2004). The quality of tissue engineered products in perfusion bioreactors has been shown to be a function of the flow rate of the culture medium (Bancroft et al., 2002; Bagnaninchi et al., 2007; Cartmell et al., 2003; Davisson et al., 2002; Dvir et al., 2006). A balance between feed rate of the nutrients, removal of the waste products of the cells, retention of newly synthesized ECM within the construct and shear stress within the pores of the scaffold is crucial to establish optimum operation (Martin et al., 2004). Common types of perfusion bioreactors in tissue engineering are hollow fibre bioreactors, perfused cartridges and tubular bioreactors. An overview is given below.

1.6.4.3.1 Hollow fibre bioreactors

The hollow fibre bioreactors consist of a closed vessel which is transversed by a large number of small diameter tubes. Cells are located either within the fibres (intracapillary space) or on the shell side (extracapillary space). Medium or blood plasma is perfused in the compartment which does not contain cells. The surface of the fibres is used for cell attachment as well as a barrier against the patient's immune system (Palsson et al., 2003). Other techniques to provide adhesion support to cells include gel embedding, attachment to microcarriers and microencapsulation (Planchamp et al., 2003).

The development of hollow fibre bioreactors evolved from ultrafiltration haemodialysis cartridges and enzyme reactors; hence there are well-recognized limitations in their use for mammalian cell cultures (Palsson et al., 2003). Specifically, several researchers have reported nutrient axial and radial gradients which arise from the pressure gradient along the fibre lumen. These gradients can alter the cell metabolism resulting in nonuniform cell proliferation and death. Additionally, protein deposition on the fibre walls has been observed over time especially with fluids containing high levels of proteins like plasma causing decrease in fibre permeability (membrane fouling) (Palsson et al., 2003).

A high pressure difference along the fibre length combined with high fibre permeability induces convective flow across the fibre wall and through the shell compartment. Analytically, intercapillary medium enters the extracapillary space near the entrance of the reactor, travels down the length of the reactor and re-enters the intercapillary flow near the exit of the reactor. This secondary flow is called Starling flow (Gramer et al., 1999; Martin and Vermente, 2005; Palsson et al., 2003). It can improve nutrient and oxygen mass transfer but its effect is detrimental for solid-like scaffolds or for bioreactors at packed cell densities (Brotherton and Chau, 1996; Gramer et al., 1999; Piret and Cooney, 1991).

Alternative methods to operate hollow fibre bioreactors have been proposed that do not cause inhomogeneities of the cell and protein distribution. These

include the periodical reversal of the flow direction of the intercapillary medium (Heath et al., 1990; Piret et al., 1990), the rotation of the bioreactor to avoid gravitational protein sedimentation (Piret and Cooney, 1990), the addition of an oxygenation membrane close to the cells to eliminate the axial oxygen gradient (Robertson and Kim, 1994) and the addition of convection by forcing medium through the extracapillary space to increase nutrient delivery and waste removal (Brotheron and Chau, 1995). However, the first two methods cannot affect the operation of the bioreactor at high cell densities and the last two require a more complicated design than the one required for a conventional bioreactor. Additionally, none of those methods offer a solution to the long-term problem of membrane fouling (Gramer et al., 1999).

Hollow fibre bioreactors are used mainly as liver assist devices (LADs) to sustain liver function and to cover the time between liver failure and implantation. This is a first step towards the construction of an artificial implantable liver which will offer a solution to the problem of severe donor liver shortage, high cost, and complexity of orthotropic liver transplantation (Chan et al., 2004; Kulig and Vacanti, 2004). LADs pass the blood through active charcoal column, oxygenators and heaters and finally through the hollow fibre module before being introduced to the patient's body (Kulig and Vacanti, 2004). There are four LADs in different stage of clinical trials which are the HepatAssist (Cedar-Sinai Medical Centre, Los Angeles, California USA), the ELAD (Vitagen, Inc., La Jolla, California USA), the modular extracorporeal liver support (MELS, Charité Virchow, Berlin, Germany) and the Bioartificial Liver Support System (BLSS, Excorp Medical Oakdale, Minnesota USA). Studies for improvements on the design of LADs are focused towards the maximization of the functional stability of the hepatocytes in an inhospitable environment, the manufacture of scalable units without creating transport limitations or excessive priming volumes that must be filled with patient's blood or plasma, the identification of a reliable cell source and a way to procure the large number of cells needed for a clinically effective device (Chan et al., 2004).

1.6.4.3.2 Perfused cartridges

In a perfusion bioreactor based on perfused cartridges, culture medium is forced through the porous network of the scaffold (Bancroft et al., 2003, Dvir et al., 2006; Vunjak-Novakovic et al., 2006). The design of a flow path which ensures that the fresh medium is flowing through the scaffold and not around its edges is crucial to achieve perfusion through the scaffold (Bancroft et al., 2003). Characteristics of this type of perfusion bioreactor include enhanced external and internal mass transfer as fresh medium is delivered not only around but also through the internal porous network of the scaffold (Bancroft et al., 2003; Cartmell et al., 2002, Vunjak-Novakovic et al., 2006). Additionally, the internal flow provides mechanical stimulation through shear forces with their variability to be dependent on the scaffold's microarchitecture. The intensiveness of the mechanical stimulation can be regulated by varying the flow rate (Bancroft et al., 2003). However, it has to be under consideration that the shear rates will increase with culture time as the produced matrix will decrease the porosity of the scaffolds causing an increase in the shear forces to a stimulatory for the cell metabolism levels (Bancroft et al., 2002). Non-invasive monitoring of the changes in the microarchitecture of the scaffold can be used to control the flow rate within the porous network.

Perfusion bioreactors with cartridges have been used in bone and cardiac tissue engineering. All studies have shown higher viability, increased cell proliferation, enhanced ECM production and constant cardiac contraction frequency (cardiac cell constructs) in comparison with static cultures (Bancroft et al., 2002; Carrier et al., 2002; Cartmell et al., 2003; Dvir et al., 2003; Freed et al., 2000).

1.6.4.3.3 Tubular reactors

Tubular reactors have been used to engineer artificial arteries (Hoerstrup, et al., 2001; Mironov et al., 2003; Narita et al., 2004; Niklason et al., 1999; Sodian et al., 2002; Thomson et al., 2002; Weinberg and Bell, 1986; Williams and Wick, 2004). The tubular bioreactors are fed with fresh medium, which diffuses to the tubular shaped scaffold, and it is consumed by the immobilized cells. They are composed also of an oxygenator, a pump and a medium culture reservoir (Bilodeau and Mantovanni, 2006). Pulsatile radial stress has been applied in order to improve collagen composition and promote mechanical properties (Hoerstrup, et al., 2001; Kim et al., 1999; Niklason, 1999; O'Callaghan and Williams, 2000; Seliktar et al., 2003). Bioreactor design for artificial arteries is still at an early stage of development and, up to now, the engineered arteries do not possess the physiological functions of the native arteries. In future, a better understanding of the physiological environment of the cells will help to design bioreactors capable of producing engineered artery substitutes.

1.6.4.4 Rotating wall vessel reactor

The rotating wall vessel (RWV) reactor, also referred to as the slow turning lateral vessel (STLV) reactor, is a cylindrical vessel that maintains cells in suspension by slow rotation about its horizontal axis with a coaxial tubular silicon membrane for oxygenation. It was designed initially at NASA's John Space Centre to simulate the effects of microgravity on cells in a ground-based system and protect tissue culture during space flight (Barron et al., 2003; Navran, 2006). To date, it has been used both for Earth-based and space experiments focusing on the construction of engineered bone, cardiac and cartilage tissue as well as on cell biology research including work with adult stem cells, cancer cells and haematopoietic cells (Martin and Vermente, 2006, Navran, 2006).

An updated version of the STLV is the high aspect ratio vessel (HARV). Its design is similar to the design of the STLV but it permits lower speeds to keep

the constructs stationary. Additionally, the oxygenation has been enhanced by the presence of a gas exchange membrane at its base. The area for exchange is more than twice as large as the area of the STRV (Martin and Vermente, 2005). The SLTV and HARV reactors are commercialized by Synthecon Inc. (Synthecon Inc., Houston, USA).

A perfusion-based version of rotating wall vessel reactor is also commercially available from Synthecon Inc. In this version the culture medium is added continually to and removed from the reactor. Additionally, two of these chambers have been linked together sharing the same nutrient loop (Eisenstein, 2006). This gives the capability for coculture experiments in which growth factors and other molecules can be secreted in the first chamber and they can be taken up to the second chamber as in a helper-cell or feeder-cell format (Eisenstein, 2006).

The procedure to build 3D constructs with immobilized cells in the rotating wall vessel reactor starts with the inoculation of cells on microcarriers. When 100 to 200 cells are formed on each of microcarrier, they attach to form larger tissue assemblages under a mechanism which has not been established yet. Cartilage cell assemblages have reached 5 mm in diameter whereas human liver cell ones have reached 3 mm in diameter. Scaffolds instead of beads have also been used to generate engineered tissues (Martin and Vermente, 2005).

The RWV reactor offers a solid body rotation so when the vessel is rotating the culture media rotates at the same angular velocity as the vessel wall with laminar fluid flow. Gravitational, centrifugal and Coriolis forces (force which causes deflection of objects from a straight path if the objects are viewed from a rotating frame of reference) are applied to the culture medium and result in a slow sedimentation of cells as the vessel turns, minimizing damaging shear forces and allowing cells to form 3D tissue-like assemblages. This gentle mixing of media is induced also by particle sedimentation. Unlike roller bottles, the vessel chamber is completely filled with culture media, avoiding the turbulence created by a headspace. Oxygenation via a coaxial silicone membrane prohibits bubble formation and consequently creation of cell-damaging turbulence (Navran, 2006).

The orbit of the assemblages orbit depends on the vessel dimensions, fluid rotational rate, external gravitational fields, particle sedimentation rate, viscosity and density of the culture medium. The rotation is slower in space than in Earth because it has only to enhance the mass transfer of nutrients to the cells. For example for a 2 mm cancer-cell assemblage the Reynolds number in Earth and space was 86 and 0.19 respectively whereas the shear stress was 0.11 Pa and $0.2x10^{-3}$ Pa respectively (Martin and Vermente, 2005).

The size of the assemblages may change during the culture due to cell proliferation and / or recruitment of additional cells into an assemblage, causing an increase in sedimentation velocity by the square of the radius. To counteract the increase in sedimentation velocity, the speed of rotation should be increased to prevent the assemblages from hitting the vessel wall. At some point their size may become so large that it is impossible to maintain them in suspension without striking the vessel wall. Even with this limitation, tissue-like assemblages approaching 10 mm are possible (Goodwin and Parker, 2006).

1.7 Organisation of thesis

The preceding sections have provided a description of tissue engineering efforts to date and the challenges involved in the design and operation of bioreactors to generate these tissues. The importance of being able to predict the supply of nutrients and removal of metabolites has been highlighted. Hence the aims of the thesis were (a) to develop models of transport phenomena in order to predict the fluid flow and mass transfer requirements of a prototype bioreactor for the formation of engineered tissues and and (b) to design micro scale experiments in order to evaluate from measurements, effective diffusivities of substrates and metabolites in alginate matrices as well as substrate consumption and metabolite production rates in matrices with immobilized cells. The advantage of such micro scale experiments was that greater data sets could be generated with the small number of cells available but in a way which predicts the larger scale.

The layout of the thesis is as follows. Chapter 2 presents the materials and methods which were used for the development of the mathematical models and the conduction of micro scale experiments. Chapter 3 presents the use of windows of operation to predict the fluid flow and oxygen mass transfer requirements of a prototype bioreactor for the production of artificial tissues. Chapter 4 presents a theoretical analysis to predict substrate and metabolite concentration profiles and cell proliferation in the artificial artery as an effect of feed and recycle rate. Chapters 5 and 6 describe the design of scale-down experiments in order to measure indirectly the oxygen, glucose and lactate effective diffusivity in an alginate gel / cell mix and the oxygen uptake rate, glucose consumption rate and lactate production rate of human adult cells. Chapter 7 outlines the final conclusions and suggests directions for future work.

Chapter 2

Materials and methods

2.1 Protocols for fibroblast cell culture

2.1.1 Creation of frozen cell bank

Normal human dermal fibroblasts under passage 11 (Karocell Tissue Engineering AB, Sweden) were kindly provided by Dr. S. Minger (Kings University, London UK). A vial was thawed in a tissue culture flask with 75 cm^2 surface area (T-75, Corning, Fisher Scientific, Loughborough UK) containing 20 mL Iscove's modified Dulbecco's medium (IMDM) supplemented with 4 mM glutamine, 25 mM HEPES, 10 % heat inactivated foetal bovine serum (all from Invitrogen, Paisley UK) and 100 U mL^{-1} penicillin/streptomycin (BioWhittaker, Walkersville, MD) and in a humidified 37°C, 5% CO_2 environment (Heraeus, HERAcell 150, Jencons-PLS, East Sussex, UK). Upon 80% confluency, the cells were passaged into one T-150 flask. They were then expanded as above using one to three flasks progression till obtaining nine T-150 confluent flasks. Following trypsinization and cell counting in the Guava cytometer (Guava Technologies, Hayward, California USA) the cells were centrifuged and resuspended in cryopreserved medium to yield a cell suspension with a cell density of 10^6 cells mL^{-1}. The cryopreserved medium was 95% complete medium with the same formulation used in the cell passaging and 5% DMSO (Sigma, Gilligham UK). Upon addition of around 1 mL of cell suspension into cryovials (Nalgene, Nalge Nunc International, Rochester, New York USA) the cells were frozen slowly in an insulated Styrofoam box in a -80°C freezer overnight and were transferred to liquid nitrogen for long term storage.

2.1.2 Cell passaging in tissue flasks

The fibroblasts were thawed and cultured in cell tissue culture flasks with a surface area of 150 cm^2 (T-150, Corning, Fisher Scientific, Loughborough UK) in a humidified 37°C, 5% CO_2 environment. The culture medium was Iscove's modified Dulbecco's medium (IMDM) supplemented with 4 mM glutamine, 25 mM HEPES ,10% heat inactivated foetal bovine serum (all from Invitrogen, Paisley UK) and 10 U mL^{-1} penicillin/streptomycin (BioWhittaker, Walkersville, Maryland USA). From here on this is denoted as the "complete medium".

The fibroblasts were passaged every two days (at 70-80% confluence) at one T-150 flask to three new T-150 flasks split using 0.25% trypsin / 0.02% EDTA (Sigma, Gilligham UK) for their detachment. Analytically, the spent medium was removed and 15 mL free of calcium and magnesium phosphate buffered saline solution (PBS, BioWhittaker, Walkersville, Maryland USA) were added to remove residual serum proteins which are otherwise decreasing trypsin activity. The PBS was removed and 5 mL of 0.25% trypsin / 0.02% EDTA solution were added. After 300 s, the cells were dislodged by tapping the flask against the palm of the hand and 10 mL of complete medium was added to deactivate the trypsin. This is necessary because eventually the trypsin will diffuse through the cell membrane initiating apoptosis. A sample was withdrawn for cell counting in a Guava Easy-Cyte cytometer (Guava Technilogies, Hayward, California USA) and then 5 mL of cell suspension were added in each T-150 flask which had previously been supplemented with 25 mL of complete medium. The flasks were placed in the incubator and the cultures were monitored for cell morphology characteristics like confluency, changes in the colour of medium as an indication of pH change and amount of cell debris.

2.2 Fibroblast-alginate construct

2.2.1 Fibroblast suspension and alginate mixture preparation

Sterile sodium alginate Pronova SLG-100 (FMC Biopolymer AS, Drammen Norway) with the molecular weight in the range of 20-30x10^3 Da, the guluronic to mannuronic acid ratio above 60% and the apparent viscosity at 25°C of the 1% (w/v) aqueous solution above 100 mPa s was used for all the experiments. Calcium-free Dulbecco's Modified Eagle's medium DMEM supplemented with L-glutamine and 10% heat inactivated foetal bovine serum (all from Invitrogen, Paisley UK) was used to dissolve the alginate and obtain a 2% (w/v) solution after mixing overnight at room temperature on a platform roller (Roller Mixer SRT2, Bibby Stuart Scientific, Stone UK). The 2% (w/v) alginate solution was mixed with the cell suspension at equal volume to yield a cell - alginate mixture with an alginate concentration of 1% (w/v).

Upon reaching 80% confluency the fibroblasts were detached from the surface of T-flasks (Corning, Fisher Scientific, Loughborough UK) using 0.25% trypsin / 0.02% EDTA solution (Sigma, Gilligham UK). A sample was withdrawn for cell counting using a Guava cytometer. The cell suspension was centrifuged (5810R Centrifuge, Eppendorf AG, Hamburg Germany) in 50 mL centrifuge tubes at 200 g at low deceleration for 300 s. The supernatant was removed and discarded and the cell pellet was resuspended in calcium free Dulbeccos's Modified Eagle's medium DMEM supplemented with L-glutamine and 10% heat inactivated foetal bovine serum (all from Invitrogen, Paisley UK) in order to dilute the residual EDTA. The second resuspension is necessary because EDTA binds Ca^{2+} therefore it would inhibit the formation of the alginate construct. The cells were centrifuged again and resuspended in medium with the previous composition. The cell density in the cell suspension was double the desired one in the alginate-cell mixture as it was mixed later on with an equal volume of alginate solution.

2.2.2 Set up of alginate in cell culture inserts and customized microplates

Falcon cell culture inserts (BD Labware, Frankin Lakes USA) were used in order to create alginate-cell construct at their bottom. The volume of the alginate-cell mixture in each one was 0.15 mL. The inserts incorporate a non tissue culture treated polyethylene terephthalate (PET) track-etched membrane with a pore size of 3 μm and a pore density $8x10^5$ pores cm^{-2}. This pore size does not allow the passage of cells through the membrane so substrates and metabolites are consumed and produced only within the alginate construct. Additionally, the "non tissue culture" membrane inhibits the cell attachment which can otherwise slow down the mass transfer of nutrients and metabolites. The inserts were placed in 12-well Falcon companion plates (BD Labware, Frankin Lakes USA) and immersed in 1.25 mL Iscove's modified Dulbecco's complete medium (IMDM) supplemented with 1% (w/v) cell culture tested $CaCl_2$ solution (Sigma, Gilligham UK) and the plates were placed in the incubator (5% CO_2, 37° C). After 1.0 h, the supplemented with $CaCl_2$ culture medium was discarded and replaced with complete IMDM medium. Its amount in each insert was 0.75 mL and in the well 2.3 mL. Additionally, the inserts were tilted while they were lowering into the well in order to avoid trapping air under them. Trapped air can delay the mass transfer of substrates and metabolites through the membrane and affect the calculations of any consumption / production rates and diffusivities. In order to improve nutrient delivery, oxygen transfer and waste removal from the alginate construct the companion plate was shaken at 220 rpm in an orbital shaker (IKA KS260, Camlab, Cambridge UK). At the end of the experiment, photos of the companion plate and the Falcon cell culture inserts were taken under the microscope to verify the non attachment of cells at their bottom.

Low volume, non tissue culture treated microwells (Luxcel Biosciences, Cork Ireland) were cut into individual wells and were glued to the bottom of the wells of ultra low attachment 24-well plates (Corning Life Sciences, New York USA). Then, oxygen or pH sensor spots (Presens, Regensburg Germany) were glued

(Nusil, Polymer Systems, Ltd., Buckinghamshire UK) at the bottom of each of the low volume wells (Figure 2.1). The sterilization of the customized plates was conducted by gamma irradiation (Isotron, Swindon UK). The selection of this type was based on the surface coating used which inhibits the attachment of any cells released from the alginate construct. Additionally, the spots are highly hydrophilic thus they do not support cell attachment on their surface. Following sensor spot calibration, an alginate-cell mixture was slowly syringed through a sterile 0.1 mm diameter blunt needle and dripped into the low volume well. Individual millicell (Millipore, Bedford UK) with a polycarbonate membrane with a pore size of 3 μm and a pore density of $8x10^6$ pores cm^{-2} were filled with complete IMDM medium supplemented with 1% (w/v) $CaCl_2$ solution and were placed on top of the low volume wells in each of the wells of the customized 24 well plate. The plate was transferred to the incubator and the $CaCl_2$ started diffusing through the polycarbonate membrane of the millicell, reacting with the alginate and forming the alginate gel. After an hour the transwells were removed and 1 mL of complete medium was added to the wells after having washed them twice with it in order to remove residual $CaCl_2$. The plate was placed in the incubator again where oxygen and pH measurements were carried out by using the oxygen and pH meter devices (Presens, Regensburg Germany). At the end of all the experiments, the sensor spots were exposed to the calibration standards solutions to check their performance. Additionally, photos of the customized plate were taken under the microscope to check in case any cells had attached to the well bottom.

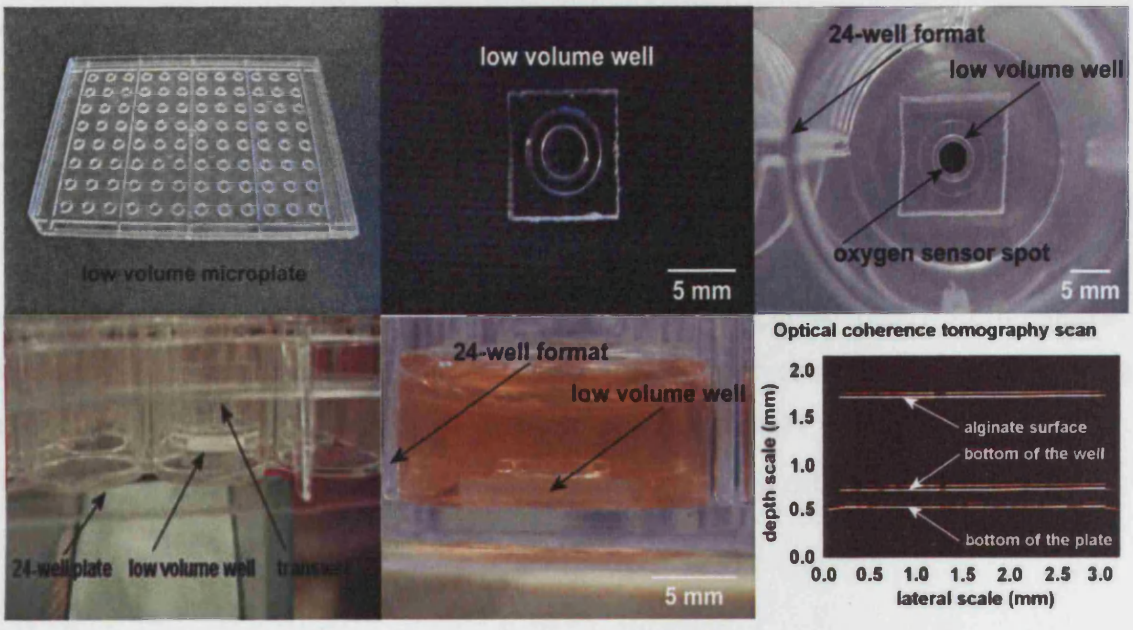

Figure 2.1: Construction of a customized plate. Low volume non tissue culture treated microwells (Luxcel Biosciences, Cork Ireland) were cut into individual wells and were glued to the bottom of the wells of ultra low attachment 24 well plates (Corning Life Sciences, New York USA). Then, either oxygen or pH sensor sports (Presens, Regensburg Germany) were glued at the bottom of each of the low volume wells. The sterilization of the customized plates was conducted by gamma irradiation (Isotron, Swindon UK). After the addition of cell / alginate solution to the low volume well, a millicell (Millipore, Bedford UK) filled with 1 % (w/v) $CaCl_2$ (Sigma, Gilligham UK) will be placed on the top of it for an hour. The $CaCl_2$ will diffuse through the millicell's membrane and cause the alginate to gel. Optical coherence tomography was used to validate the flatness of the alginate surface. It was conducted at Professor Ruikang Wang's Lab at Cranfield University, UK.

2.3 Fibroblast / alginate evaluation

2.3.1 Fibroblast recovery from alginate constructs

The fibroblasts were recovered by dissolution of the alginate constructs in a solution of 0.3 M trisodium citrate in trypsin / EDTA (both from Sigma, Gillingham UK). Trisodium citrate plays the role of chelator of calcium ions dissociating them from the alginate hydrogel (Lee, 1991; Smidsrcd and Skj&k-Braek, 1990). The trypsin / EDTA solution was used in order to achieve a single cell suspension.

The dissolution of the alginate constructs formed in cell culture inserts was conducted by placing the insert in 15 mL of the above solution in 50 mL centrifuge tubes (Corning, Fisher Scientific, Loughborough UK). Then, the tubes were placed in a roller (Roller Mixer SRT2, Bibby Stuart Scientific, Stone UK) for 10 min.

The dissolution of the alginate constructs formed in customized microplates was conducted by replacing the culture medium with 1 mL of 0.3 M trisodium citrate in trypsin / EDTA. The plate was placed in an orbital shaker (IKA KS260, Camlab, Cambridge UK) for 10 min. In both cases the recovery of the fibroblasts in a single cell suspension was verified by phase contrast microscopy.

2.3.2. Flow cytometric methods

2.3.2.1 Guava Easy-Cyte cytometer

A Guava EasyCyte cytometer (Guava Technologies, Hayward, California USA) was used for cell enumeration, cell cycle analysis and recognition of Ki-67 expression. It is an automated desktop single-cell analysis system which accommodates both a 96-well plate and microcentrifuge tubes. The system

uses a flow cell with an inner diameter of 100 µm. It is made of fused silica with a polyimide coating that requires no alignment following replacement. There is a high-pressure purge of the flow cell available for removing obstructions in the flow cell and the sample is aspirated through the flow cell using a high precision microsyringe. Sheath fluid is not required for operation. The particles are excited by light from a suitable light source such as a diode laser (488 nm) and scattered light is detected providing an absolute count of all particles passing through. Three fluorescence detectors / photomultipliers with 583 ± 26 nm (PM1), 680 ± 30 nm (PM2), and 525 ± 30 nm (PM3) filters are used. The instrument requires as little as 20 µL of neat sample and as few as 1000-2000 total cells to perform an analysis and works with both adherent and non-adherent cells. However, accurate results are only obtained for a cell size between 7 to 60 µm (Goix, 2004).

2.3.2.2 Cell enumeration

The Guava ViaCount assay distinguishes between viable and non-viable cells based on the differential permeability of two DNA-binding dyes in the ViaCount Reagent; the laser dye styril (LDS) and the propidium iodide (PI) dye. The LDS (Exciton Laboratories, USA) is membrane permeable, stains all nucleated cells and its fluorescent signal is detected by the PM2. The PI dye (Sigma, USA) will only penetrate cells with compromised membrane integrity (non-viable cells) and is detected by the PM1. Events are counted if they emit nucleated cell fluorescent signal and if the forward light scatter (FSC) intensity is appropriate to a particle of the size of a cell (Figure 2.2) (Phi-Wilson et al, 2002).

Cell suspension, 196 µL, with a cell concentration in the range of 0.01 to 0.50 $x10^6$ cells mL^{-1} was added in each wells of a 96 well plate. Viacount dye, 4 µL, was added in each well and the sample was mixed by pipeting repeatedly. The 96-well plate was incubated at room temperature for 15 min in the dark to allow dye to equilibrate. The data acquisition was achieved by using the Express Plus application software within Cytosoft. Cell samples were assayed for cell count and viability.

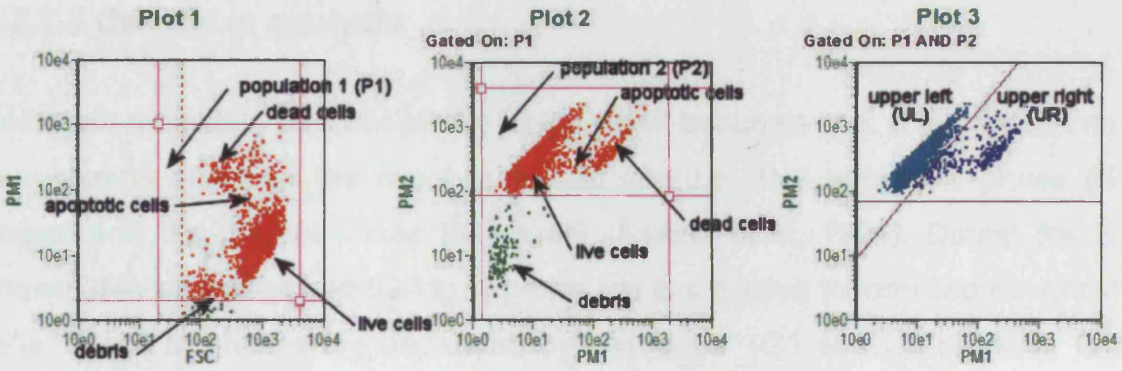

Analysis Results Plot 3 - DotPlot: PM1 vs PM2

	Count	Cells /mL	% of Gated	x-Mean	y-Mean
LL	0	0.00e00	0.00%	0.00	0.00
LR	0	0.00e00	0.00%	0.00	0.00
UL	2624	1.24e05	90.83%	11.60	342.32
UR	265	1.25e04	9.17%	150.11	417.54
Gated by P1 & P2	2889		95.50% (% of All Events)		

Figure 2.2: Typical results obtained using the Guava EasyCyte cytometer for cell concentration and cell viability determination. The results are presented in three plots. Plot 1 shows the fluorescent signal which is detected by the photomultiplier 1 (PM1) versus the forward side scatter signal (FSC). The PM1 detects PI which penetrates cells with compromised membrane integrity (non-viable cells) and the FSC is related with the size of the particle with a low intensity signal to correspond to low size particles. Plot 2 shows the fluorescent signal which is detected by the PM2 versus the one which is detected by the PM1. The PM2 detects the LDS which stains all nucleated cells. Plot 3 uses Plot 1 to help define different cell type in Plot 2 and help create two quadrants, UL and UR which are containing the live cell (UL) and the apoptotic and dead cell population (UR). The table gives the cell count and cell concentration for each of these regions.

2.3.2.3 Cell cycle analysis

Cell cycle describes the process by which a cell becomes two. It is divided into four phases of which the two basic ones are the DNA synthesis phase (S phase) and the mitosis phase (M phase) (Alberts et al, 1994). During the S phase DNA replicates and during M phase the cell divides to form two daughter cells. S and M phases are separated by two "gaps" (G1 and G2 phases). G1 phase controls entry into the S phase by checking if the cell is large enough, DNA is undamaged and if external conditions are favourable. G2 phase controls entry into the M phase. It checks if DNA has been replicated without damage and if the cell is big enough to divide into daughter cells (Alberts et al, 1994). Cells in a quiescent state are out of the cell cycle and they are in the so-called G0 phase. They can remain there for days, weeks or even years. (Alberts et al, 1994)

By using PI the nuclear DNA can be stained and cells can be discriminated at different stages of cell cycle. Cells at G0 / G1 phase contain two copies of each chromosome. They start synthesizing DNA by entering the S phase. As a result the PI fluorescence intensity is increasing till it reaches twice the intensity of the G0 / G1 population. At this point cells have entered the G2 / M phase and eventually they will divide into two cells.

PI staining requires cell fixation in order to make the cells permeable to the dye. Analytically, 200 µL of cell sample with an adjusted concentration between 0.5 to $1x10^6$ cells mL^{-1} were transferred to a round bottom 96 well plate. The plate was centrifuged twice at 450 g for 300 s with the brake on low at room temperature. After the first centrifugation the supernatant was replaced with 200 µL of phosphate buffer saline (Sigma, UK) and after the second one with 200 µL of 70% ice cold ethanol which was added dropwise. The plate was sealed and refrigerated for 12 h. Following cell fixation the plate was centrifuged twice under the same conditions as above. After the first centrifugation the supernatant was replaced with 200 µL PBS and after the second one with 200 µL cell cycle reagent (Guava Technologies, Hayward, California USA). The plate was incubated at room temperature in the dark for 0.5 h and it was then

located in the Guava EasyCyte cytometer. The data acquisition was achieved by using the Express Plus application software within Cytosoft. The file was exported to Modfit 3.1 software (Verity Software House, Topsham USA) for gating and deconvolution of the curves (Figure 2.3).

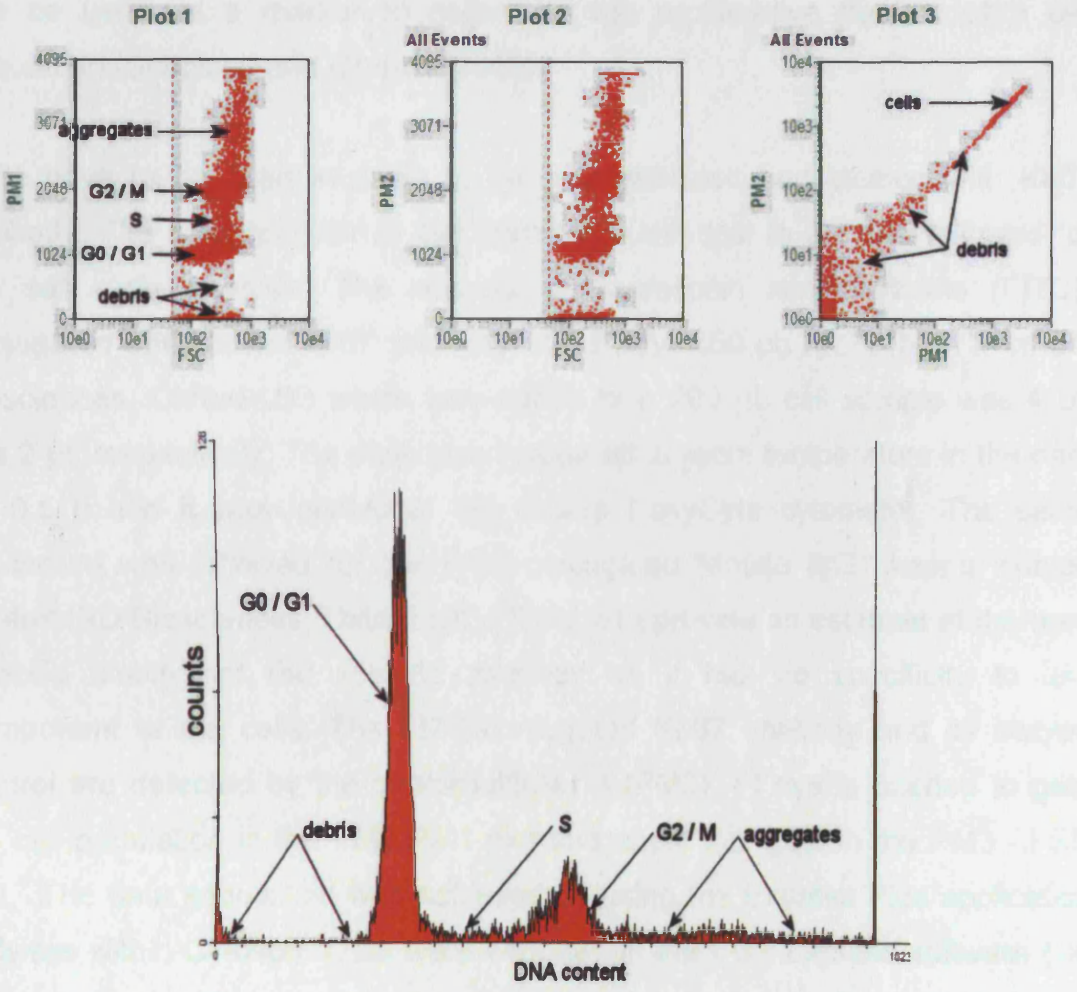

Figure 2.3: Typical results from cell cycle analysis using the Guava EasyCyte cytometer. The cells are fixed, permealized and stained with the Guava cell cycle reagent. Following incubation in the dark at room temperature for 0.5 h, cell cycle data are acquired in the Guava Express software within Cytosoft and are exported as a single parameter FCS 2.0 file to Modfit 3.1 software (Verity Software House, Topsham USA) for gating and deconvolution of the curves.

2.3.2.4 Ki-67 expression as a cell proliferation marker

The Ki-67 antigen can be detected within the nucleus of cells. Detailed analysis has revealed that it was presented in all the phases of the cell cycle but absent from resting cells in the G0 phase (Scholzen and Gerdes, 2000). Therefore, it can be used as a marker to determine the proliferative fraction of a cell population (Scholzen and Gerdes, 2000).

Cells have to be fixed in order to be permeabilized and stained with Ki-67 antibody. The protocol prior to cell staining is identical to the one followed for the cell cycle analysis. The amount of fluorescein isothiocyanate (FITC)-conjugated anti-human Ki-67 antibody and PI dye (50 μg mL^{-1}) (both from BD Biosciences, Oxford UK) which was added to a 200 μL cell sample was 4 μL and 2 μL respectively. The plate was incubated at room temperature in the dark for 0.5 h and it was located in the Guava EasyCyte cytometer. The same procedure was followed for the FITC-conjugated Mouse IgG1 kappa isotype control (BD Biosciences, Oxford UK). This is to provide an estimate of the non-specific binding of the specific antibody as it has no specificity to any component of the cells. The FITC-conjugated Ki-67 antibody and its isotype control are detected by the photomultiplier 3 (PM3). PI dye is needed to gate the cell population in the PM2-PM1 plot and apply that gate in the PM3 - FSC plot. The data acquisition was achieved by using the Express Plus application software within Cytosoft. Data were exported in the FCS Express software (De Novo Software, Ontario Canada). Samples were assayed for percentage of cells expressing Ki-67 (Ki-67 positive cells) (Figure 2.4).

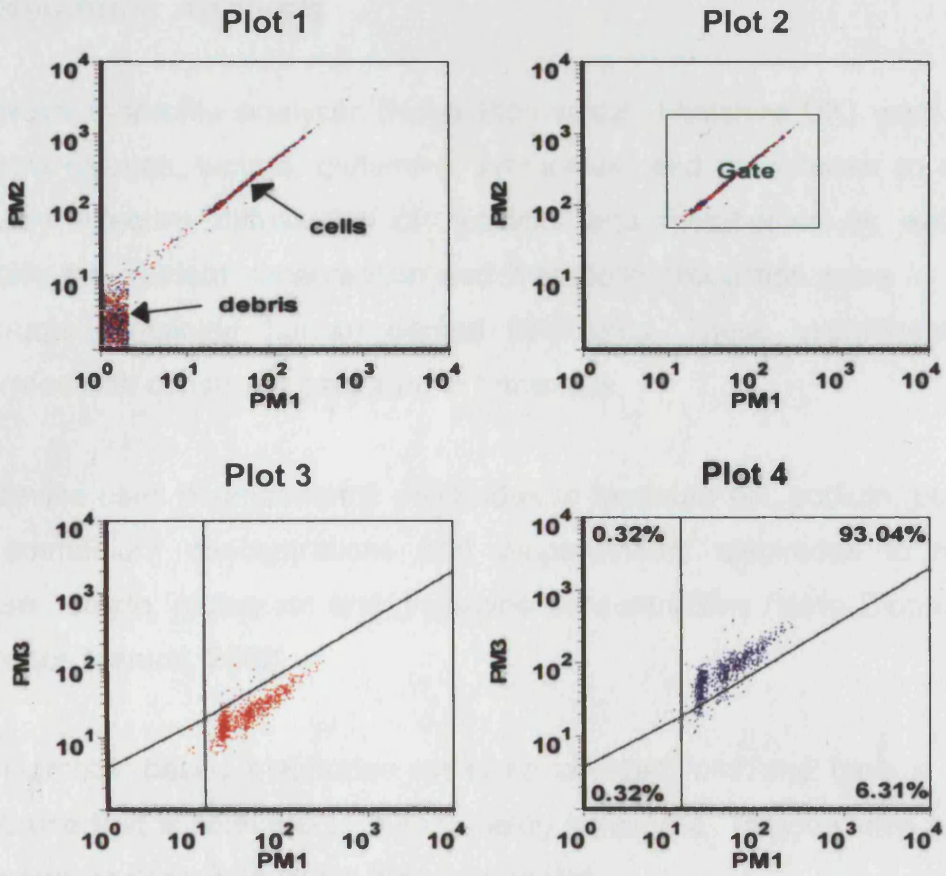

Figure 2.4: Typical results from Ki-67 expression analysis using the Guava EasyCyte cytometer. The cells are fixed, permeabilized and stained with FITC-conjugated Ki-67 antibody and PI dye. FITC-conjugated IgG1 kappa antibody is used as an isotype control. Cells are incubated in the dark at room temperature for 0.5 h. Data derived from staining with Ki-67 and IgG1 (isotype control) antibodies are acquired in the Guava Express software within Cytosoft and exported to FCS Express software (De Novo Software, Ontario Canada). FCS Express has been chosen because it offers the capability to overlay data derived from Ki-67 antibody staining with data derived from isotype control antibody staining. Plots 1 and 2 contain overlaid events from PI staining derived from the cell sample stained with Ki-67 antibody and from the one stained with its isotype control. The cell population is gated and that gate is applied in Plot 3 and Plot 4 which contain events derived from isotype control and Ki-67 staining respectively. The quadrants in Plot 3 are applied in Plot 4 and events within the upper left quadrant are corresponding to Ki-67 positive cells.

2.4 Metabolic Analysis

The Nova Bioprofile analyser (Nova Biomedical, Flintshire UK) was used to measure glucose, lactate, glutamine, ammonium and pH in order to evaluate indirectly effective diffusivities of nutrients and metabolites as well as to evaluate the nutrient consumption and metabolic production rates in alginate constructs containing human dermal fibroblasts. These experiments were performed with constructs prepared in transwells.

The device uses potentiometric electrodes to measure pH, sodium, potassium and ammonium concentrations and amperometric electrodes to measure glucose, lactate, glutamate and glutamine concentrations (Nova Bioprofile 400 Reference Manual, 2002).

Potentiometric-based electrodes measure charged ions and have a sensing membrane that is selective to the ion being measured. They develop a voltage which can be described by the Nernst equation:

$$E_m = E_0 + 2.303\frac{RT}{nF}\log_{10} a_i \tag{2.1}$$

where E_m is the membrane potential, a_i is the activity of the ion, R is the universal gas constant, T is the temperature, F is the Faraday's constant and n is the charge of the measured ion.

The potential of the sample is compared against the potential of a standard solution and their difference is dependent on the ratio of the activity of the ion of interest in the sample and the activity of the ion of interest in the standard solution. This statement is expressed mathematically by the following equation (Nova Bioprofile 400 Reference Manual, 2002)

$$\Delta E = E_x - E_{std} = S\log_{10}\frac{a_x}{a_{std}} \tag{2.2}$$

where S is the electrode slope (30.8 mV per decade change in activity for a divalent ion and 61.6 mV for a univalent ion), E_x and a_x are the potential and activity of the measured ion in the sample, E_{std} and a_{std} the potential and activity of the measured ion in the standard solution.

The activity of an ion is the product of its concentration and ionic coefficient. The latter relates concentration and activity and is a function of the ionic strength of the solution. The standard solution has been formulated to reflect the same ionic strength as that of serum and therefore the difference in potential between the sample and the standard solution is only dependent on the concentration (Nova Bioprofile 400 Reference Manual, 2002). It can be expressed mathematically as follows:

$$\Delta E = S\log_{10}\frac{c_x}{c_{std}} \tag{2.3}$$

$$c_x = c_{std}10^{\Delta E/S} \tag{2.4}$$

where c_x is the concentration of the ion of interest.

Amperometric electrodes consist of a membrane with immobilized enzymes and a platinum electrode. The substrate or metabolite diffuses through the membrane and is oxidised. Consequently, the hydrogen peroxide produced is oxidized at the platinum electrode producing electrons. The current generated by the flow of electrons is proportional to the concentration of the substrate or metabolite (Nova Bioprofile 400 Reference Manual, 2002).

The relevant chemical equations are the following

for glucose

$$\beta\text{-D-glucose} + H_2O \xrightarrow[oxidase]{glucose} gluconic\ acid + H_2O_2$$

$$H_2O_2 \xrightarrow{-2e^-} O_2 + 2H^+$$

for lactate

$$lactate + H_2O \xrightarrow[oxidase]{lactate} pyruvate\ acid + H_2O_2$$

$$H_2O_2 \xrightarrow{-2e^-} O_2 + 2H^+$$

for glutamine and glutamate

$$glutamine + H_2O \xrightarrow{glutaminase} glutamate + NH_3$$

$$glutamate + O_2 \xrightarrow[oxidase]{glutamate} ketoglutarate + NH_3 + H_2O_2$$

$$H_2O_2 \xrightarrow{-2e^-} O_2 + 2H^+$$

2.5 Oxygen and pH measurements

The Presens 4-channel fiber-optic oxygen and pH meters (Presens GmbH, Regensburg, Germany) based on 2 mm spots (polyester base) were used to acquire oxygen concentration and pH measurements on-line. The spots were glued at the bottom of customized wells and measurements were acquired non-invasively and non-destructively from outside through the bottom of the customized microplate.

Oxygen is measured in the range of 0 to 250% of air saturation and pH in the range of 5.5 to 9. The accuracy and the resolution of the oxygen measurements depend on its level. Specifically, at 1% oxygen of air saturation (20°C) the accuracy and resolution of the measurements are 0.15% and 0.05% of air saturation respectively, whereas at 250% oxygen of air saturation (same temperature) are 0.5% and 1% of air saturation respectively. Similarly, the pH can be measured in the range of 5 to 9 (20°C) with an accuracy of 0.05 pH units and a resolution of 0.005 pH units. The drift of the sensor spots is 0.5% oxygen of air saturation per 100000 measurements and 0.1 pH units per 5000 measurements. The response time (90% of the signal change) for gaseous and dissolved oxygen (non-stirred solution) is 10 and 40 s respectively while the response time for pH is 30 s. A two-point calibration in oxygen free water and humidified air or air-saturated water is followed for the oxygen sensor and a calibration based on a series of buffer solutions for the pH sensor (Presens Fibox-3 Instruction Manual, 2004).

The principle of measurement is based on the effect of dynamic luminescence quenching which is caused by collision between molecular oxygen / protons and luminescent dye molecules in the excited state. After collision, energy transfer takes place from the excited indicator molecule to the quencher. As a result, the indicator molecule does not emit luminescence and the measurable luminescence signal decreases (Presens Fibox-3 Instruction Manual, 2004).

Both the devices use the phase-modulation technique to evaluate the luminescence decay time of the indicators. If the luminophore is excited with a

sinusoidally intensity modulated light, its decay time causes a time delay in the emitted light signal. In technical terms, this delay is the phase angle between the exciting and the emitted signal. The relation between decay time τ and the phase angle Φ is shown by the following equation (Presens Fibox-3 Instruction Manual, 2004)

$$\tau = \frac{tan\Phi}{2\pi f_{mod}} \tag{2.5}$$

where f_{mod} is the modulation frequency.

The phase-modulation technique is used because the decay time does not depend on the intensity of the light source, the sensitivity of the detector or the concentration of the dye. Additionally, it is not influenced by the shape and size of the sensor spot or by variations in the optical properties of the sample including turbidity, refractive index and coloration (Presens Fibox-3 Instruction Manual, 2004).

The dual luminophore reference method (DLR) is used exceptionally to measure pH because the decay time of the pH-indicator dyes is in the nanosecond time scale. A direct measurement in this time scale requires expensive and sophisticated instrumentation. Instead, the DLR method uses the measurement of average decay times. Analytically, the pH sensor consists of an indicator with short decay time (ns time scale) and a reference dye with long decay time (µs time scale). Ideally, the two luminophores have overlapping excitation and emission spectra. The reference luminophore gives a constant background signal while the fluorescence signal of the indicator depends on the proton concentration. The average phase shift directly reflects the intensity of the indicator dye and, consequently, the proton concentration (Presens pH-1 mini Instruction Manual, 2004).

The relation between the oxygen concentration in the sample and the luminescence intensity as well as the luminescence decay time is described by the Stern-Volmer equation (Presens Fibox-3 Instruction Manual, 2004).

$$\frac{I_0}{I} = \frac{\tau_0}{\tau} = 1 + K_{SV}[O_2] \tag{2.6}$$

where τ_0 and τ are the luminescence decay times in absence and presence of oxygen, I_0 and I are the respective luminescence intensities in absence and presence of oxygen, $[O_2]$ the oxygen concentration and K_{SV} the overall quenching constant.

The Boltzman equation describes the relationship between pH and phase angle because of the sigmoidal shape of the pH calibration curve (Presens pH-1 mini Instruction Manual, 2004).

$$\Phi = \frac{\Phi_{min} - \Phi_{max}}{1 + e^{\frac{(pH - pH_0)}{dpH}}} + \Phi_{max} \qquad (2.7)$$

where Φ_{min}, Φ_{max} *are the* minimum and maximum phase angle, pH_0 defines the pH where the phase angle is equal to the average of the two limiting phase angles ($\Phi=(\Phi_{min} + \Phi_{max})/2$) and dpH is the width of the pH range which the phase angle changes significantly.

2.6 The finite element method

The mathematical formulation of the whole class of transport phenomena due to conservation of mass, momentum species and energy leads to partial differential equations in the continuum approximation (Zimmerman, 2006). Their solution by exact methods of analysis is often impossible either because of complex geometry and material properties or because of the complicated functions involved. In such cases approximate methods of analysis are used.

The finite element method is a technique where a given domain is divided into subdomains. Each subdomain is called an element and their union gives the so called finite element mesh. When all elements are of the same length the mesh is characterized as uniform; otherwise it is called a non-uniform mesh. The points where the elements are connected to each other are called nodes. This subdivision allows the accurate representation of complex geometries and inclusion of materials with anisotropic properties as well as accurate approximation of local large gradients in the solution (Reddy, 2003).

The functions which approximate the solution are developed over each of the elements. They are usually based on the idea that any continuous function can be represented by a linear combination of suitable algebraic polynomials and undetermined coefficients. The latter are obtained by satisfying the governing equations in a weighted-integral sense over each element with the nodes to play the role of interpolation points. This is needed in order to obtain as many algebraic equations as there are unknown coefficients in the approximation of the dependent functions of the equation (Reddy, 2003).

The dimensionality of the elements depends on the dimensionality of the problem to be solved. In one-dimensional problems the element is a line segment. In two-dimensional problems the fundamental element is a triangle and in three-dimensional problems the fundamental element is a tetrahedron. Additionally, the elements are categorized according to the type of interpolation functions used with them. The elements are called simplex if the interpolation polynomials have linear parts and complex if the interpolation polynomials have high-order polynomial parts (Zimmerman, 2006).

There are three sources of error in a finite element method. They are those due to the approximation of domain, those due to the approximation of the solution and those due to the numerical computation (numerical integration and round-off errors in a computer). The higher the number of elements the higher will be the accuracy of the solution and the larger will be the computation time. However, above a number of elements the sensitivity of the accuracy becomes negligible. There is no formula which can predict the optimum number of elements (Reddy, 2003). When the solution cannot be verified by comparing the results to values from the literature a convergence test is necessary to determine if the mesh density is sufficient. The approach is to begin with a mesh which is believed to be adequate and solve the problem. Then, a finer mesh is selected and a new solution is obtained. If the difference between the two solutions is significant further mesh refinements are needed till the obtained solution agrees with the previous one to the desired number of significant figures (Comsol Multiphysics manual, 2006; Reddy, 2003; Zimmerman, 2006).

The model is solved using the finite element solver Comsol Multiphysics v.3.3a. Data analysis and visualization can be extended by combining Comsol Multiphysics with technical computing languages like C++ and Matlab (Comsol Multiphysics manual, 2006). The set up of a model in Comsol Multiphysics is shown in the following flowchart:

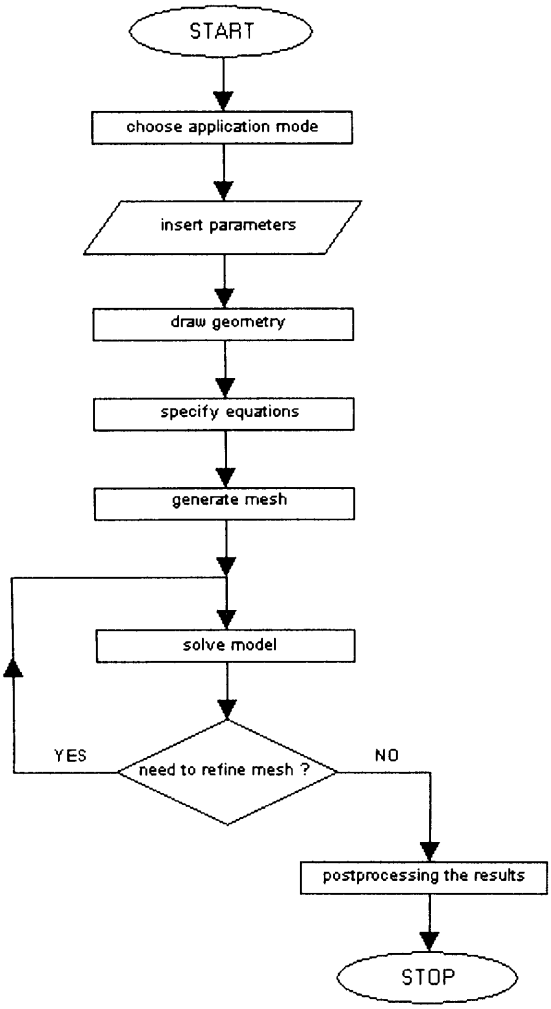

Figure 2.5: Flowchart for the formulation and solution of a model in Comsol Multiphysics. There are 7 steps involved. In the first step the application mode which describes the physics phenomena in a model has to be selected. In the second step the values of the parameters of the model are inserted in the model. In the third and fourth step the geometry is drawn and meshed. In the fifth step the equations are specified in the subdomains and boundaries. In the sixth step the model is solved and if the solution is not satisfactory the mesh is refined and the model is solved again. In the last step the results are exported for processing.

2.7 Inverse method

The inverse method was used to evaluate from measurements the substrate / metabolite effective diffusivities as well as the substrate consumption and metabolite production rates in alginate constructs with immobilized human dermal fibroblasts (Figure 2.6). The measurements have to be sensitive to the parameters of interest in order to achieve the parameters' accurate evaluation.

The inverse method was implemented in Comsol Multiphysics wrapped around Matlab in four steps. In the first one the partial differential equation of the mass transfer of substrates and metabolites in alginate constructs was solved for values of parameters derived from literature. In the second step the Comsol model was saved as a Matlab file. This file was edited as a function having as input the parameters of interest and output the concentrations of nutrients and metabolites. It was referred to as the forward model function. Its role is to help Matlab to recognize which are the parameters of interest of the Comsol model which will be estimated. In the third step the function which gives the sum of the squares of the relative errors between experimental and simulated nutrient / metabolite concentration values at various instants was created having as input the forward model function. The function of the third step was referred to as the error function. In the fourth step the best-fit values of the parameters of interest were estimated by creating a new Matlab file which was based on the non-linear programming Matlab function "lsqnonlin" and was referred to as the optimizer function. This function was minimizing the output of the error function by changing repeatedly the initial estimates of the values of the parameters of interest following the Levenberg-Marquardt algorithm. Additionally, the Matlab statistical toolbox function "nlparci" was used to obtain the parameters' confidence intervals.

In equations with non-linear parts the above algorithm could converge to a local minimum instead of a global minimum. In this case the algorithm will give wrong best-fit values for the parameters of interest. In order to check the accuracy of the results the algorithm was rerun with different initial guesses of the values of the parameters of interest.

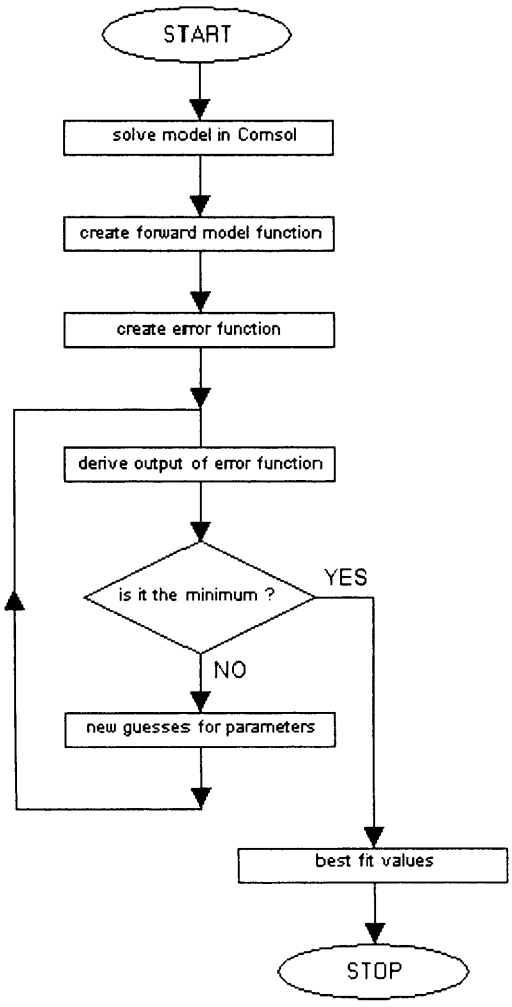

Figure 2.6: Flowchart for evaluating from measurements the glucose and lactate effective diffusivities as well as the glucose consumption and lactate production rates in alginate constructs with immobilized human dermal fibroblasts by using the inverse method implemented in Comsol Multiphysics and Matlab. The algorithm involved four steps. In the first step the model is solved in Comsol Multiphysics. In the second step the forward model function is created and helps Matlab to recognize which are the parameters of interest of the Comsol model which will be estimated. In the third step the error function is created and gives the sum of the squares of the relative errors between experimental and simulated glucose and lactate concentration values at various instants having as input the forward model function. In the last step the optimization function is created and finds the best-fit values for the parameters of interest by minimizing the value of the error function.

2.8 The use of Comsol Multiphysics wrapped around Matlab in the construction of windows of operation

The data needed to construct the windows of operation for the artificial artery reactor were obtained by using Comsol Multiphysics wrapped around Matlab. The procedure involved three steps. Firstly the Comsol Multiphysics model of the artificial artery reactor was created and saved as a Matlab file. In the second step this Matlab file was converted to a Matlab function. Its input was the flowrate in the lumen and its output was the profile of the oxygen concentration at the exit of the artificial artery at its outer wall during cell proliferation. In Matlab this profile is given as a matrix. Every element of this matrix and consequently every oxygen concentration corresponds to a cell concentration at the exit of the artificial artery at its outer wall. In the third step a Matlab program with a double loop structure gave the oxygen concentration at the exit of the artificial artery at its outer wall as a function of the cell concentration there and the flowrate in the lumen.

2.9 Statistical Analysis

One-way analysis of variance (ANOVA) was used for statistical analysis and it was performed with Minitab 13.2 (Minitab Ltd., Coventry, UK). Differences were considered significant when p values were <0.05. All data are presented as means ± standard error.

Chapter 3

Oxygen transfer and metabolism in the artificial artery

3.1 Introduction

The availability of large numbers of engineered tissues would offer significant benefits to the clinical management of surgery. In this scheme, bone marrow stromal cells will be isolated from bone marrow aspirates and seeded onto the polymer scaffold designed to facilitate and direct the growth of a fully functional tissue. During operation, nutrients are fed through the lumen, diffuse though the scaffold and are consumed by the cells; the products of cell respiration / metabolism would diffuse back to the lumen. No generic bioreactor design currently exists. There is a need to establish a robust, automated manufacturing process for the production of engineered tissues.

A critical issue of this tissue engineered construct is the supply of sufficient oxygen. Cells within the scaffold can be supplied with oxygen by diffusion so the oxygen concentration decreases between the lumen and the outer limit of the construct. Within any particular simulation of scaffold preparation it is assumed that the effective oxygen diffusivity in the scaffold remains constant and that the only way to control diffusion is by increasing the convective transport in the lumen.

Models of transport phenomena are developed in order to predict the fluid flow and oxygen mass transfer requirements of a prototype bioreactor for the production of artificial tissues. The use of windows of operation is demonstrated to accommodate design variables.

A "window of operation" can be characterized as an operational space determined by the system and process constraints and correlations governing a particular process or operation under consideration (Woodley and Titchener-Hooker, 1996). Windows of operation enable the engineer to visualize rapidly the variable region in which it is possible to achieve a specific level of

performance and to investigate the effects of altering the key operating variables (Zhou and Titchener-Hooker, 1999).

3.2 Governing equations

A mathematical model was set up to describe oxygen mass transfer phenomena in the tubular reactor. This involved setting up equations to predict mass transfer during cell proliferation. The tubular reactor can be considered as having two key zones; the lumen, where oxygen and nutrients are supplied and the alginate matrix where cell proliferation occurs (Figure 3.1).

The mathematical model includes the following simplifying assumptions.
For the lumen: (i) the system is isothermal, (ii) the flow is laminar with a parabolic, developed velocity profile, (iii) no reaction occurs in the bulk of the lumen, (iv) the diffusion coefficient is a time-independent variable, (v) diffusion obeys Fick's first law, (vi) the culture medium has water-like physical properties.

For the alginate matrix: (i) the suspension is homogenous, (ii) component consumption follows Monod kinetics, (iii) there is no convective transport, (iv) the effective diffusion coefficient is a time-independent variable and equal to the 75% of its diffusion coefficient in culture medium, (v) diffusion obeys Fick's first law, (vi) there is no cell differentiation.

The continuity equation for oxygen in cylindrical coordinates is expressed mathematically by the following equation:

$$\frac{\partial c}{\partial t} + v_r \frac{\partial c}{\partial r} + v_\theta \left(\frac{1}{r}\frac{\partial c}{\partial \theta}\right) + v_z \frac{\partial c}{\partial z} = D\left(\frac{1}{r}\frac{\partial}{\partial r}\left(r\frac{\partial c}{\partial r}\right) + \frac{1}{r^2}\frac{\partial^2 c}{\partial \theta^2} + \frac{\partial^2 c}{\partial z^2}\right) + q \qquad (3.1)$$

where c is the concentration, r,θ,z are the radial, angular and axial coordinate respectively, v_r, v_Θ, v_Z are the radial, angular and axial velocity respectively, D is the diffusion constant and q is the production rate.

The term $\frac{\partial c}{\partial t}$ represents the accumulation rate per unit volume. The term $D(\frac{1}{r}\frac{\partial}{\partial r}(r\frac{\partial c}{\partial r})+\frac{1}{r^2}\frac{\partial^2 c}{\partial \theta^2}+\frac{\partial^2 c}{\partial z^2})$ represents the rate per unit volume of mass transfer by diffusion, the term $v_r\frac{\partial c}{\partial r}+v_\theta(\frac{1}{r}\frac{\partial c}{\partial \theta})+v_z\frac{\partial c}{\partial z}$ represents the rate per unit volume of mass transfer by convection and the term q represents the production rate per unit volume based on cell metabolism. It is negative for the consumed substrate and positive for produced metabolite.

In the lumen, there is no chemical reaction so q is zero. The radial velocity v_r and angular velocity v_θ are zero as well because the flow in the lumen is laminar. Additionally, the term $\frac{1}{r^2}\frac{\partial^2 c}{\partial \theta^2}$ is zero because the artificial artery is rotationally symmetric due to its cylindrical shape. After the above considerations the equation (3.1) gives for the lumen:

$$\frac{\partial c^{lumen}}{\partial t}+v_z\frac{\partial c^{lumen}}{\partial z}=D_{lumen}(\frac{1}{r}\frac{\partial}{\partial r}(r\frac{\partial c^{lumen}}{\partial r})+\frac{\partial^2 c^{lumen}}{\partial z^2}),\ 0<r<R_1,\ 0<z<L \qquad (3.2)$$

where c^{lumen}, D^{lumen} is the concentration and diffusivity of the component n in the lumen, R_1 is the radius of the lumen and L is the length of the artificial artery. In the alginate matrix the terms $\frac{1}{r^2}\frac{\partial^2 c}{\partial \theta^2}$, v_r and v_θ are zero for the reasons that have been mentioned for the lumen. Therefore, equation (3.1) simplifies to the following equation:

$$\frac{\partial c^{alginate}}{\partial t}+v_z\frac{\partial c^{alginate}}{\partial z}=D^{alginate}(\frac{1}{r}\frac{\partial}{\partial r}(r\frac{\partial c^{alginate}}{\partial r})+\frac{\partial^2 c^{alginate}}{\partial z^2})+q \qquad (3.3)$$

where $c^{alginate}$ and $D^{alginate}$ are the oxygen concentration and oxygen effective diffusivity in the alginate scaffold.

The boundary conditions are specified as follows. At $r=0$ there is radial symmetry because of the cylindrical shape of the artificial artery. This condition is expressed mathematically by the following equation:

$$D^{lumen}\frac{\partial c^{lumen}}{\partial r}=0 \qquad (3.4)$$

At $r=R_1$, the molecular flux of oxygen per unit area in the lumen is equal to its molecular flux per unit area in the alginate-matrix as there is no accumulation at the interface. This statement is expressed mathematically as

$$D^{lumen}\frac{\partial c^{lumen}}{\partial r} = D^{alginate}\frac{\partial c^{alginate}}{\partial r} \tag{3.5}$$

$$c^{lumen} = c^{alginate} \tag{3.6}$$

In the lumen at the exit of the artificial artery, the diffusive flux for the component n which is perpendicular to this boundary is zero. This statement can be described by the following equation:

$$D^{lumen}\left(\frac{1}{r}\frac{\partial}{\partial r}\left(r\frac{\partial c^{lumen}}{\partial r}\right)\right) = 0,\ 0<r<R_1,\ z=L \tag{3.7}$$

At $r=R_2$, the molecular flux of component n per unit area out of the reactor is zero. This can be stated by the following equation:

$$D^{alginate}\frac{\partial c^{alginate}}{\partial r} = 0 \tag{3.8}$$

Finally, in the alginate matrix at the end of reactor the molecular flux of component n per unit area is zero. Stated mathematically,

$$D^{alginate}\frac{\partial^2 c^{alginate}}{\partial z^2} = 0 \tag{3.9}$$

The kinetic expression for oxygen considers consumption for proliferation and maintenance and it is described by the following equation.

$$R=\frac{1}{Y_{X/n}}\frac{dX}{dt}+mX, \tag{3.10}$$

where $Y_{X/n}$ is yield coefficient of cell concentration on the concentration of the component n, X is the cell concentration, m is the specific maintenance rate.The kinetic term for consumption due to proliferation is given by the following expression:

$$\frac{1}{Y_{X/n}}\frac{dX}{dt}$$

and the kinetic term for consumption due to maintenance by the expression:

mX

The cell proliferation cannot continue indefinitely even if there is not substrate depletion or metabolite inhibition. Instead, the cell concentration will reach a maximum value due to space limitations within the alginate construct. The logistic equation has been chosen for phenomenological description of the cell proliferation. In the specific case it assumes an inhibition in proliferation proportional to the square of the cell concentration. The mathematical definition of the logistic equation is given by the following equation

$$\frac{dX}{dt}=\mu X(1-\frac{X}{X_{MAX}}) \tag{3.11}$$

where μ is the specific proliferation rate and X_{MAX} is the maximum cell concentration achievable.

It is possible that the proliferation is oxygen limited. Such a dependency of the specific proliferation rate to the concentrations of limited oxygen can be described by Monod kinetics as follows:

$$\mu=\mu_{MAX}\frac{c}{k_M+c} \tag{3.12}$$

where μ_{MAX} is the maximum specific proliferation rate and k_M is the half saturation constant of oxygen. The equation (3.10) becomes

$$R=q_{MAX}\frac{c}{k_M+c}X(1-\frac{X}{X_{MAX}})+mX \tag{3.13}$$

where q_{max} is the maximum specific oxygen uptake rate and is equal to the maximum specific proliferation rate divided by the yield coefficient of cell concentration on the oxygen concentration. The specific maintenance rate is assumed to be equal to 10% of the specific oxygen uptake rate.

The system of the above equations was solved by using the finite element method with the commercial software package Comsol Multiphysics 3.3a (Comsol Ltd., Cambridge UK). One half of the system was simulated due to symmetry at the tubular reactor's centreline. It was chosen to use the transient non-linear solver as the proliferation rate is a nonlinear term. The convergence was tested by refining the mesh up to 1800 elements. Each simulation took around 4 h on a Pentium IV PC with a 3 GHz processor and 2 Gb memory.

3.3 Windows of operation

The use of windows of operation has been chosen to describe the operation of the tissue-engineered construct. This kind of technique visualizes the key parameters for the design of the reactor in a clear and rapid way. The sensitivity of the operation can be defined by how the area enclosed by the window of operation alters by changing the values of the key parameters. This area can even shrink to a point for a singular, optimal and design solution. The window of operation approach gives the opportunity to someone to conceive the engineering evaluation of such a complex system without the need of having advanced mathematical knowledge.

The windows of operation were set up for cell concentration against flow rate in the lumen. They define the area in order to simulate coronary artery function. A short analysis, which explains the way to set up the windows of operation, is given below.

Oxygen in the scaffold is being provided by diffusion (convective flow is assumed negligible). The only way to enhance diffusion in the scaffold is by increasing the flow rate in the lumen. The higher the flow rate is, the lower the oxygen gradient in the lumen will be. Thus, oxygen concentration at the interface between lumen and scaffold will be almost equal to the oxygen concentration at the entrance of the reactor. As a consequence, all the cells along the reactor will have almost equal access to it and as a result similar metabolic behaviour.

The upper limit of oxygen concentration is identified at the entrance of the reactor in the interface between lumen and alginate matrix and the lower limit is identified in the exit of the reactor. The difference between the upper and the lower limit is high then the creation of microenvironments of varying characteristics is very possible. This problem can be avoided by arranging the oxygen concentration to be at that level, which exists in the bone marrow and it has been reported to be 52.0 ± 14.5 mmHg (0.069 ± 0.020 mM) (Ishikawa and Ito, 1988). By solving the mathematical model a correlation between cell

concentration and flow rate can be achieved as the values for the lowest and highest oxygen concentration are known. This correlation is not enough to set up the window of operation. It needs a second figure to visualize the cell concentration constraints. The upper limit of this range is defined by the maximum cell concentration in a coronary artery, which is $262x10^6$ cells mL^{-1} (Dahl et al, 2007; Niklason et al., 1999). The lower one is defined by the minimum cell concentration that has to be achieved in a tissue engineered coronary artery to lead to a physiological coronary artery when it will be implanted in a patient. This limit is equal to $116x10^6$ cells mL^{-1} (Dahl et al, 2007; Niklason et al., 1999). The overlap of the two figures gives the window of operation.

3.4 Results

Figure 3.3 shows the cell concentration and the oxygen concentration in the alginate at the exit of the artificial artery at its outer wall as a function of the culture time for a representative flow rate. Initially, the oxygen concentration decreases because of the high metabolic activity of the proliferating cells. It increases when the cells start entering the less metabolically demanding maintenance phase. The oxygen concentration is minimum when the cell concentration in the construct reaches the value of $130x10^6$ cells mL^{-1}.

The window of operation, which describes the effect of cell concentration in the scaffold, has been set up for an initial cell concentration of $10x10^6$ cells mL^{-1} and a final one of $116x10^6$ cells mL^{-1}. The oxygen diffusivity in the tissue-engineered construct is $2.25x10^{-9}$ m^2 s^{-1} (Table 3.1), its length is 0.33 m, its wall thickness is 300 μm and the specific oxygen uptake rate is $0.11x10^{-18}$ mol $cell^{-1}$ s^{-1}. The procedure to set up a window of operation is described below (Figure 3.4).

In the Figure 3.4A the light shaded area indicates the region where it is possible to provide sufficient oxygen to maintain it above the minimum prescribed level. The unshaded area indicates the region where is not possible to supply oxygen

at a sufficient rate to support cell proliferation while maintain oxygen level above the prescribed minimum. So the bioreactor has to operate in the shaded area.

In Figure 3.4B the light shaded area defines the cell concentration constraint. The reactor has to operate in the shaded area, which corresponds to concentrations higher than $116x10^6$ cells mL^{-1} and lower than $262x10^6$ cells mL^{-1}. By combining the two last figures Figure 3.4C is obtained which also defines the window of operation as the dark-shaded region. From this figure it can be concluded that there is a critical flow rate in the lumen below which it is not possible to maintain proliferating cells at an acceptable concentration. Concerning the non-shaded area below the concentration of $116x10^6$ cells mL^{-1}, it has to be mentioned that not only the concentration range has larger value, but the cell concentration is lower than $116x10^6$ cells mL^{-1}. In the light-shaded area below the cell concentration of $116x10^6$ cells mL^{-1} the range is acceptable, but the cell concentration is lower than $116x10^6$ cells mL^{-1}. Above the cell concentration of $262x10^6$ cells mL^{-1}, the cell concentration is higher than the maximum cell concentration in a coronary artery.

The effect of wall thickness, length and effective oxygen diffusivity in the area which is defined by a window of operation is presented below. For every window of operation the minimum required cell concentration is $116x10^6$ cells mL^{-1} and the specific oxygen uptake rate is $0.11x10^{-18}$ mol $cell^{-1}$ s^{-1} (Figure 3.5). Each variable was changing by 10% and the effect on the critical flow rate in particular was addressed.

It can be concluded that the critical flow rate is more sensitive to changes in the tube wall thickness than in the length and effective oxygen diffusivity. It can be increased either by increasing the feed rate in the reactor or by increasing the recycle rate in the artificial artery. The former will lead to the increased usage of fresh culture medium which will raise the operational cost of the reactor and the latter will lead in the recycle of the waste products of the cells which will inhibit their metabolism and consequently it will increase the time for the artery to be ready for implantation. Later on a more detailed discussion of the acceptable flow rates is given.

The previous windows of operation have been set up based on the assumption that there is no error in the values of specific oxygen uptake rate, wall thickness, length and diffusivity coefficient. Those errors have to be taken into account in order to achieve a functional operation of the tissue engineered construct. The worst case scenario could be when there is a positive error in the values of cell concentration, length and wall thickness of the scaffold and a negative one in the value of the oxygen diffusivity.

The effect of a positive error in the above variables can be eliminated by increasing the flow rate in the lumen. Concerning the diffusivity, a lower value decreases the rate of diffusion in the scaffold according to the first Fick's law. A way to re-establish the diffusional flux is to increase the concentration gradient in the scaffold by increasing the concentration at the interface between scaffold and lumen. This can be achieved by decreasing the concentration gradient along the axial direction of the construct through an increase of the flow rate in the lumen.

As the purpose of this chapter is not to give quantitative solutions to specific values of variables, realistic values for the errors in the variables have been chosen. The above window of operation was set up again assuming a +5% error for wall thickness and specific oxygen uptake rate, a +1% for the length, and a negative error -5% for the oxygen diffusivity (Figure 3.6). If the errors are taken account to the set up of the window of operation the flow rate to sustain a cell concentration 116×10^6 cells mL^{-1} has to rise from 3600 mL h^{-1} to 8100 mL s^{-1}.

The effect of geometry and oxygen diffusivity of the alginate matrix on the critical flow rate is presented in Figure 3.7. The critical flow rate is expressed as the ratio of the critical flow rate to the one for the initial setting as it is defined in Figure 3.4. This interaction is visualized for the case of the original setting with no errors in the mentioned variables and for the case of the robust one (Figure 3.7).

In Figure 3.8 the effect of the mean oxygen concentration and critical flow rate on the range of the oxygen concentration in the artificial artery is explored. The range is expressed as deviation of the maximum (entrance of the artificial artery) and minimum oxygen concentration (exit of the artificial artery at the outer limit of the alginate). Assuming no changes in the metabolic behaviour of the cells for the range of the oxygen concentrations studied it can be concluded that the higher the critical flow rate the smaller the difference between the maximum and minimum concentration in the artificial artery will be. Use as an example the mean oxygen concentration of 0.07 mM. When the critical flow rate is low and specifically 470 mL h^{-1}, the minimum oxygen concentration, the maximum oxygen concentration and their difference is 0.039, 0.101 and 0.062 respectively. For medium values of critical flow rate and specifically 1500 mL s^{-1} the minimum oxygen concentration, the maximum oxygen concentration and their difference is 0.046, 0.095 and 0.049 mM respectively. Similarly, for high values of critical velocity and specifically 7000 mL h^{-1} the minimum oxygen concentration, the maximum oxygen concentration and their difference is 0.053, 0.088 and 0.035 mM.

Table 3.1: Parameters used in Chapter 3

Parameter	Value	Unit	Reference
lumen radius (R_1)	1.7×10^{-3}	m	
outer radius (R_2)	2×10^{-3}	m	
axial length (L)	0.33	m	
initial cell concentration ($C_{initial}$)	10×10^{6}	cells mL^{-1}	
cell concentration of native coronary artery (X_{max})	262×10^{6}	cells mL^{-1}	Dahl et al., 2007
cell concentration of engineered coronary artery (X_{eng})	116×10^{6}	cells mL^{-1}	Dahl et al., 2007
specific oxygen uptake rate (q_{max})	10.6×10^{-18}	mol $cell^{-1}$ s^{-1}	Peng and Palsson, 1996
oxygen half-saturation constant (K_{ox})	10^{-3}	mM	Peng and Palsson, 1996
oxygen diffusivity in the lumen (D_{ox}^{lumen})	3×10^{-9}	m^2 s^{-1}	Palsson et al., 2003

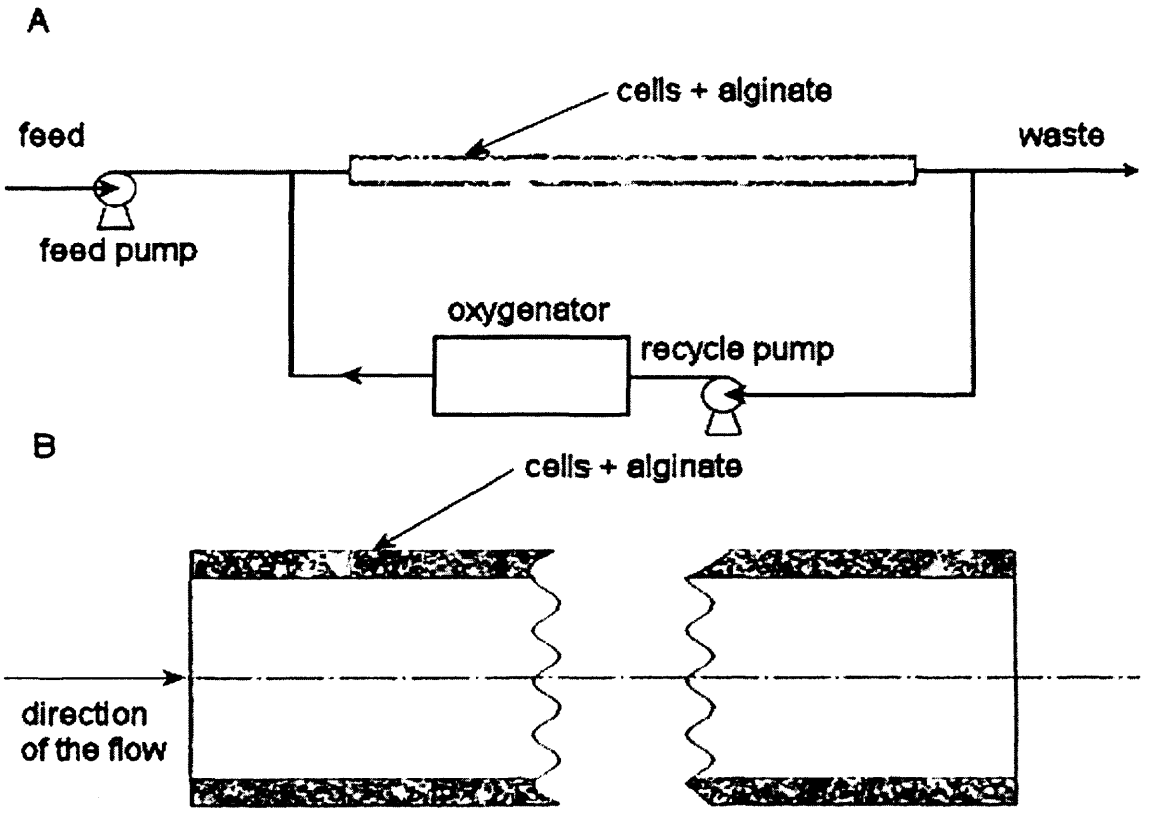

Figure 3.1: Prototype bioreactor for the production of artificial arteries. The bioreactor operates in recycle mode with feed and bleed of medium (Figure 3.1A). The artificial artery is composed of two concentric cylindrical zones corresponding to two regions: the lumen and the alginate matrix. The oxygen and other nutrients are supplied by flow through the lumen, diffuse through the alginate matrix and are consumed by the cells (Figure 3.1B).

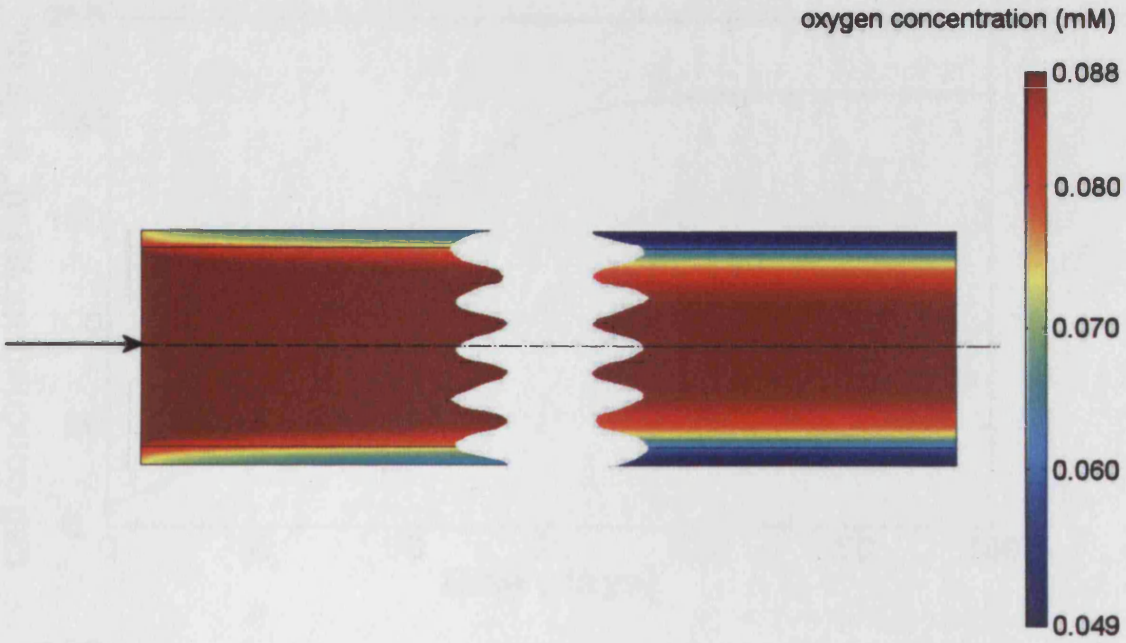

Figure 3.2: The oxygen distribution has been modelled for a tubular bioreactor of length 0.33 m, wall thickness 300 μm and inner diameter 3.4 mm. The oxygen effective diffusivity in the scaffold is assumed to be 2.25×10^{-9} m^2 s^{-1}, the flow rate in the lumen is 3600 mL h^{-1} and the maximum and minimum oxygen concentration are 0.049 mM and 0.088 mM respectively. The cell concentration is 116×10^6 cells mL^{-1} with a specific oxygen uptake rate equal to 0.11×10^{-18} mol $cell^{-1}$ s^{-1}.

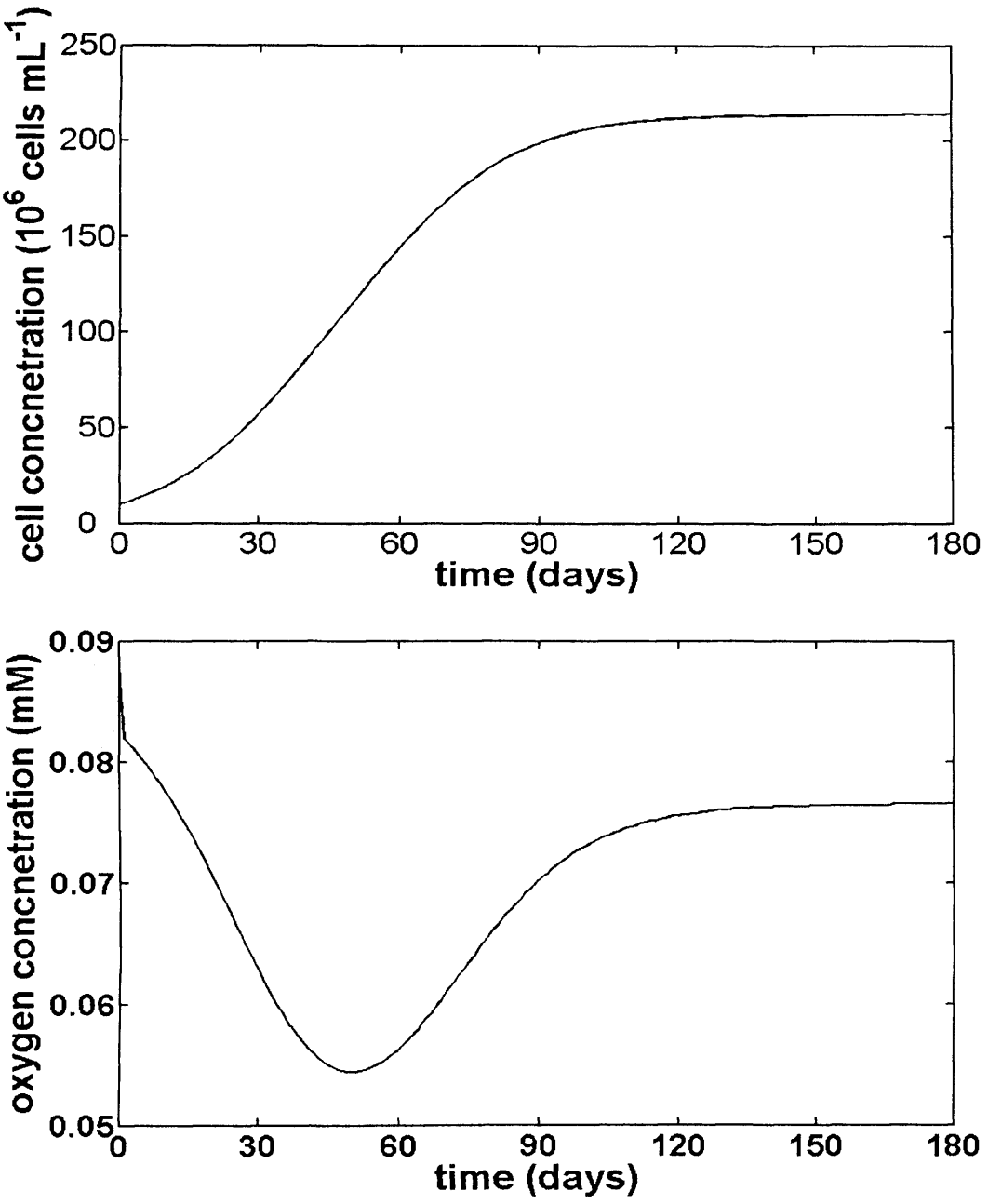

Figure 3.3: Cell concentration and oxygen concentration in the alginate at the exit of the artificial artery at its outer wall as a function of the culture time for a representative flow rate (3600 mL h^{-1}).

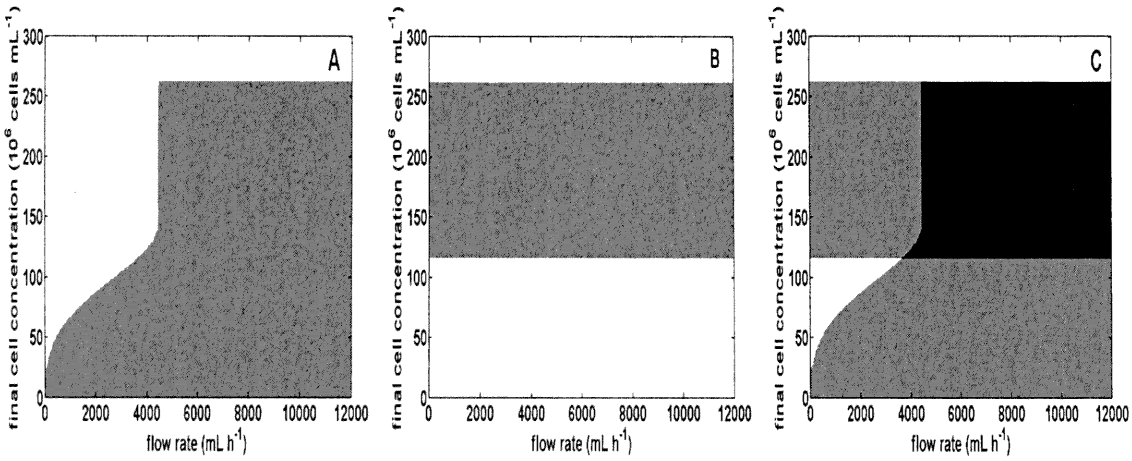

Figure 3.4: Development of a window of operation for cell growth in a scaffold.

Figure 3.4A: Shaded region is that area where the oxygen transfer rate available exceeds the oxygen transfer rate required to support cell growth for a range of cell concentrations. In this case the conditions are defined for tube of length 0.33 m, wall thickness 300 μm and inner diameter 3.4 mm. The oxygen diffusivity in the scaffold is assumed to be 2.25×10^{-9} m^2 sec^{-1} and the maximum and minimum oxygen concentrations are 0.088 mM and 0.049 mM respectively. The specific oxygen uptake rate of the cells is 0.11×10^{-18} mol $cell^{-1}$ s^{-1}. Oxygen transfer is via flow of nutrient solution over the internal surface of the tube at the average velocity given.

Figure 3.4B: Shaded region is that area where cell concentration is considered to be acceptable for tissue engineering purposes. The lower limit is defined by the value of 116×10^6 cells mL^{-1}; the upper limit is defined by the value of 262×10^6 cells mL^{-1}.

Figure 3.4C: The overlap of figures 3A and 3B gives a window of operation where an acceptable concentration of cells is achieved without exposing them to oxygen concentrations above or below specified values.

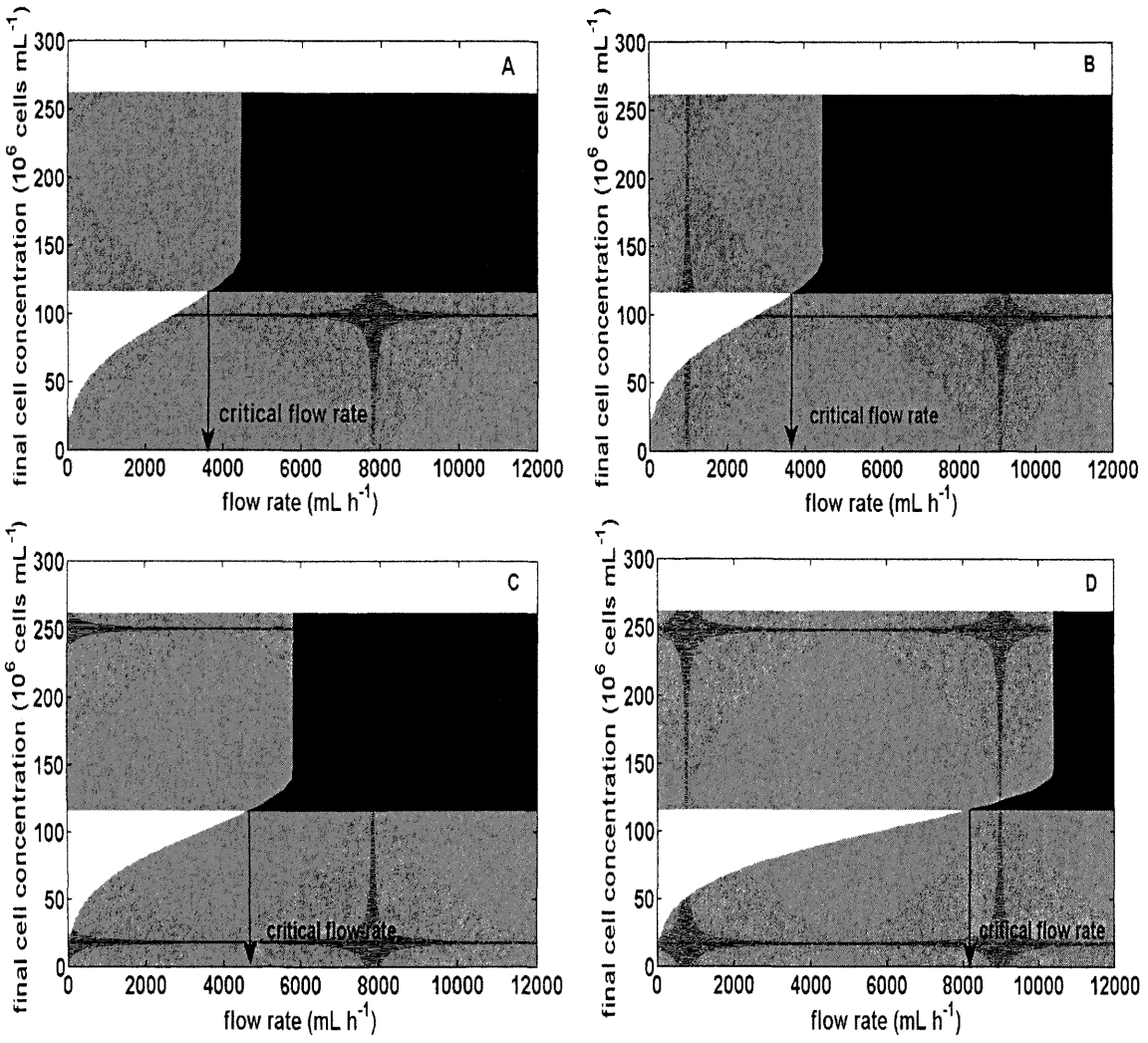

Figure 3.5: Analysis of window of operation for feasibility of cell-scaffold preparation as determined by the critical flow rate needed for sufficient oxygen supply.

Figure 3.5A: Conditions as defined in Figure 2 - critical flow rate 3600 mL h^{-1}.

Figure 3.5B: Effect of 10% decrease in the effective oxygen diffusivity of the alginate-matrix (2.25×10^{-9} to 1.99×10^{-9} m^2 s^{-1}) - new critical flow rate 3750 mL h^{-1}.

Figure 3.5C: Effect of 10% increase in tube length (0.33 to 0.36 m) – new critical flow rate 4800 mL h^{-1}.

Figure 3.5D: Effect of 10% increase in tube wall thickness (3 to 3.30×10^{-3} mm) - new critical flow rate 8050 mL h^{-1}.

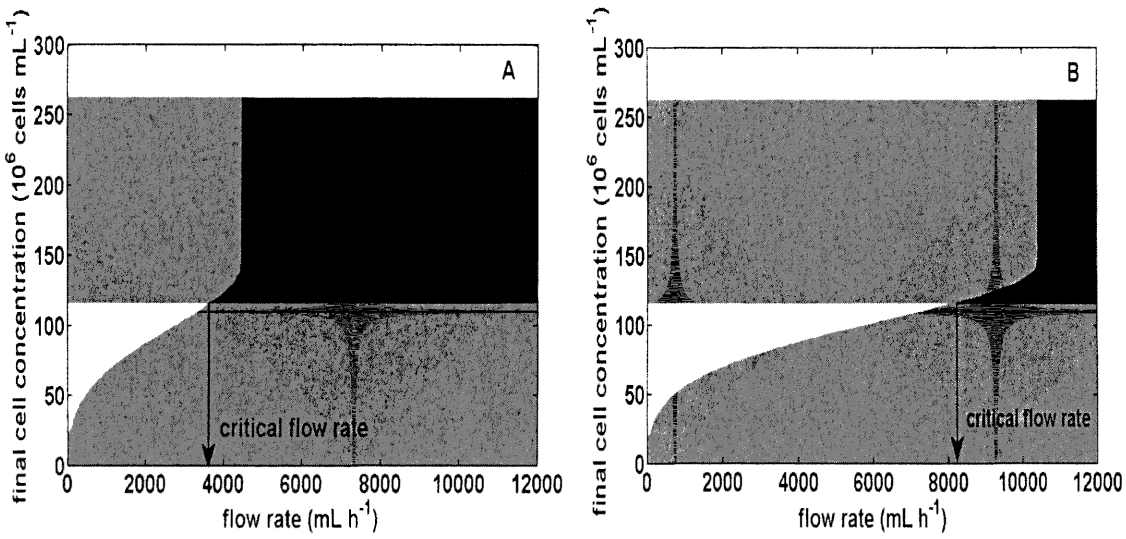

Figure 3.6: Impact of errors in variables in the window of operation.

Figure 3.6A: Original window of operation with conditions as defined in Figure 3.1 - critical average velocity 3600 mL h^{-1}.

Figure 3.6B: Robust operating window under the effect of +5% error for wall thickness and specific oxygen uptake rate, a +1% for the length, and -5% for the oxygen diffusivity-new critical flow rate 8100 mL h^{-1}.

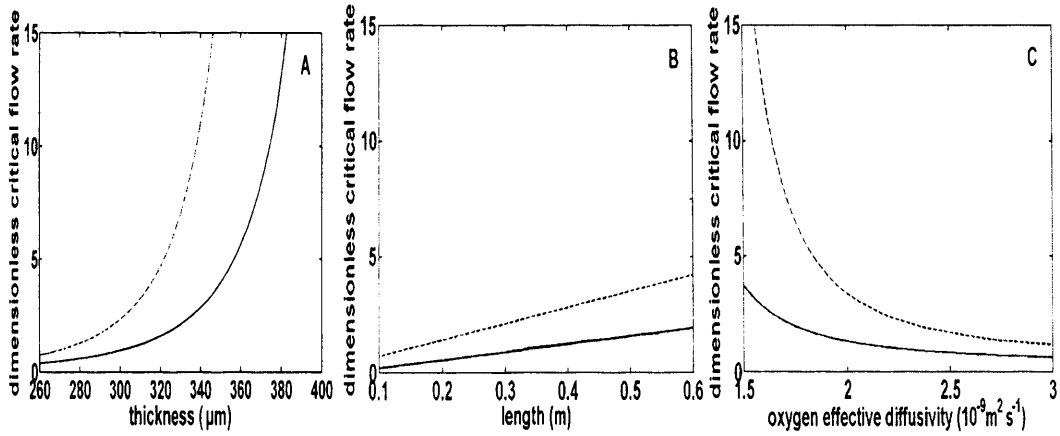

Figure 3.7: Effect of geometry and oxygen diffusivity on the dimensionless critical flow rate (ratio of the critical flow rate to the initial one as it is defined in Figure 3.4) for the original setting (—) (as defined in Figure 3.4) and for the robust setting (---) (as defined in Figure 3.6).

Figure 3.7A: Effect of wall thickness.

Figure 3.7B: Effect of length.

Figure 3.7C: Effect of effective oxygen diffusivity.

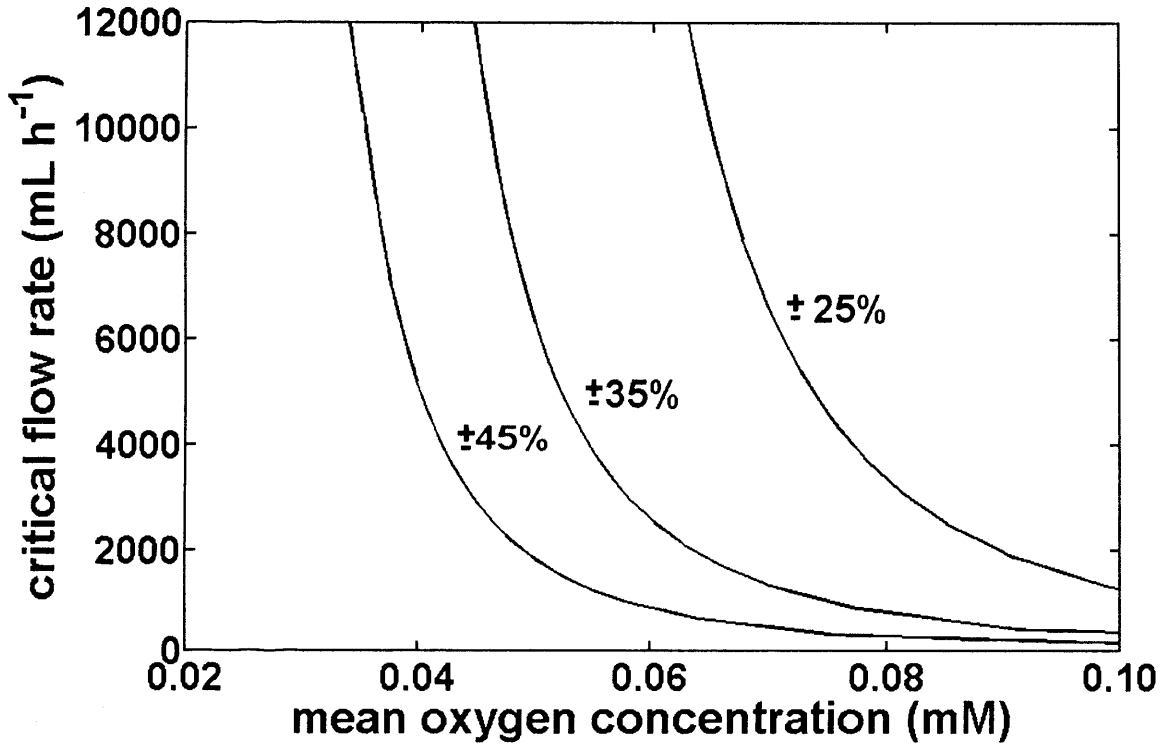

Figure 3.8: Effect of the mean oxygen concentration and critical average velocity on the range of the oxygen concentration (values shown on relationship) in the artificial artery. This range is expressed as deviation around the mean oxygen concentration with the upper and lower limits defined by the maximum (entrance of the artificial artery) and minimum oxygen concentration (exit of the artificial artery at the outer limit of the alginate) respectively. It has been assumed that the metabolic behaviour of the cells does not change in the range of the oxygen concentrations studied. It can be concluded that the higher the oxygen acceptable mean concentration or critical flow rate the smaller the difference between the maximum and minimum concentration in the artificial artery will be.

Chapter 4

Substrate and metabolite transfer and metabolism in the artificial artery

4.1 Introduction

The bioreactor for the production of artificial arteries operates in recycle mode with feed and bleed of medium. The oxygen and other nutrients are supplied by flow through the lumen, diffuse through the alginate matrix and are consumed by the mesenschymal stem cells. In the previous chapter a mathematical model was developed in order to predict the effect of the cell concentration, tube geometry, alginate effective diffusivity and oxygen concentration levels on the oxygen mass transfer in the alginate. Similar studies for other substrates have not been conducted because their mass transfer rates in alginate are considerably higher than that of the oxygen as a consequence of their higher concentration in the culture medium. However, the feed and recycle rate of the culture medium can influence the concentrations of substrates and metabolites and consequently the cell proliferation.

In this chapter a theoretical analysis has been conducted to predict the effect of feed and recycle rate on the substrate and metabolite concentration profiles and cell proliferation in the artificial artery. Glucose, glutamine and oxygen have been chosen as the main substrates and lactate and ammonia as the main metabolites. For simplicity reasons, the engineering analysis will be presented by giving the mass balance, mass transfer and kinetic expressions for the component n, instead of giving these expressions for every substrate and metabolite separately.

4.2 Mathematical model to describe substrate and metabolite concentration profiles in the artificial artery

4.2.1 Mass balance expressions for the recycle loop

The feed rate in the bioreactor is equal to its waste rate assuming equal densities at its entrance and exit. The overall material balance for the bioreactor is expressed mathematically as:

$$F = W, \tag{4.1}$$

where F, W are the feed and waste rate respectively.

The input rate to the artificial artery is equal to the sum of the feed rate to the bioreactor and the recycle rate assuming constant medium density. Thus the overall material balance expression between the entrance of the bioreactor and the entrance of the artificial artery states that

$$F+R=V, \tag{4.2}$$

where R, V are the recycle and input rate to the artificial artery respectively.

The influx of the component n in the artificial artery is equal to the sum of its feed flux in the bioreactor and its recycle flux. This is expressed mathematically as:

$$Fc_{F,n}+Rc_{R,n}=Vc_{A,n}, \tag{4.3}$$

where $c_{F,n}$, $c_{R,n}$, $c_{A,n}$ are the feed, the recycle and the inlet concentration to the artificial artery respectively. Additionally, the output rate from the artificial artery is equal to the sum of the recycle and waste rate of the bioreactor assuming constant medium density. Accordingly, the outflux of the component n from the artificial artery is equal to its recycle flux and its waste flux from the bioreactor

Mathematically, the above statements are expressed as:

$$V=R+W, \tag{4.4}$$

$$Vc_{A,n}=Rc_{R,n}+Wc_{W,n}, \tag{4.5}$$

where W, $c_{W,n}$ are the waste rate and concentration of the component n in waste stream respectively.

4.2.2 Mass transfer expressions in the artificial artery

The artificial artery can be considered as having two subdomains; the lumen and the alginate matrix (Figure 4.1). The artificial artery has a cylindrical shape so it is possible to reduce the problem from 3D to a 2D axi-symmetric problem. The mathematical equations which describe the mass transfer as well as the consumption of substrates and production of metabolites in the artificial artery are based on the following assumptions:

For the lumen: (i) the system is isothermal, (ii) the flow is laminar with a parabolic, developed velocity profile, (iii) no reaction occurs in the bulk of the lumen, (iv) the diffusion coefficient is a time-independent variable, (v) diffusion obeys Fick's first law, (vi) the culture medium has water-like physical properties.

For the alginate matrix: (i) the suspension is homogenous, (ii) component consumption follows Monod kinetics, (iii) there is no convective transport, (iv) the effective diffusion coefficient of component *n* is a time-independent variable and equal to the 75% of its diffusion coefficient in culture medium, (v) diffusion obeys Fick's first law, (vi) there is no cell differentiation.

The continuity equation for the component *n* in cylindrical coordinates is expressed mathematically by the following equation:

$$\frac{\partial c}{\partial t} + v_r \frac{\partial c}{\partial r} + v_\theta \left(\frac{1}{r}\frac{\partial c}{\partial \theta}\right) + v_z \frac{\partial c}{\partial z} = D\left(\frac{1}{r}\frac{\partial}{\partial r}\left(r\frac{\partial c}{\partial r}\right) + \frac{1}{r^2}\frac{\partial^2 c}{\partial \theta^2} + \frac{\partial^2 c}{\partial z^2}\right) + q \qquad (4.6)$$

where c is the concentration, r,θ,z are the radial, angular and axial coordinate respectively, v_r, v_Θ, v_Z are the radial, angular and axial velocity respectively, D is the diffusion constant and q is the production rate.

The term $\frac{\partial c}{\partial t}$ represents the accumulation rate per unit volume. The term $D\left(\frac{1}{r}\frac{\partial}{\partial r}\left(r\frac{\partial c}{\partial r}\right) + \frac{1}{r^2}\frac{\partial^2 c}{\partial \theta^2} + \frac{\partial^2 c}{\partial z^2}\right)$ represents the rate per unit volume of mass transfer by diffusion, the term $v_r \frac{\partial c}{\partial r} + v_\theta \left(\frac{1}{r}\frac{\partial c}{\partial \theta}\right) + v_z \frac{\partial c}{\partial z}$ represents the rate per

unit volume of mass transfer by convection and the term q represents the production rate per unit volume based on cell metabolism. It is negative for the consumed substrate and positive for produced metabolite.

In the lumen, there is no chemical reaction so q is zero. The radial velocity v_r and angular velocity v_θ are zero as well because the flow in the lumen is laminar. Additionally, the term $\frac{1}{r^2}\frac{\partial^2 c}{\partial \theta^2}$ is zero because the artificial artery is rotationally symmetric due to its cylindrical shape. After the above considerations the equation (4.6) gives for the lumen:

$$\frac{\partial c_n^{lumen}}{\partial t} + v_z \frac{\partial c_n^{lumen}}{\partial z} = D_n^{lumen}\left(\frac{1}{r}\frac{\partial}{\partial r}\left(r\frac{\partial c_n^{lumen}}{\partial r}\right) + \frac{\partial^2 c_n^{lumen}}{\partial z^2}\right),\ 0<r<R_1,\ 0<z<L \qquad (4.7)$$

where c_n^{lumen}, D_n^{lumen} is the concentration and diffusivity of the component n in the lumen, R_1 is the radius of the lumen and L is the length of the artificial artery. In the alginate matrix the terms $\frac{1}{r^2}\frac{\partial^2 c}{\partial \theta^2}$, v_r and v_θ are zero for the reasons that have been mentioned for the lumen. Equation (4.6) simplifies to the following equation:

$$\frac{\partial c_n^{alginate}}{\partial t} + v_z \frac{\partial c_n^{alginate}}{\partial z} = D_n^{alginate}\left(\frac{1}{r}\frac{\partial}{\partial r}\left(r\frac{\partial c_n^{alginate}}{\partial r}\right) + \frac{\partial^2 c_n^{alginate}}{\partial z^2}\right) + q \qquad (4.8)$$

where $c_n^{alginate}$ and $D_n^{alginate}$ are the oxygen concentration and oxygen effective diffusivity in the alginate scaffold.

The boundary conditions are specified as follows. At $r=0$ there is radial symmetry because of the cylindrical shape of the artificial artery. This condition is expressed mathematically by the following equation:

$$D_n^{lumen}\frac{\partial c_n^{lumen}}{\partial r} = 0 \qquad (4.9)$$

At $r=R_1$, the molecular flux of component n per unit area in the lumen is equal to its molecular flux per unit area in the alginate-matrix as there is no accumulation at the interface. This statement is expressed mathematically as

$$D_n^{lumen}\frac{\partial c_n^{lumen}}{\partial r} = D_n^{alginate}\frac{\partial c_n^{alginate}}{\partial r} \qquad (4.10)$$

$$c_n^{lumen} = c_n^{alginate} \tag{4.11}$$

In the lumen at the exit of the artificial artery, the diffusive flux for the component *n* which is perpendicular to this boundary is zero. This statement can be described by the following equation:

$$D_n^{lumen}\left(\frac{1}{r}\frac{\partial}{\partial r}\left(r\frac{\partial c_n^{lumen}}{\partial r}\right)\right) = 0,\ 0<r<R_1,\ z=L \tag{4.12}$$

At $r=R_2$, the molecular flux of component *n* per unit area out of the reactor is zero. This can be stated by the following equation:

$$D_n^{alginate}\frac{\partial c_n^{alginate}}{\partial r} = 0 \tag{4.13}$$

Finally, in the alginate matrix at the end of reactor the molecular flux of component *n* per unit area is zero. Stated mathematically,

$$D_n^{alginate}\frac{\partial^2 c_n^{alginate}}{\partial z^2} = 0 \tag{4.14}$$

4.2.4 Species kinetic expression

The kinetic expression for component *n* considers consumption for proliferation and maintenance and it is described by the following equation.

$$R=\frac{1}{Y_{X/n}}\frac{dX}{dt}+mX, \tag{4.15}$$

where $Y_{X/n}$ is yield coefficient of cell concentration on the concentration of the component n, X is the cell concentration, m is the specific maintenance rate. The kinetic term for consumption due to proliferation is given by the following expression:

$$\frac{1}{Y_{X/n}}\frac{dX}{dt}$$

and the kinetic term for consumption due to maintenance by the expression:

mX

The cell proliferation cannot continue indefinitely even if there is not substrate depletion or metabolite inhibition. Instead, the cell concentration will reach a

maximum value due to space limitations within the alginate construct. The logistic equation has been chosen for phenomenological description of the cell proliferation. The mathematical definition of the logistic equation is given by the following equation

$$\frac{dX}{dt}=\mu X(1-\frac{X}{X_{MAX}}) \tag{4.16}$$

where μ is the specific proliferation rate and X_{MAX} is the maximum cell concentration achievable.

It is possible that the proliferation is substrate limited and simultaneously there are inhibitions caused by high metabolite concentrations. Such a dependency of the specific proliferation rate to the concentrations of limited substrates and inhibited metabolites can be described by Monod kinetics as follows:

$$\mu=\mu_{MAX}\frac{c_n}{k_n+c_n}\frac{c_{n+1}}{k_{n+1}+c_{n+1}}\cdots\frac{K_p}{K_p+c_p}\frac{K_{p+1}}{K_{p+1}+c_{p+1}}\cdots \tag{4.17}$$

where μ_{MAX} is the maximum specific proliferation rate and k_n, k_{n+1} are the half saturation constants of the substrates n and $n+1$ and K_p, K_{p+1} are the inhibition constants of the metabolites p and $p+1$ (Bailey and Ollis, 1986).

The equation (4.15) becomes

$$R=q_{MAX,n}(\frac{c_n}{k_n+c_n}\frac{c_{n+1}}{k_{n+1}+c_{n+1}}\cdots\frac{K_p}{K_p+c_p}\frac{K_{p+1}}{K_{p+1}+c_{p+1}}\cdots)X(1-\frac{X}{X_{MAX}})+mX \tag{4.18}$$

where q_{max} is the maximum specific consumption / production rate of component n and is equal to the maximum specific proliferation rate divided by the yield coefficient of cell concentration on the concentration of the component n. The specific maintenance rate is assumed to be equal to 10% of the specific consumption/production rate of component n.

4.2.5 Numerical method

The system of the above equations was solved by the finite element method. The mathematical package which was used was Comsol Multiphysics 3.3 using

two dimensional axial symmetry. It was chosen to use the transient non-linear solver as the proliferation rate is a nonlinear term. The convergence was tested by refining the mesh up to 3600 elements. The concentration profiles were obtained by solving the system of the above equations for different values of feed and recycle rate. Specifically, the Comsol model was connected to a Matlab loop structure which was providing the solution of the governing equations of the bioreactor in the range of 1-5 mL h^{-1} for the feed rate and 1000-6000 mL h^{-1} for the recycle rate. The simulation took 95 h on a Pentium IV PC with a 3 GHz processor and 2 Gb memory.

4.3 Results and conclusions

The bioreactor operates in recycle mode with feed and bleed of medium. The culture medium is diffused in alginate through the lumen where the substrates are consumed by the mesenchymal stem cells producing metabolites. The culture medium is oxygenated via a gas exchanger located in the recycle loop. The initial cell concentration has been set to $10x10^6$ cells mL^{-1} and the artificial artery is cultured in the bioreactor for 90 days. The critical cell concentration which has to be reached is $116x10^6$ cells mL^{-1}. This value is the one of constructs which has been used as tissue-engineered arteries (Dahl et al, 2007; Niklason et al., 1999).

Figure 4.2 gives the minimum required glucose, glutamine and oxygen as well as the maximum resulting lactate and ammonia concentration in the artificial artery during the proliferation of undifferentiated bone marrow mesenchymal stem cells immobilized in alginate as a function of feed and recycle rate. The minimum substrate and the maximum metabolite concentration exist at the exit of the artificial artery at its outer wall. The shaded area corresponds to combinations of feed and recycle rates which give after 90 days of culture a construct with a cell concentration below the critical one.

Glucose and glutamine concentration increase and lactate and ammonia concentration decrease by increasing the feed rate (Figure 4.2). High substrate

concentrations favour cell proliferation therefore the higher the feed rate is the higher the cell concentration in the artificial artery will be (Figure 4.3).

A high recycle rate enhances the aeration of the artificial artery increasing the concentration of lactate and ammonia and decreasing the concentration of the glucose and glutamine (Figure 4.2). This can be explained from the fact that at high recycle rates the medium is passing through the artificial artery more times than at low ones. Thus more lactate and ammonia is produced and more glucose and glutamine is consumed after every pass of the recycled medium. Consequently, this will inhibit the cell proliferation resulting in constructs with a lower cell concentration (Figure 4.3).

Oxygen is provided through the oxygenator in the recycle loop where the flow rate is around two orders of magnitude higher than the flow rate of the fresh culture medium. Thus, the oxygen of the feed stream does not affect its concentration level in the artificial artery. At low feed rates oxygen concentration depends not only on the recycle rate but also on the feed rate. It is a result of the low glucose and glutamine supply which slows down the cell proliferation rate and consequently the oxygen uptake rate. At high feed rates the dependency of the oxygen concentration on the recycle rate prevails against its dependency on the feed rate. Therefore at high feed rates oxygen concentration is a function of the recycle rate only.

Figure 4.4 gives the time which is needed in order to obtain a construct with the critical cell concentration. The higher the feed rate is the sooner the construct will obtain the required cell concentration. This can be explained from the fact that at high feed rates there is excess of substrates therefore the cells are metabolically more active proliferating at a higher rate. On the opposite, this time increases as the recycle rate increases. As mentioned above high recycle rates increase the concentration of the metabolites. This increase inhibits cell proliferation and consequently increases the time for the cell population to reach a specific concentration.

The concentration of the substrates decrease and the concentration of the metabolites increase in a direction towards the exit of the artificial artery as a result of the substrate consumption and metabolite production by the cells. Therefore, the cell concentration is lower in areas close to the exit of the artificial artery than in areas close to its entrance as a result of substrate limitation and metabolite inhibition. Figure 4.5 gives an indication of the homogeneity of cell concentration in alginate as a function of the feed and recycle rate. The homogeneity is expressed as the ratio of the cell concentration at the exit of artificial artery at its outer wall to the cell concentration at its entrance at its inner wall. It was calculated when the cell concentration at the exit of the artificial artery at its outer wall reaches the critical one ($116x10^6$ cells mL^{-1}). It is relatively uniform for all the combinations of feed and recycle rates which can give within 90 days a construct with a cell concentration of a tissue-engineered artificial artery. Therefore, it can be concluded that there is sufficient substrate supply and efficient metabolite removal to produce an artificial artery with homogenous cell concentration even when the feed and the recycle rate are relatively low.

Figure 4.6 shows the substrate and metabolite concentrations in the alginate at the exit of the artificial artery at its outer wall as a function of the culture time for representative values of feed and recycle rate. Initially, the substrate concentrations decrease as the cells start proliferating but then they start increasing as a fraction of the cells enters the less metabolically demanding maintenance phase lowering the overall substrate uptake from the cells. The substrate concentrations stabilize when all cells have entered the maintenance phase. There is a sharp decrease in substrate concentrations early at the beginning of the culture which lasts till the priming of the reactor with fresh medium.

Table 4.1: Parameters used in Chapter 4

Parameter	Value	Unit	Reference
lumen radius (R_1)	1.7×10^{-3}	m	
outer radius (R_2)	2×10^{-3}	m	
axial length (L)	0.33	m	
initial cell concentration ($C_{initial}$)	10×10^{6}	cells mL^{-1}	
cell concentration of native coronary artery (X_{max})	262×10^{6}	cells mL^{-1}	Dahl et al., 2007
cell concentration of engineered coronary artery (X_{eng})	116×10^{6}	cells mL^{-1}	Dahl et al., 2007
glucose concentration in fresh medium (C_{gluc0})	5.55	mM	manufacturer's data
glutamine concentration in fresh medium (C_{glut0})	2	mM	manufacturer's data
specific oxygen uptake rate (q_{max})	10.6×10^{-18}	mol $cell^{-1}$ s^{-1}	Peng and Palsson, 1996
yield of glucose from oxygen ($Y_{glu/ox}$)	1	mol mol^{-1}	Zeng et al., 1998
yield of glucose from glutamine ($Y_{glu/gln}$)	0.35	mol mol^{-1}	Zeng et al., 1998
yield of lactate from glucose ($Y_{lac/glu}$)	1.3	mol mol^{-1}	Zhao et al., 2005
yield of glutamine from ammonia ($Y_{gln/amm}$)	0.80	mol mol^{-1}	Xie and Wang, 1994
glucose half-saturation constant (K_{glu})	0.75	mM	Xie and Wang, 1994
lactate inhibition constant (K_{lac})	60	mM	assumed
glutamine half-saturation constant (K_{gln})	0.15	mM	Xie and Wang, 1994
ammonia inhibition constant (K_{amm})	2	mM	assumed
oxygen half-saturation constant (K_{ox})	10^{-3}	mM	Peng and Palsson, 1996
glutamine chemical decomposition rate constant ($K_{glutdec}$)	1.33×10^{-6}	s^{-1}	Glacken et al., 1986
glucose diffusivity in the lumen (D_{gluc}^{lumen})	0.92×10^{-9}	m^2 s^{-1}	Sengers et al., 2005
lactate diffusivity in the lumen (D_{lact}^{lumen})	1.4×10^{-9}	m^2 s^{-1}	Sengers et al., 2005
glutamine diffusivity in the lumen (D_{glut}^{lumen})	3×10^{-9}	m^2 s^{-1}	Perry and Green, 1984
ammonia diffusivity in the lumen (D_{amm}^{lumen})	3×10^{-9}	m^2 s^{-1}	Perry and Green, 1984
oxygen diffusivity in the lumen (D_{ox}^{lumen})	3×10^{-9}	m^2 s^{-1}	Palsson et al., 2003

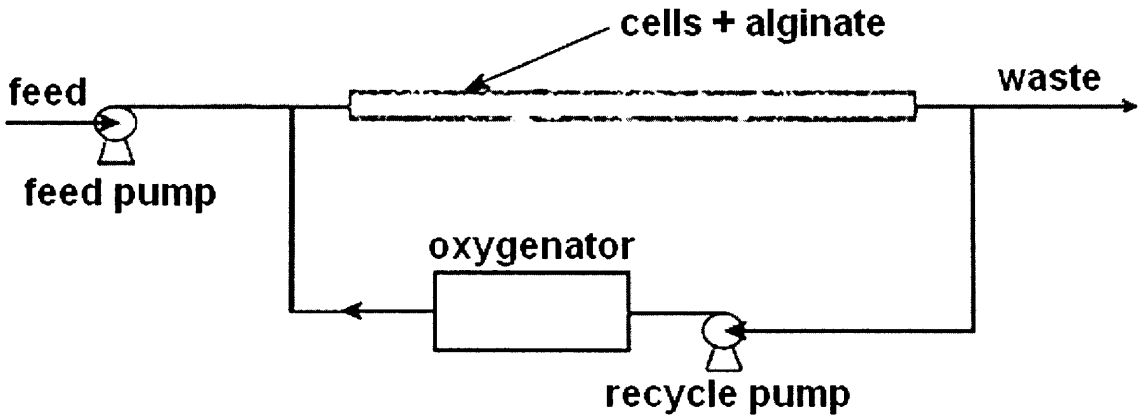

Figure 4.1: The bioreactor operates in recycle mode with feed and bleed of medium. The feed flow rate is in the order of 1-5 mL h^{-1} and the recycle flow rate is in the order of 1000-6000 mL h^{-1}. The artificial artery is composed of two concentric cylindrical zones corresponding to two regions: the lumen and the alginate matrix with the adult mesenchymal stem cells. The culture medium is diffused in alginate through the lumen where the substrates are consumed by the cells producing metabolites. The culture medium is oxygenated via a gas exchanger located in the recycle loop.

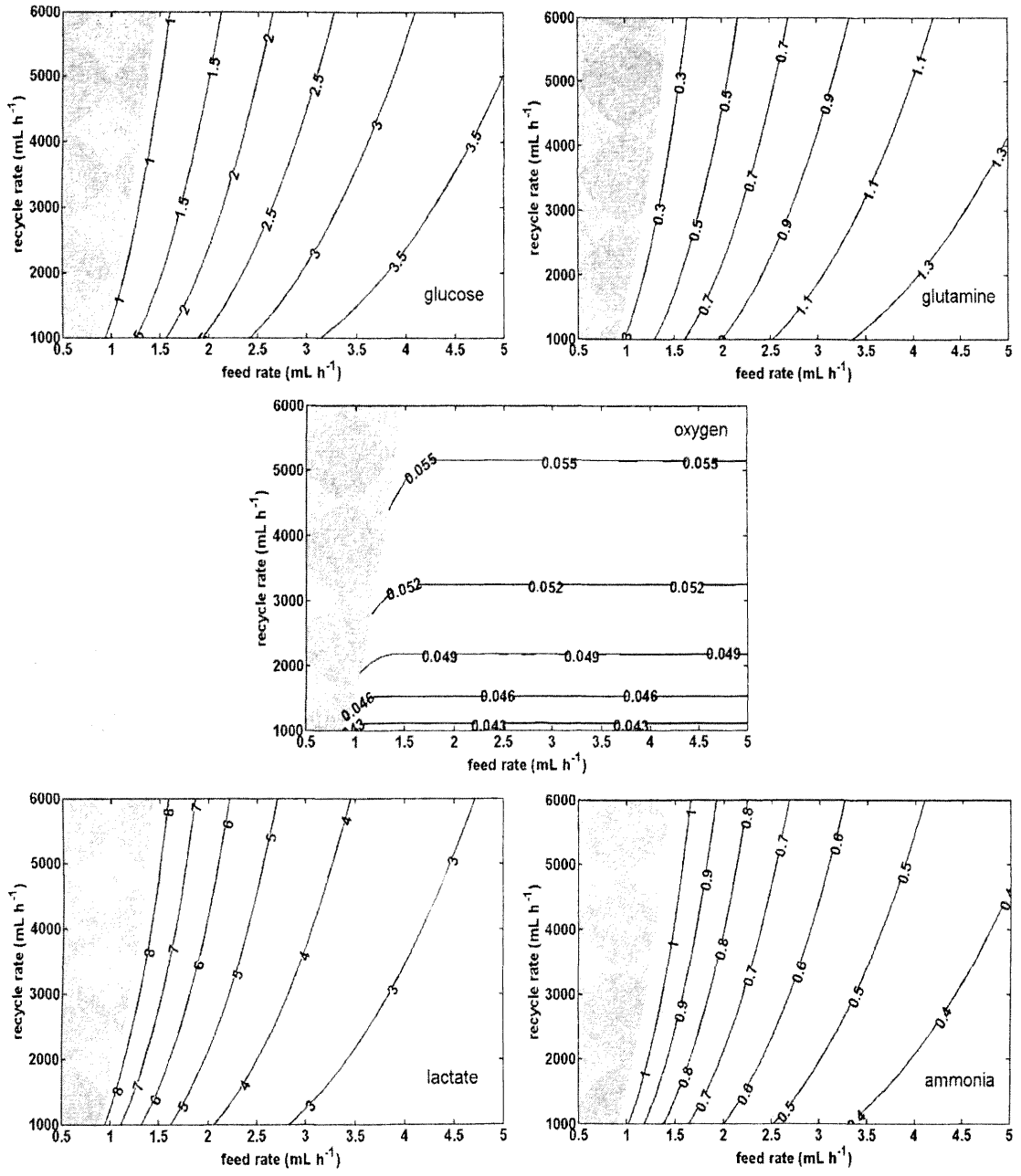

Figure 4.2: Minimum substrate and maximum metabolite concentration expressed in mM as a function of the feed and recycle rate. The minimum substrate and maximum metabolite concentration exists at the exit of the artificial artery at its outer wall. The bioreactor for the production of artificial arteries operates in recycle mode with feed and bleed of medium. Alginate has been used as scaffold and it has been seeded initially with $10x10^6$ cells mL^{-1} mesenchymal stem cells. The shaded area corresponds to combinations of feed and recycle rates which give after 90 days of culture a construct with a cell concentration below the critical one ($116x10^6$ cells mL^{-1}).

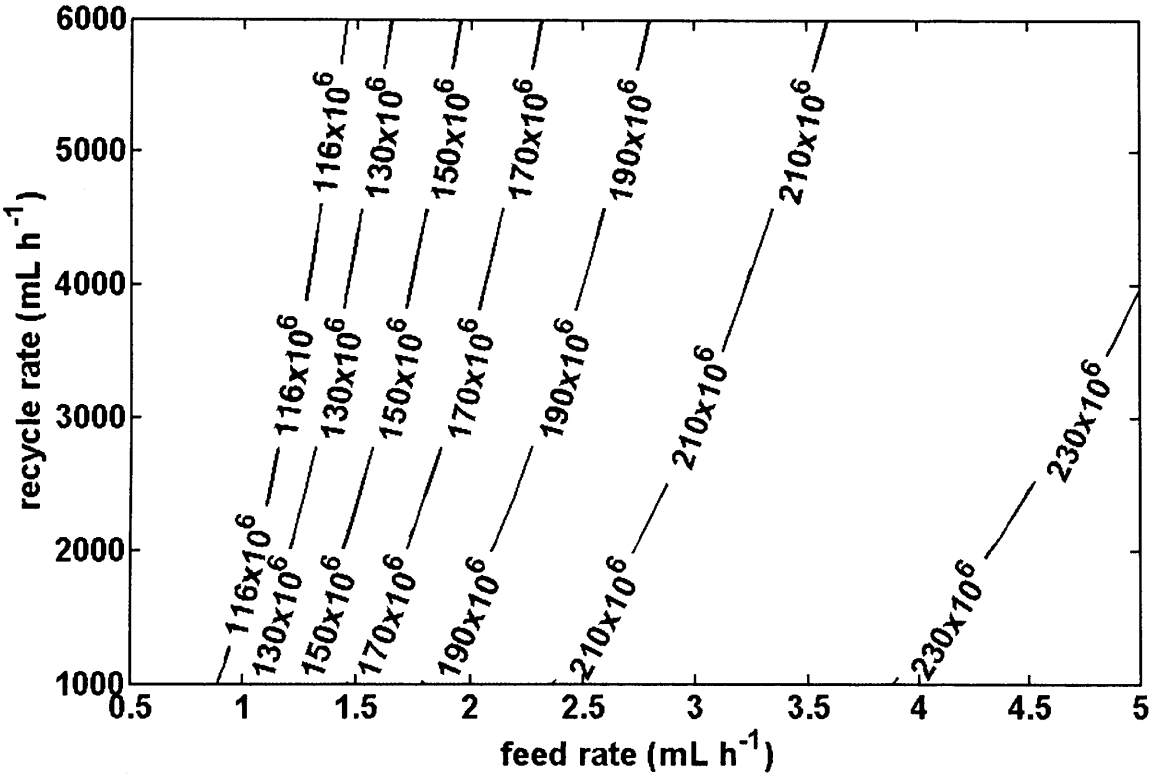

Figure 4.3: Cell concentration (in 10^6 cells mL^{-1}) at the exit of the artificial artery at its outer wall after 90 days of culture as a function of feed and recycle rate. The bioreactor for the production of artificial arteries operates in recycle mode with feed and bleed of medium. Alginate has been used as scaffold and it has been seeded initially with $10x10^6$ cells mL^{-1} mesenchymal stem cells.

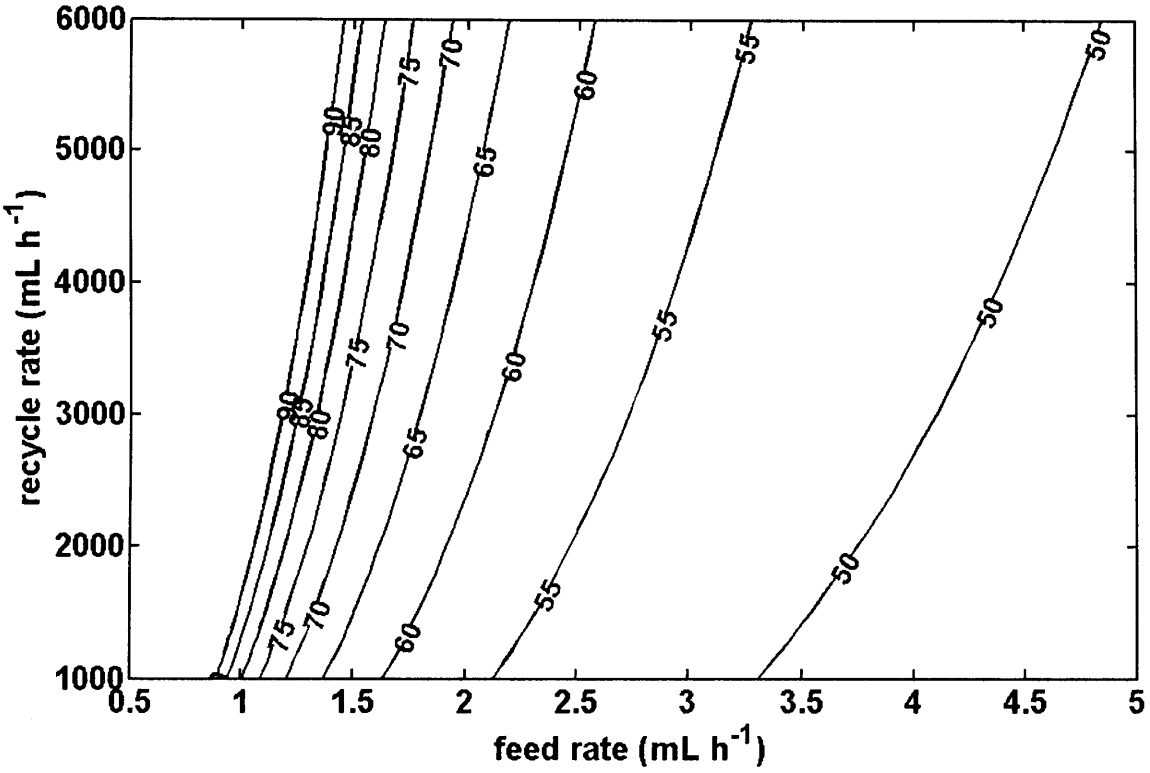

Figure 4.4: Time (in days) which is needed in order to obtain a tissue-engineered artery. This artery should have a cell concentration above the critical one ($116x10^6$ cells mL^{-1}) at its exit at its outer limit. The bioreactor for the production of artificial arteries operates in recycle mode with feed and bleed of medium. Alginate has been used as scaffold and it has been seeded initially with $10x10^6$ cells mL^{-1} mesenchymal stem cells.

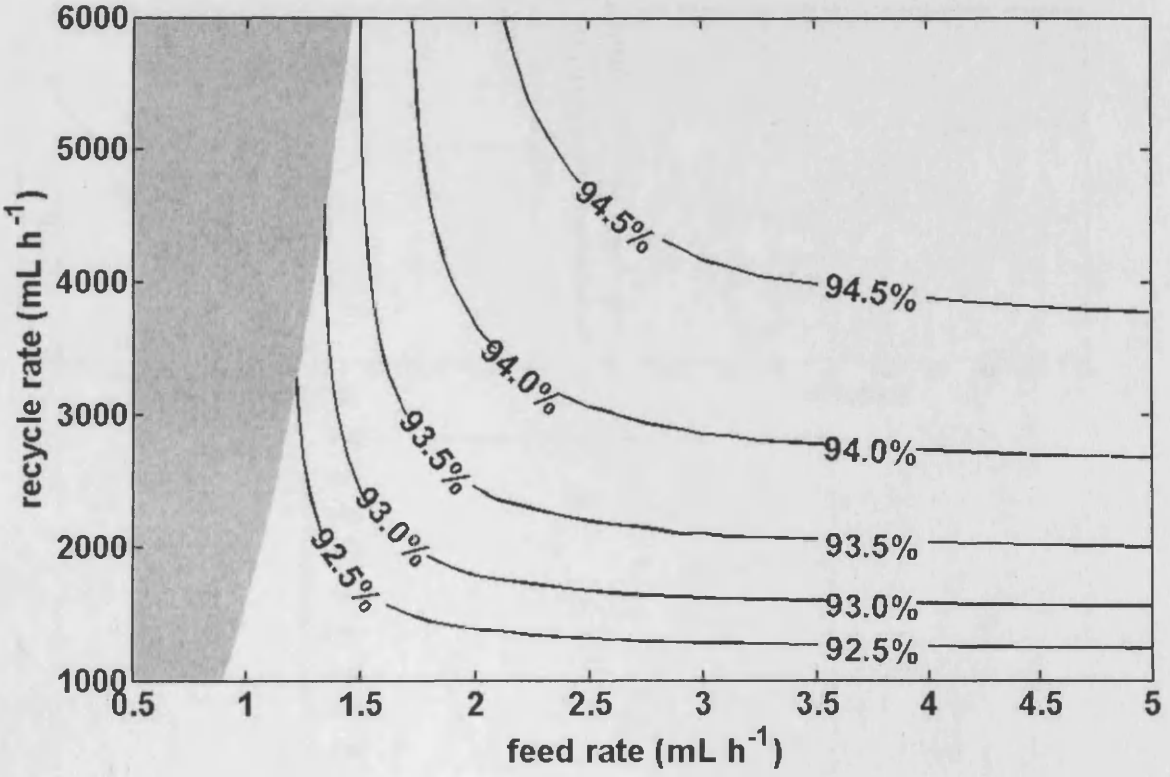

Figure 4.5: Homogeneity of the cell concentration in the artificial artery as a function of the feed and recycle rate when the cell concentration at the exit of the artificial artery at its outer wall reaches the critical cell concentration ($116x10^6$ cells mL^{-1}). The homogeneity is expressed as the ratio of the cell concentration at the exit of the artificial artery at its outer wall to the cell concentration at its entrance at its inner wall. The shaded area corresponds to combinations of feed and recycle rates which give a construct with a cell concentration below the critical one.

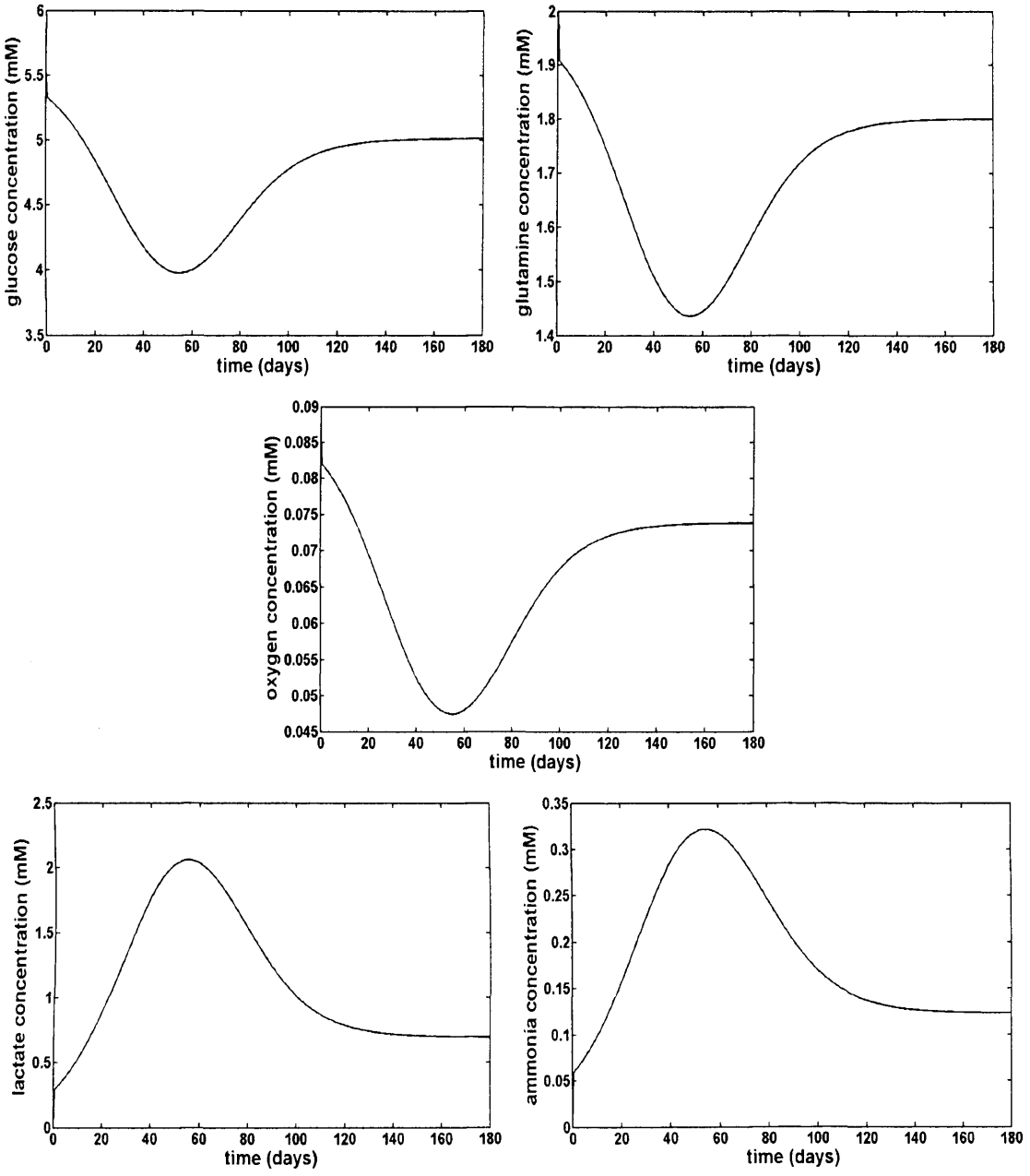

Figure 4.6: Minimum substrate and maximum metabolite concentration as a function of the culture time for a representative feed rate of 5 mL h^{-1} and a representative recycle rate of 30 mL h^{-1}. The minimum substrate and maximum metabolite concentration exists at the exit of the artificial artery at its outer wall. The bioreactor for the production of artificial arteries operates in recycle mode with feed and bleed of medium. Alginate has been used as scaffold and it has been seeded initially with $10x10^6$ cells mL^{-1} mesenchymal stem cells.

5. Oxygen transfer and metabolism in alginate

5.1 Introduction

Scale-down experiments at 7 μL level were designed to measure oxygen gradients in an alginate gel / cell mix and hence evaluate the oxygen effective diffusivity and the oxygen uptake rate of human adult cells. In this way amounts of human cells in an alginate construct can be used to measure experimentally parameters which will define the windows of operation.

Alginate constructs with immobilized human dermal fibroblasts were formed in customized 24-well plates with integrated oxygen and pH sensor spots. Their volume was 7 μL and their shape was cylindrical with a diameter of 3 mm and a height of 1 mm. Human fibroblasts were selected as a cell source due to their availability and ease of handling (Alberts et al, 1994). Additionally, alginate constructs with and without cells were used to study the effect of immobilized cells on the oxygen effective diffusivity.

The fibroblasts were immobilized in alginate at the concentration of $7x10^6$ cells mL^{-1} and cultured in 1 mL of static IMDM medium. Oxygen transfer occurs from the gas phase of the well to the alginate construct by diffusion where it was consumed by the cells.

Oxygen concentration and pH were recorded for the first 2.5 days and during that time cell enumeration, viability determination, Ki-67 expression and cell cycle analysis were conducted in order to evaluate the cell culture in alginate. The evaluation of the cell culture was necessary as the state of the cells defined the assumptions of the mathematical model which simulated the experiment for the calculation of the parameters.

This experiment was initiated by lowering the oxygen level in the incubator from 18.5% to 5% and the decrease in the oxygen concentration at the bottom of the alginate construct was recorded. The fibroblasts were evaluated in terms of cell

enumeration, viability, Ki-67 expression and cell cycle distribution after the end of the experiment in order to verify if the assumptions of the mathematical model had not been compromised. The oxygen decrease in the gas phase of the customized microwell was recorded in a separate experiment by using empty customized wells located at the same position in the plate as the wells used in the experiment for the calculation of the parameters.

The parameters and their confidence intervals were calculated by using the inverse method (section 2.6). Briefly, they are derived by minimisation of the sum of the squared differences between experimental and simulated data by using the Matlab Statistical Toolbox function "nlintool".

An additional experiment with conditions that differed from those of the experiment above was conducted as a verification of the calculations. The oxygen tension in the incubator was lowered from 18.5% to 10% and kept at that level until the oxygen concentration at the bottom of the alginate construct was stable. The oxygen tension was then increased back to 18.5%. The fibroblast culture was characterized as above.

5.2 Mathematical models

5.2.1. Mathematical model for the simulation of the oxygen diffusion and consumption in alginate constructs with immobilized human dermal fibroblasts

As illustrated in Figure 5.1 the customized well is considered as having two subdomains: the culture medium and the alginate matrix. A mathematical model has been set up to describe the oxygen diffusion and consumption in the customized well based on the following assumptions.

For the culture medium: (i) the system is isothermal, (ii) no reaction occurs, (iii) diffusion obeys Fick's first law, (iv) there is no convective transport, (v) the oxygen tension in the gas phase of the microwell is assumed to be equal to the one in the incubator, (vi) there is no resistance in the oxygen mass transfer at the air-culture medium interface, (vii) there is radial symmetry at the microwell centreline.

For the alginate matrix: (i) the system is isothermal, (ii) the cell suspension is homogenous, (iii) oxygen consumption follows Monod kinetics, (iv) there is no convective transport, (v) diffusion coefficient is a time independent parameter, (vi) diffusion obeys Fick's first law, (vii) the upper surface of the alginate construct is considered to be flat, (viii) alginate does not contract, (ix) there is symmetry at the construct centreline.

The equation of continuity for oxygen states

the rate of increase of oxygen mass per unit volume	=	*negative net rate of addition of oxygen mass per unit volume by convection and by diffusion*	+	*the rate of consumption of oxygen mass per unit volume by reaction*

For the culture medium

$$\frac{\partial c^{I}}{\partial t} = D_1(\frac{1}{r}\frac{\partial}{\partial r}(r\frac{\partial c^{I}}{\partial r}) + \frac{\partial^2 c^{I}}{\partial z^2}),$$

where D_1 is oxygen diffusivity in culture medium and c^{I} is the oxygen concentration in culture medium.

For the alginate matrix

$$\frac{\partial c^{II}}{\partial t} = D_2(\frac{1}{r}\frac{\partial}{\partial r}(r\frac{\partial c^{II}}{\partial r}) + \frac{\partial^2 c^{II}}{\partial z^2}) - q_{MAX}\frac{c^{II}}{K_M + c^{II}}X,$$

where c^{II} is the oxygen concentration in the alginate matrix, X is the cell concentration, D_2 is the oxygen diffusivity the alginate matrix, q_{MAX} is the maximum uptake rate and K_m is the Monod constant (concentration at which the half maximum oxygen uptake rate occurs).

The terms $\frac{\partial c^{I}}{\partial t}$ and $\frac{\partial c^{II}}{\partial t}$ represent the rate of increase of oxygen mass per unit volume for the culture medium and the alginate construct respectively. The terms $D_1(\frac{1}{r}\frac{\partial}{\partial r}(r\frac{\partial c^{I}}{\partial r}) + \frac{\partial^2 c^{I}}{\partial z^2})$ and $D_2(\frac{1}{r}\frac{\partial}{\partial r}(r\frac{\partial c^{II}}{\partial r}) + \frac{\partial^2 c^{II}}{\partial z^2})$ represent the negative net rate of addition of oxygen mass per unit volume by diffusion, for the culture medium and the alginate construct respectively. The term $-q_{MAX}\frac{c^{II}}{K_M + c^{II}}X$ represents the oxygen consumption rate per unit volume based on cell metabolism which occurs according to the Monod kinetics. The latter states that when the K_M constant becomes insignificant compared to the oxygen concentration the consumption rate is independent of the oxygen concentration. On the contrary, when the oxygen concentration becomes insignificant compared to the K_M constant the consumption rate becomes linearly dependent on oxygen concentration.

No flux boundary conditions are applied at the microwell and alginate construct centrelines because of the radial symmetry of their cylindrical shape. This statement is expressed mathematically by the following equations for the microwell and alginate construct centreline respectively.

$$D_1 \frac{\partial c_A^I}{\partial r} = 0 \; ; \; D_2 \frac{\partial c_A^{II}}{\partial r} = 0 \, ,$$

The bottom and the side walls of the microwell and the side walls of the construct are considered impermeable to oxygen therefore no flux boundary conditions are applied there. This statement is expressed mathematically as

$$D_1 \frac{\partial c^I}{\partial r} = 0 \; ; \; D_1 \frac{\partial c^I}{\partial z} = 0 \, ,$$

for the side walls and bottom of the microwell respectively and

$$D_2 \frac{\partial c^{II}}{\partial r} = 0 \; ; \; D_2 \frac{\partial c^{II}}{\partial z} = 0 \, ,$$

for the side walls and bottom of the alginate construct respectively.

It was assumed that there is no resistance to oxygen mass transfer at the air-culture medium interface. Therefore the oxygen concentration at the top surface of the medium can be derived from the oxygen tension in the gas phase of the microwell using Henry's law. The latter was acquired from the experiment where empty customized wells were used to record the oxygen tension decrease in the gas phase of the well caused by the oxygen tension decrease in the incubator. It was inserted into the mathematical model as an interpolation function using the cubic spline method.

The oxygen concentration profile which is developed in the microwell after 2.5 days incubation is the initial condition of the mathematical model which simulates the experiment for the calculation of the parameters. It can be derived from a mathematical model which has been set up under the same assumptions as the above and consists of the following equations and boundary conditions for the culture medium:

$$0 = D_1 \left(\frac{1}{r} \frac{\partial}{\partial r} \left(r \frac{\partial c^I}{\partial r} \right) + \frac{\partial^2 c^I}{\partial z^2} \right),$$

and for the alginate matrix:

$$0 = D_2 \left(\frac{1}{r} \frac{\partial}{\partial r} \left(r \frac{\partial c^{II}}{\partial r} \right) + \frac{\partial^2 c^{II}}{\partial z^2} \right) + q_{MAX} \frac{c^{II}}{K_A + c^{II}} X$$

No flux boundary conditions are applied at the microwell and alginate construct centrelines because of the radial symmetry of their cylindrical shape. This statement is expressed mathematically by the following equations for the microwell culture medium and the alginate construct respectively.

$$D_1 \frac{\partial c_A^I}{\partial r} = 0 ;\ D_2 \frac{\partial c_A^{II}}{\partial r} = 0$$

The bottom and the side walls of the microwell and the side walls of the construct are considered impermeable to oxygen therefore no flux boundary conditions are applied there. This statement is expressed mathematically as

$$D_1 \frac{\partial c^I}{\partial r} = 0 ,\ D_1 \frac{\partial c^I}{\partial z} = 0 ,$$

for the side walls and bottom of the microwell respectively.

$$D_2 \frac{\partial c^{II}}{\partial r} = 0 ,\ D_2 \frac{\partial c^{II}}{\partial z} = 0 ,$$

for the side walls and bottom of the alginate construct respectively.

The oxygen concentration at the top surface of the medium can be derived from the oxygen tension in gas phase of the microwell using Henry's Law.

5.2.2 Mathematical model for the simulation of the oxygen diffusion in alginate constructs without immobilized cells

The mathematical model can be derived from the one which simulates the experiment for the calculation of the parameters in alginate constructs with immobilized cells by applying the same assumptions. The difference is that the term which describes the oxygen consumption has been eliminated as there are no immobilized cells.

For the culture medium:

$$\frac{\partial c^I}{\partial t} = D_1 \left(\frac{1}{r}\frac{\partial}{\partial r}\left(r \frac{\partial c^I}{\partial r}\right) + \frac{\partial^2 c^I}{\partial z^2}\right),$$

For the alginate matrix:

$$\frac{\partial c^{II}}{\partial r} = D_2(\frac{1}{r}\frac{\partial}{\partial r}(r\frac{\partial c^{II}}{\partial r}) + \frac{\partial^2 c^{II}}{\partial z^2}),$$

No flux boundary conditions are applied at the microwell and alginate construct centrelines because of the radial symmetry of their cylindrical shape. This statement is expressed mathematically by the following equations

$$D_1\frac{\partial c_A^{I}}{\partial r} = 0\,; D_2\frac{\partial c_A^{II}}{\partial r} = 0$$

for the microwell and the alginate construct respectively.

The bottom and the side walls of the microwell and the side walls of the construct are considered impermeable to oxygen therefore no flux boundary conditions are applied there. This statement is expressed mathematically as

$$D_1\frac{\partial c^{I}}{\partial r} = 0\,,\; D_1\frac{\partial c^{I}}{\partial z} = 0\,,$$

for the side walls and bottom of the microwell respectively.

$$D_2\frac{\partial c^{II}}{\partial r} = 0\,,\; D_2\frac{\partial c^{II}}{\partial z} = 0\,,$$

for the side walls and bottom of the alginate construct respectively.

The oxygen concentration at the top surface of the medium can be derived from the oxygen tension in gas phase of the microwell using Henry's Law. It was inserted into the mathematical model as an interpolation function created from data acquired from the empty customised well experiment. The interpolation was conducted by using the cubic spline method.

5.2.3. Model solution and convergence

The system of the above equations was solved by using the commercial software package Comsol Multiphysics 3.3 (Comsol Ltd., UK). One half of the system was modelled due to symmetry at the construct centreline. Different solvers were used for the various mathematical models. A nonlinear time dependent solver was used for the mathematical model which simulates the

experiment with the immobilized cells because of the nonlinearity of the Monod kinetics term. The linear dependent solver was used for the experiments with the alginate constructs without the immobilized cells as all terms in the differential equations are linear. The nonlinear stationary solver was used to simulate the oxygen profile which was developed in the microwell after 2.5 days in the incubator. The solver is stationary because based on the assumptions of the mathematical model the oxygen concentration is time independent and it is nonlinear because of the nonlinear Monod kinetics term.

The relative and absolute tolerance in the time dependent solver has been adjusted to 10^{-3} and 10^{-4} respectively. The maximum number of iterations, the minimum step size and the tolerance for convergence in the stationary solver was adjusted to 25, 10^{-4} and 10^{-6} respectively.

In all simulations, the alginate construct has been meshed with 595 triangular elements and the culture medium with 690. The convergence was tested by increasing the number of elements to 152320 and 176640 for the alginate construct and the culture medium respectively. The oxygen concentration simulated by using the new mesh was agreed up to 4 significant figures with the oxygen concentration simulated by using the default mesh.

The values of the oxygen effective diffusivity, oxygen uptake rate and the Monod constant with their confidence intervals are obtaining by using the inverse method implemented in Comsol Multiphysics wrapped around Matlab (section 2.6). Each parameter evaluation took 23 h on a Pentium IV PC with a 3 GHz processor and 2 Gb memory.

5.3 Results and conclusions

The oxygen at the bottom of the alginate construct dropped to 1% within the first 3 hours and increased to 6 % after a day. Following a medium exchange (peak in DOT) the oxygen tension stabilized at 9.5% (Figure 5.2). The experiments for the calculations of the oxygen related parameters of the alginate / cell mix were initiated after the oxygen concentration at the bottom of the construct had stabilized.

This initial decrease in oxygen tension can be attributed to the transition from a flask to an alginate based cell culture system. Analytically, anchorage-dependent cells cannot adhere within unmodified hydrophilic substrates like alginate (lack of adhesive peptides) therefore they cannot enter their cell cycle and proliferate (Alberts et al, 1994; Palsson, 2003). However, the anchorage control operates at the G1 phase of the cell cycle and cells in S, G2 and M phase do not require adhesion to a surface to complete the cell cycle (Alberts et al, 1994). Therefore, cells which were in S, M and G2 phase just before the incubation of the alginate construct managed to complete the cell cycle. The oxygen demand was higher at the beginning of the incubation of the construct and started decreasing as the cells in the S, G2 and M phase were completing the cell cycle and entering the G0 / G1 phase which is less oxygen demanding. Thus, a decrease in oxygen concentration at the bottom of the construct was taken place the first 3 h followed by an increase as these cells were completing the cell cycle. The oxygen concentration at the bottom of the construct stabilized eventually at 9.5 % after 24 h, a time point when all cells had entered the less oxygen demanding G0 / G1 phases.

The value of the cell concentration which was inserted in the mathematical model was equal to the initial one ($7x10^6$ cells mL^{-1}) because there is no change in the live cell concentration till the end of the experiments (after 1.5 day incubation) (Figure 5.3). Additionally, no mathematical term describing the effect of cell death was inserted in the mathematical model as the viability was over 97% and remained at this level till the end of the experiments (Figure 5.3). The

slight deviation from 100% can be attributed to loss of cells from their recovery from the alginate construct.

High levels of lactate or ammonia can inhibit the cell metabolism causing a decrease in the oxygen uptake rate. Their effect though was not taken into account in the mathematical model as the pH at the bottom of the construct was relatively constant and acceptable (7.20 ± 0.05) for fibroblast cell growth (Alberts et al, 1994) (Figure 5.4).

It has been reported that oxygen uptake rate depends on the distribution of cells in the cell cycle (Freyer et al, 1985; Ramirez and Mutharasan, 1990). Therefore, cell cycle analysis was necessary in order to set up a mathematical model capable of predicting the variations in oxygen uptake rate caused by changes in the distribution of the phases of cell cycle.

The initial decrease in oxygen tension is accompanied by an increase in G0 / G1 fraction cell population and a decrease in the S fraction of the cell population (Figure 5.5). Analytically, the initial fractions of G0 / G1, and S phase cells (64.9 ± 0.9%, and 13.6 ± 0.1% respectively) remained stable for the first 3 hours ($p= 0.66$ and $p= 0.31$ respectively) and then the fraction of G0 / G1 phase cells started increasing, accompanied by a decrease in the fraction of S phase cells. Their values stabilized after a day from the beginning of the incubation at 72.9 ± 1.4% ($p= 0.87$) for G0 / G1 phase cells and 4.3 ± 0.3% ($p= 0.97$) for S phase cells. This increase in G0 / G1 phase cells accompanied by a decrease in the S phase cells is expected as cells cannot attach to alginate and it has been reported that anchorage control operates at the G1 phase (Alberts et al, 1994).

Ki-67 analysis was used to determine the percentage of the cells in quiescent state (G0 phase). Cell cycle analysis could not determine this characteristic. This was necessary because cells in G0 phase are less active metabolically than proliferating cells. The rate of protein synthesis for example is 20% of its value in proliferating cells (Alberts et al, 1994). Therefore, a mathematical model which neglects changes in the percentage of quiescent cells may lead to erroneous calculations.

The initial percentage of cells positive to Ki-67 expression was 85.8 ± 4.1%. It remained at this level throughout the experiments. However, after a week incubation a significant decrease was noted (Figure 5.6).

This experiment for the calculation of oxygen uptake rate, oxygen effective diffusivity and Monod constant was initiated by lowering the oxygen level in the incubator from 18.5% to 5%. The decrease in the oxygen concentration at the bottom of the alginate construct was recorded and analysed in a mathematical model which was set up in Matlab 7.1 and Comsol Multiphysics 3.3. The simulated data represented the best fit of the experimental data as obtained using the inverse method (section 2.6). The values for oxygen effective diffusivity, oxygen uptake rate and Monod constant with their 95% confidence intervals were 0.95 ± 0.10x10^{-9} m^2 s^{-1}, 19.42 ± 0.07x10^{-18} mol $cell^{-1}$ s^{-1} and 11.93 ± 1.28x10^{-3} mM respectively. The average absolute relative error between experimental and predicted data is 7.3% (Figure 5.7). The confidence intervals of the values of the oxygen effective diffusivity and Monod constant are much higher than the confidence interval of the oxygen uptake rate. This indicates that the variations of the experimental data are affecting more these two parameters.

The overestimation of the simulated oxygen profile may be attributed to an actual smaller thickness of the alginate construct or an inhomogeous cell distribution in alginate. Analytically, if the actual thickness of the construct is smaller than the one assumed the oxygen diffusion from the gas phase of the customized well to the alginate construct will progress faster than predicted and will lead to an overestimated simulated oxygen concentration profile.

Additionally, if the cell distribution in the construct is inhomogenous, the cell concentration can be higher above the oxygen sensor than in other areas of the construct. In this case the oxygen concentration will be lower there than in other areas of the construct. A decrease in the oxygen tension in the incubator will initiate a diffusive flux from the gas phase of the incubator to the alginate construct. The diffusive flux will be higher above the oxygen sensor than in other areas of the construct. Therefore, faster oxygen diffusion will take place.

Assuming a homogenous cell concentration, slower oxygen diffusion is predicted above the oxygen sensor which leads to an overestimation of the experimental oxygen concentration profile with the magnitude of the deviation to follow the progress of the oxygen diffusion.

The value of the oxygen effective diffusivity in alginate was $2.54 \pm 0.57 \times 10^{-9}$ cm^2 s^{-1} in constructs without cells and $0.95 \pm 0.10 \times 10^{-9}$ m^2 s^{-1} in constructs with immobilised cells. This can be attributed to the presence of ECM and cells which hinder the diffusion by occupying space within the alginate construct.

The average absolute relative error between experimental and simulated data was 6.8%. This error can be attributed in the error in the thickness of the construct. In this case it seems that the actual thickness of the construct is higher than the one assumed in the simulations producing an underestimated oxygen concentration profile due to slower oxygen diffusion from the construct to the gas phase of the customized well (Figure 5.8).

To verify the calculation of the oxygen related parameters of the alginate / cell mix, the oxygen tension in the incubator was lowered from 18.5% to 10%, and kept at that oxygen level till the oxygen concentration at the bottom of the alginate construct was stable and then was increased back to 18.5%. Results showed that the mathematical model was reliable as the average absolute relative error between experimental and predicted data was only 0.2% (Figure 5.9).

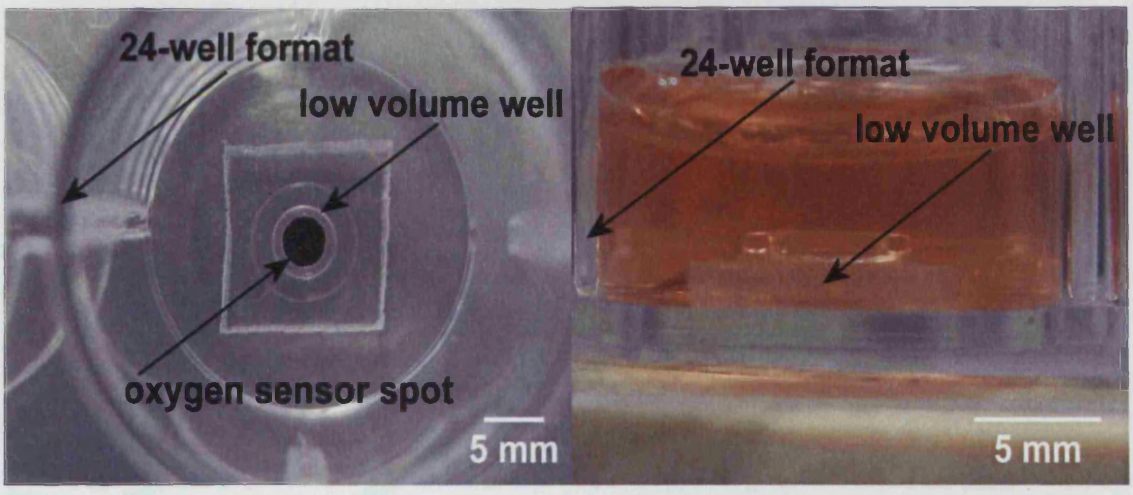

Figure 5.1: Photos of a customized well in 24-format used for the calculation of oxygen effective diffusivity in an alginate / cell mix and the oxygen uptake rate of human dermal fibroblasts. The alginate construct was formed within the well insert (volume of 7 µL, diameter of 3 mm and thickness of 1 mm). It was incubated in static IMDM culture medium at 37°C and under 5% CO_2. Oxygen was transferred to the alginate matrix by diffusion. Sensor spots with a diameter of 2 mm (polyester base) were glued at the bottom of the well insert and were used to provide oxygen concentration and pH on-line measurements. The values of the oxygen effective diffusivity and oxygen uptake rate were determined by inserting the data in a mathematical model set up in Comsol Multiphysics wrapped around Matlab.

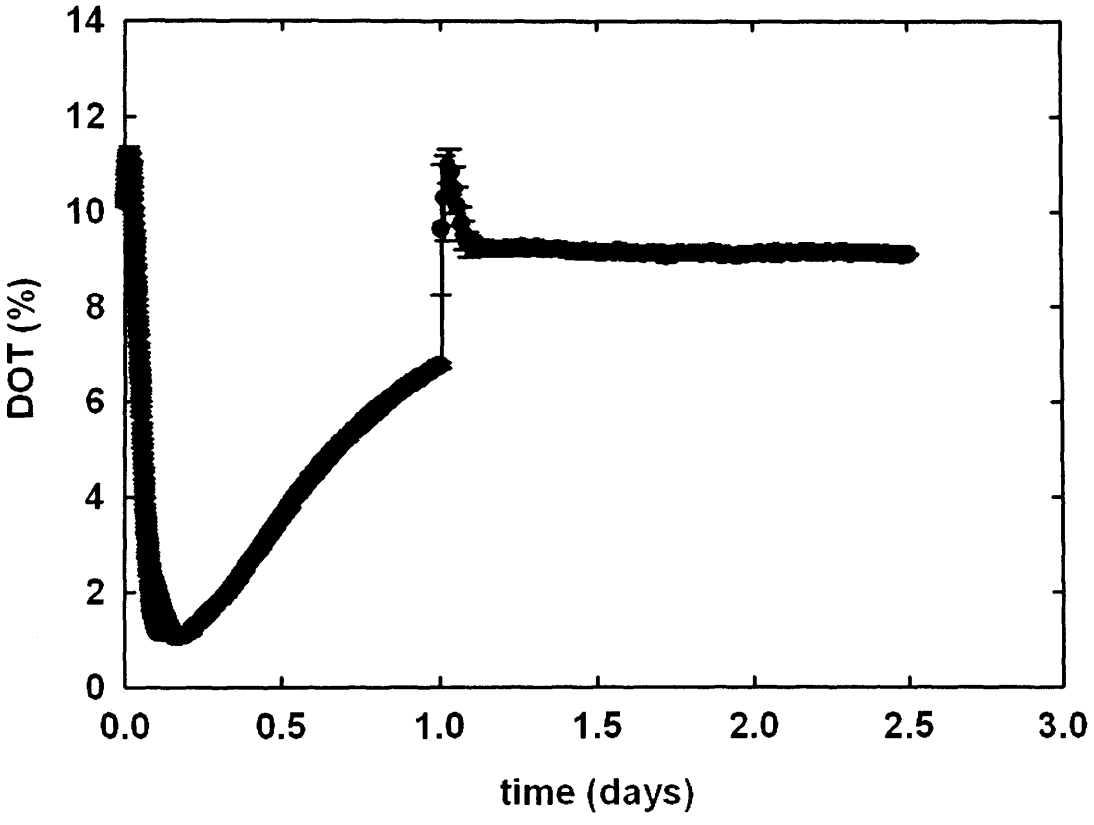

Figure 5.2: Oxygen profile at the bottom of newly formed alginate constructs with immobilized human dermal fibroblasts at a concentration of $7x10^6$ cells mL^{-1}. The constructs were formed in customized wells having cylindrical shapes with a volume of 7 µL and a thickness of 1 mm each. The fibroblasts were incubated in 1 mL static IMDM culture medium (37°C, 5% CO_2). The experimental data are represented as average ± standard error of measurements acquired from 3 customized wells operating simultaneously. The oxygen dropped to 1% within the first 3 hours, increased to 6 % after a day. Medium exchange was conducted after a day (peak in DOT). It then stabilized at 9.5 %. The initial transient decrease in oxygen concentration was accompanied by a decrease in the fraction of the proliferating cells. This metabolic shift can be attributed to the transition from a flask to a hydrogel based cell culture system (section 5.3).

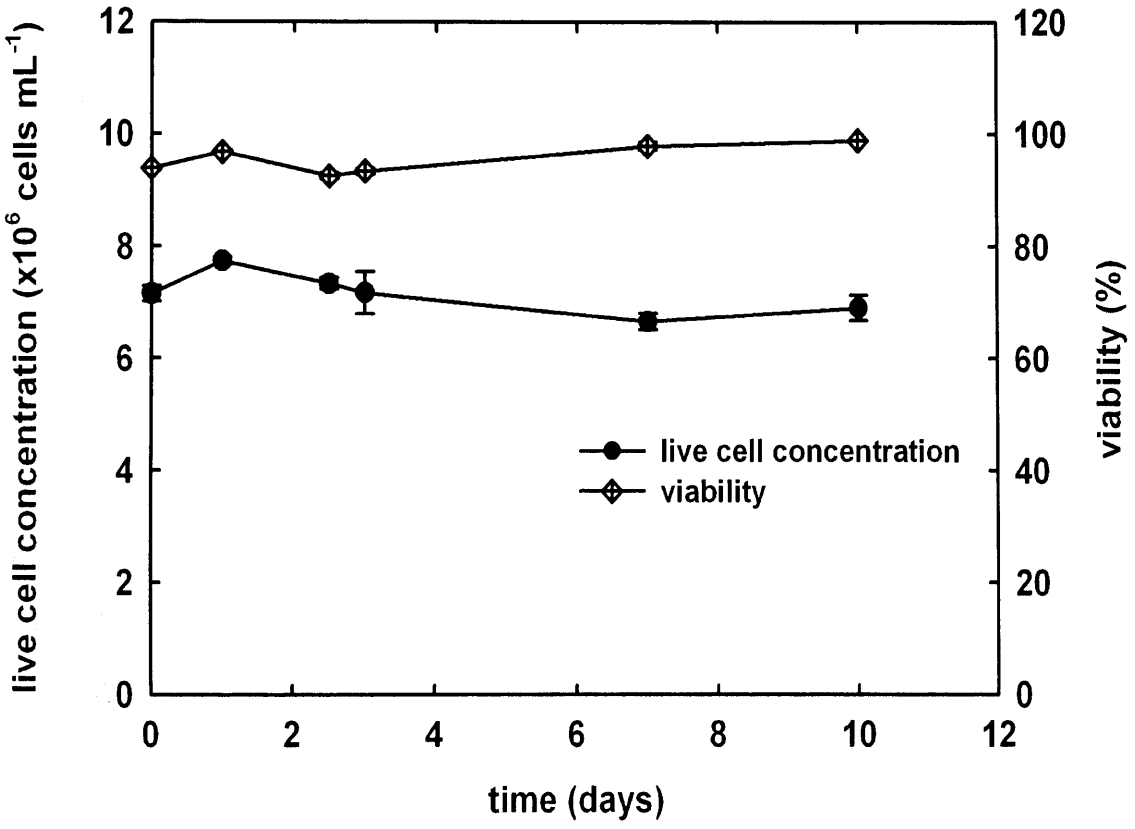

Figure 5.3: Live cell concentration (—●—) and viability (—◈—) profile of human dermal fibroblasts immobilized in alginate. The alginate constructs were formed in customized wells having cylindrical shapes with a volume of 7 µL and a thickness of 1 mm each. Following incubation for 2.5 days in 1 mL IMDM culture medium (37°C, 5% CO_2), the oxygen tension in the incubator was lowered transiently from 18.5% to 5% in order to calculate the oxygen effective diffusivity in the alginate construct and the oxygen uptake rate of the fibroblasts. Live cell concentration and viability data were acquired as described in section 2.3.2.2. Data are represented as average ± standard error of measurements acquired simultaneously from 3 customized wells. No change in the live cell concentration ($p=0.22$) and viability ($p=0.21$) at the 5% significance level was observed during the time period of 10 days.

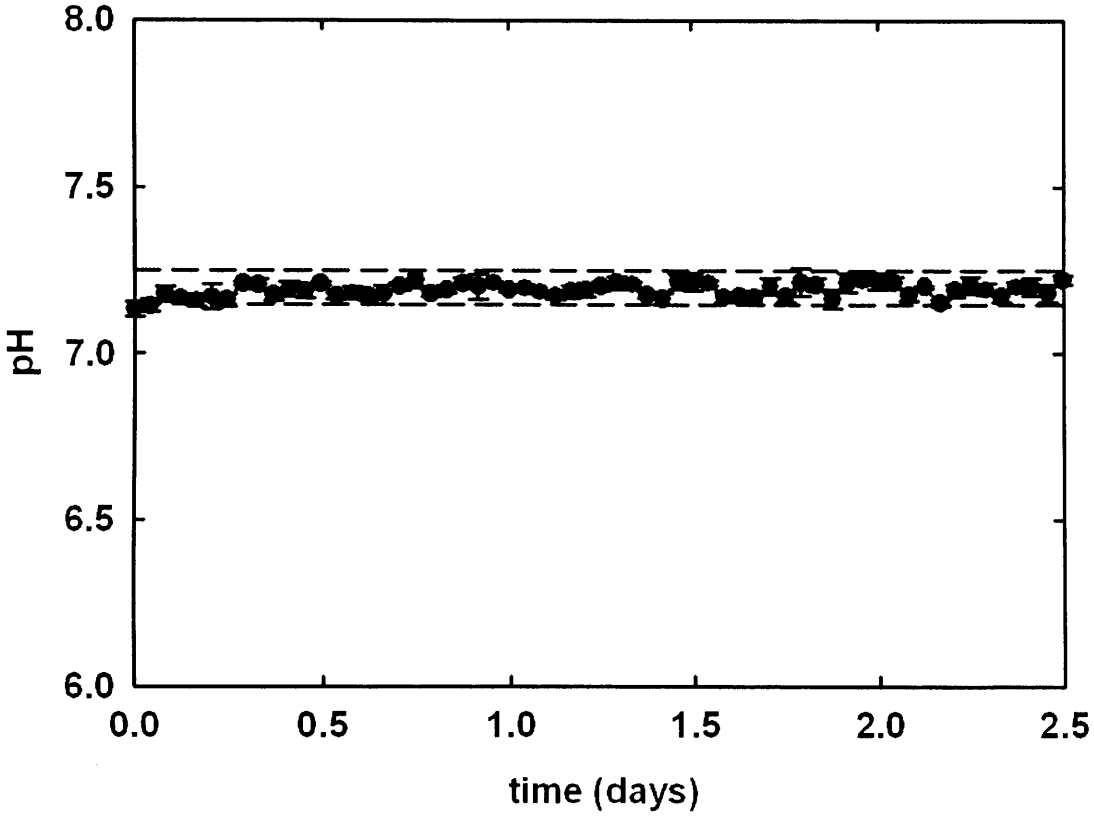

Figure 5.4: pH measurements were carried out from the bottom of alginate constructs with immobilized human dermal fibroblasts at a concentration of $8x10^6$ cells mL^{-1}. Each of the constructs was formed in a customized well and it had cylindrical shape with a volume of 7 µL. The cells were incubated in 1 mL static IMDM culture medium (37°C, 5% CO_2). HEPES, 25 mM, was used to buffer the medium. The pH of fresh complete medium was 7.18 ± 0.02 (3 independent measurements) and HEPES proved to be effective for maintaining constant pH. pH varies from 7.15 to 7.25 (dotted lines). The fibroblasts were reefed with fresh medium after a day with no effect on pH. The experimental data are represented as average ± standard error of measurements acquired from 3 customized wells.

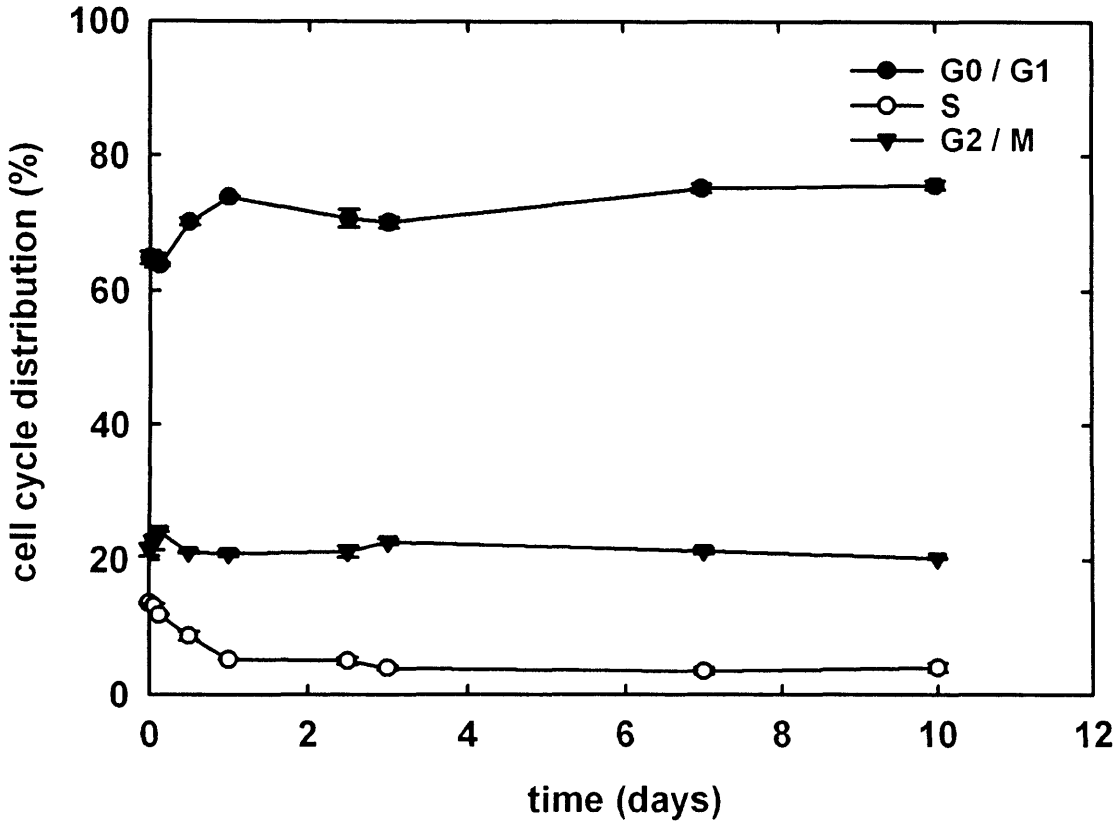

Figure 5.5: Cell cycle distribution of human dermal fibroblasts immobilized in cylindrical alginate constructs. Following incubation for 2.5 days in 1 mL IMDM culture medium (37°C, 5% CO_2), the oxygen tension in the incubator was lowered transiently from 18.5% to 5% in order to calculate the oxygen effective diffusivity in the alginate construct and the oxygen uptake rate of the fibroblasts. Data are represented as average ± standard error of measurements acquired from 3 customized wells. The fractions of cells in each phase of the cell cycle were calculated using ModFit-LT software. The initial fractions of G0 / G1, S, and G2 / M phase cells were 64.9 ± 0.9%, 13.6 ± 0.1% and 21.5 ± 0.9% respectively. The fractions remained stable for the first 3 hours ($p= 0.66$, $p= 0.31$ and $p= 0.56$ respectively) and then the fraction of G0 / G1 phase cells started increasing, accompanied by a decrease in the fraction of S phase cells. Their values stabilized after a day from the beginning of the incubation at 72.9 ± 1.4% ($p= 0.87$) and 4.3 ± 0.3% ($p= 0.97$).

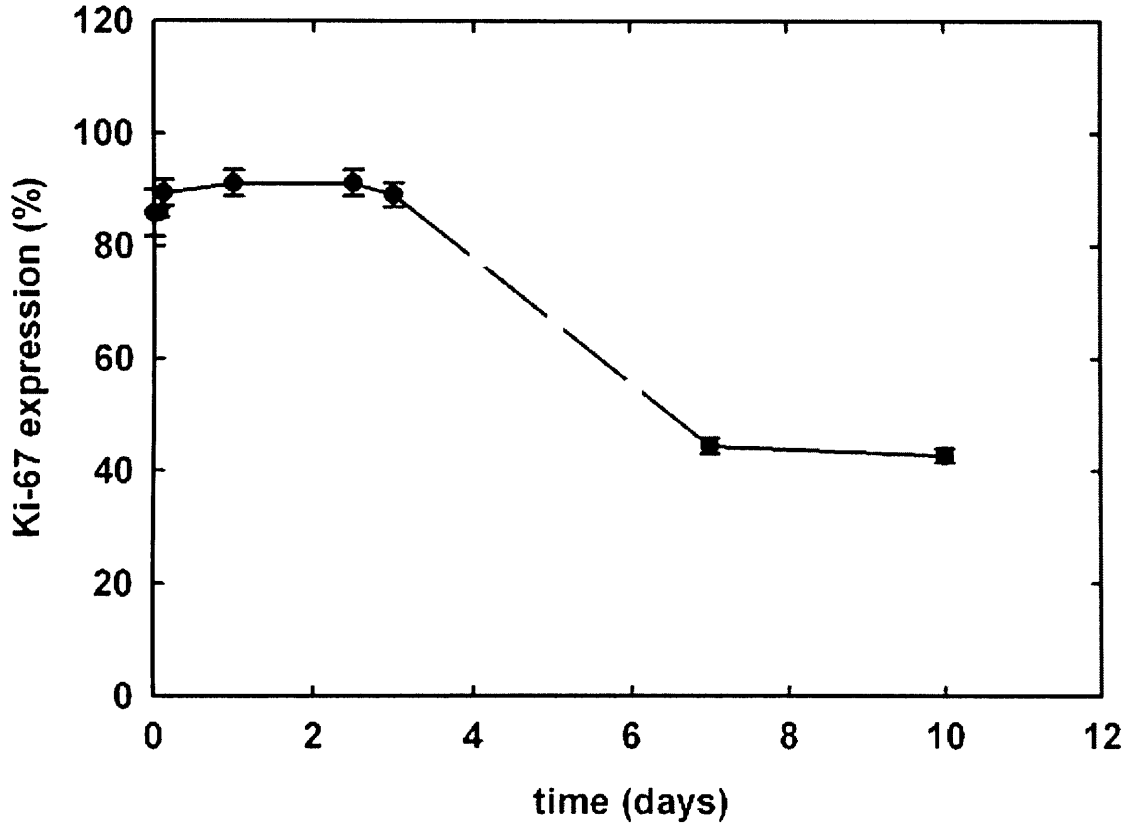

Figure 5.6: Percentage of Ki-67 expression of human dermal fibroblasts immobilized in cylindrical alginate constructs. Following incubation for 2.5 days in 1 mL IMDM culture medium (37°C, 5% CO_2), the oxygen tension in the incubator was lowered transiently from 18.5% to 5% in order to calculate the oxygen effective diffusivity in the alginate construct and the oxygen uptake rate of the fibroblasts. Data were assayed for Ki-67 expression using the Guava Express Plus application within the Guava cytometer software. They are represented as average ± standard error of measurements acquired simultaneously from 3 customized wells. The initial percentage of cells expressing Ki-67 was 85.8 ± 4.1%. However, it remained at this level for 3 days ($p= 0.54$) and then decreased to 44.4 ± 1.4% within a week.

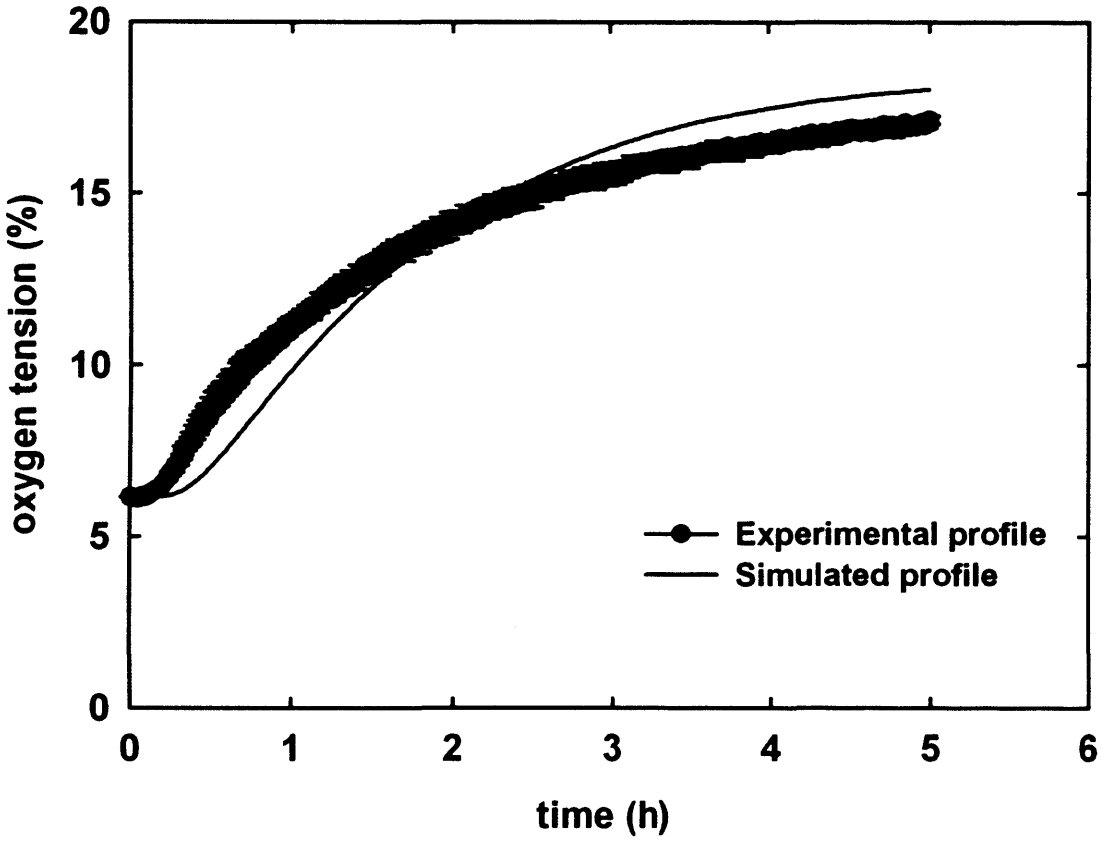

Figure 5.7: Oxygen profile at the bottom of alginate constructs without immobilized cells. The constructs were formed in customized wells having cylindrical shapes with a volume of 7 μL and a thickness of 1 mm each. IMDM culture medium, 1mL, was added to the customized well. Following incubation (static conditions, 37°C, 5% CO_2) for 2.5 days, the oxygen tension was lowered from 18.5% to 6%. When the system reached steady state conditions (6% at the bottom of the alginate construct), the oxygen tension in the incubator was increased back to 18.5% and the dissolved oxygen tension at the bottom of the construct was recorded by using the Presens device. The experimental data are represented as average ± standard error of measurements acquired simultaneously from 3 customized wells. The simulated data represent the best fit of the experimental data and they were obtained by combining Comsol Multiphysics and Matlab. The derived value for the oxygen effective diffusivity in alginate was 2.54 ± 0.57x10^{-9} m^2 s^{-1}. The average absolute relative error between experimental and predicted data was 6.83%.

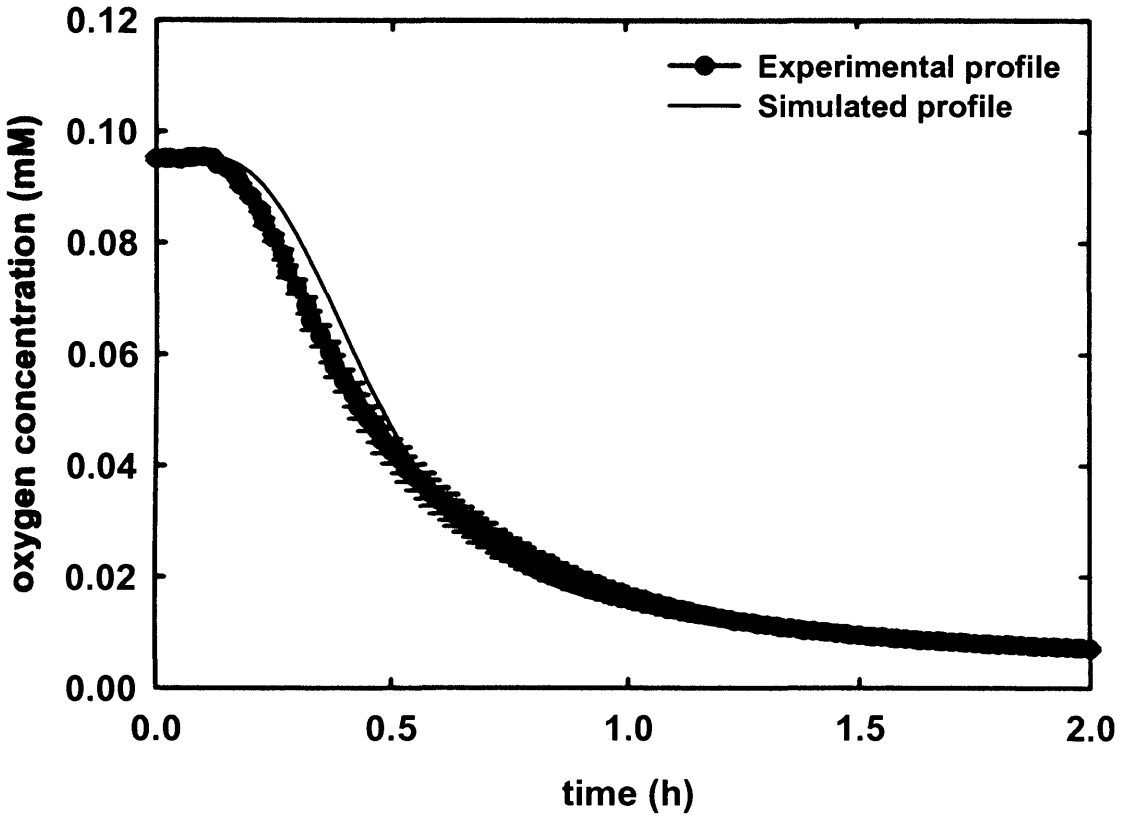

Figure 5.8: Experimental (—●—) and simulated (——) oxygen profiles at the bottom of an alginate construct with immobilized human dermal fibroblasts at a concentration of $7x10^6$ cells mL^{-1}. The construct was formed in a customized well and it had a cylindrical shape with a volume of 7 µL and a thickness of 1 mm. Following incubation in 1 mL static IMDM culture medium (37°C, 5% CO_2) for 2.5 days, the oxygen tension in the incubator was lowered from 18.5 to 5% and the oxygen concentration at the bottom of the alginate construct was recorded. The experimental data are represented as an average ± standard error of measurements acquired from 3 customized wells. The simulated data represent the best fit of the experimental data and they were obtained by combining Comsol Multiphysics and Matlab. The output values for oxygen effective diffusivity, oxygen uptake rate and Monod constant with their 95% confidence intervals were 0.95 ± $0.10x10^{-9}$ m^2 s^{-1}, 19.42 ± $0.07x10^{-18}$ mol $cell^{-1}$ s^{-1} and 11.93 ± $1.28x10^{-3}$ mM respectively. The average absolute relative error between experimental and predicted data is 7.3%.

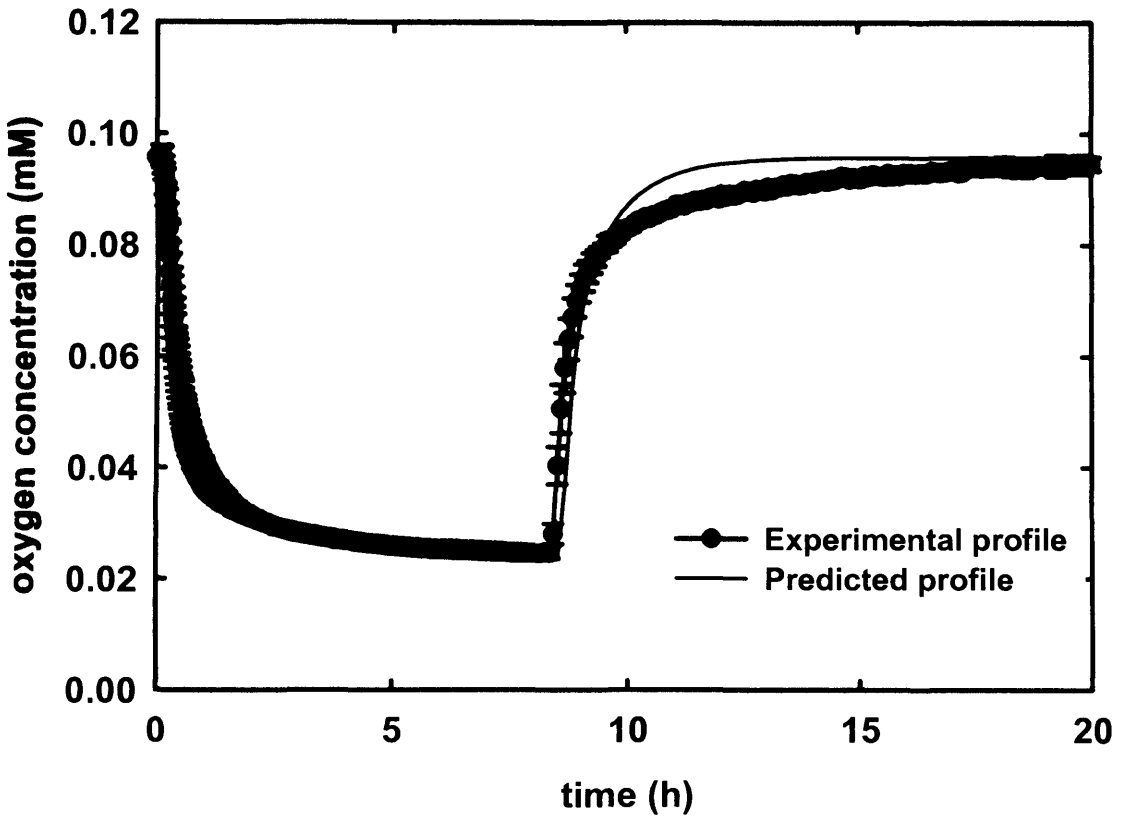

Figure 5.9: Validation of the calculation of the oxygen related parameters of the alginate / cell mix through the comparison of experimental (—●—) and predicted (——) oxygen profile at the bottom of alginate constructs with immobilized human dermal fibroblasts at a concentration of $7x10^6$ cells mL^{-1}. The constructs were formed in customized wells having cylindrical shapes with a volume of 7 µL and a thickness of 1 mm each. Following incubation in 1 mL static IMDM culture medium (37°C, 5% CO_2) for 1 day, the oxygen tension in the incubator was lowered from 18.5% to 10%, was kept at that level till the oxygen concentration at the bottom of the alginate construct was stable and then was increased back to 18.5%. The experimental data are represented as average ± standard error of measurements acquired from 3 customized wells. The predicted oxygen concentration profile has been generated by inserting the values of the oxygen related parameters of the alginate / cell mix in the mathematical model which describes the oxygen diffusion in the construct (section 5.2). The average absolute relative error between experimental and predicted data is 0.2%.

Chapter 6

Glucose / lactate transport and metabolism in alginate

6.1 Introduction

Alginate constructs with immobilized human dermal fibroblasts were formed in transwells in order to measure indirectly the effective diffusivities of glucose, and lactate as well as the glucose consumption and the lactate production rate. These values in conjunction with those for oxygen which were derived from the customized well experiments (previous chapter) help to inform better the construction of windows of operation as glucose and lactate should be balanced properly at the time as oxygen is delivered.

The constructs were formed at the bottom of the transwell within its conical frustum shape. The volume was 0.15 mL and the diameter of the top and bottom surface was 10.9 and 10.5 mm respectively. Their initial thickness was 1.34 mm stabilizing at 1.61 mm after 2 hours in culture medium (swelling effect) (Figure 6.1).

The transwells with the alginate constructs were placed in 24-format companion microplates and the immobilized fibroblasts were cultured in IMDM medium. The volume in each transwell was 0.75 mL and in each well 2.3 mL. Nutrient delivery and waste removal from the construct was enhanced by shaking the microplate at 220 rpm in an orbital shaker. The culture medium in each well and transwell was analysed over time for glucose and lactate. The effect of the cell concentration on the values of parameters of interest was studied by forming constructs with $25x10^6$ and $60x10^6$ cells mL^{-1}.

Constructs without cells were used as controls. Serum supplemented with 18 mM lactic acid and IMDM culture medium were used for the diffusivity studies. Mass transfer in the shake alginate constructs was considered to be diffusion dominant. The rate of diffusion of glucose and lactate is proportional to the

difference of their concentration in (i) the serum supplemented with lactic acid (initially 1mM glucose, 18 mM lactate) and (ii) IMDM medium (initially 23 mM glucose, 0.1 mM lactate). The proportionality is governed by the relative diffusion coefficient. The osmolarities of the serum supplemented with lactic acid and the IMDM culture medium were equal (Nova Bioprofile analyser measurements). Therefore there was no osmotic pressure difference between the serum in the well and the IMDM culture medium in transwell which could have affected the mass transfer in the alginate construct.

It is assumed in the mathematical models which simulated the above experiments that the mass transfer in the alginate constructs is governed by diffusion and that there is negligible external mass transfer resistance. However, flow of culture medium between the alginate constructs and the sidewalls of the transwell as well as interstitial flow through the alginate constructs caused by shaking can lead to a convection dominant mass transfer in them increasing potentially the value of the calculated effective diffusivity.

Additionally, the external resistance to mass transfer is regarded as lying in a layer to the top and bottom surface of the alginate construct. It is possible the resistance to mass transfer in this layer is the same order of magnitude as for the alginate construct. In this case by assuming in the mathematical models a negligible external mass transfer resistance, the simulated one is lying only within the alginate construct. Therefore, the calculated effective diffusivity will be lower than the real one in order for the simulated mass transfer resistance to be balanced with the increased real one which lies within the alginate construct and the two layers.

The assumption of a diffusion dominant mass transfer in the alginate construct with negligible external mass transfer resistance was validated by comparing the effective diffusivity of lactate in static and shake alginate constructs without immobilized cells.

All experiments for the calculations of the glucose and lactate based parameters were started 1.5 days after incubation and lasted at most 1.5 days.

This was necessary because the oxygen experiments (previous chapter) have shown that during that period there are no significant changes in the cell cycle distribution and Ki-67 expression, therefore unchanged metabolic behaviour can be assumed in the mathematical models.

The culture medium in each well and transwell was analysed over time for glucose and lactate. A computer program written in Matlab 7.1 and Comsol Multiphysics 3.3 yielded the effective diffusivities and the consumption / production rates of the species of interest in alginate as well as their confidence intervals by using the inverse method (section 2.7).

6.2 Mathematical models

6.2.1 Mathematical model for the simulation of glucose and lactate diffusion and their consumption and production in alginate constructs with human dermal fibroblasts

A mathematical model was set up to describe glucose consumption, lactate production and their diffusion in alginate constructs formed in transwells. The equations of the mathematical model will be presented for a representative species *n*, instead of giving them for glucose and lactate separately.

The assumptions of the mathematical model are the following:
(i) the system is isothermal, (ii) the cell suspension is homogenous, (iii) glucose consumption is independent of its concentration, (iv) lactate level does not affect the cell metabolism (v) there is no convective transport in the alginate construct, (vi) diffusion coefficient is a time independent parameter, (vii) diffusion obeys Fick's first law, (viii) there is no external mass transfer resistance (ix) the upper surface of the alginate construct is considered to be flat, (x) alginate does not contract, (xi) there is radial symmetry at the construct centreline, (xi) mass transfer resistance though the membrane of the transwell is negligible.

The equation of continuity for the species *n* states

$$\frac{\partial c}{\partial t} = D\left(\frac{1}{r}\frac{\partial}{\partial r}\left(r\frac{\partial c}{\partial r}\right) + \frac{\partial^2 c}{\partial z^2}\right) - qX \tag{6.1}$$

where *c* is the concentration, *X* is the cell concentration, *D* is the effective diffusivity in the alginate construct and *q* is the production rate.

The term $\frac{\partial c}{\partial t}$ represents the accumulation rate of mass of the species *n* per unit volume for the culture medium and the alginate construct respectively. The terms $D\left(\frac{1}{r}\frac{\partial}{\partial r}\left(r\frac{\partial c}{\partial r}\right) + \frac{\partial^2 c}{\partial z^2}\right)$ represents the mass transfer rate of species *n* per unit volume. The term *qX* represents the production rate of species *n* per unit volume based on cell metabolism. It is negative for the consumed glucose and positive for produced lactate.

No flux boundary conditions are applied at the alginate construct's centreline and at the transwell's sidewalls. At the construct's centreline there is radial symmetry and the transwell's sidewalls are impermeable to species *n*. Both boundary conditions are expressed mathematically by the following equation:

$$D\frac{\partial c}{\partial r} = 0 \tag{6.2}$$

It is assumed that there is no external mass transfer resistance so the concentration of species *n* at the top surface of the construct and the bottom surface of the transwell's membrane is equal to its bulk concentration.

The amount of glucose in the culture medium is given by the original level minus the amount which has been transferred to the alginate construct and consumed by the cells. Similarly, the amount of lactate in the culture medium is equal to its initial value plus the amount which has been produced in the alginate construct by the cells and transferred to the culture medium. The mass transfer occurs because the consumption or production by the cells creates a concentration gradient between construct and culture medium.

The continuity equation for the species *n* in the culture medium of the well and transwell states that

$$V(c - c_{t=0}) = -AD\frac{\partial c}{\partial z} \tag{6.3}$$

where V is the volume of the culture medium in transwell or well, c is the concentration of species n after time t, $c_{t=0}$ is the initial concentration of species n and A is the area of the top or bottom surface of the alginate construct.

The term $V(c - c_{t=0})$ represents the increase of the mass of species n and the term $-AD\frac{\partial c}{\partial z}$ represents the amount which is transferred from the alginate construct to the culture medium. Both terms are positive sign for the produced lactate and negative for the consumed glucose.

The initial concentration of species n in the transwell and in the well is its amount in the fresh culture medium. Concerning the alginate construct the initial condition is the concentration profile of species n developed after incubation for 1.5 days. An approximation of this profile is provided by solving the pseudo-steady state of the mathematical model developed above. The pseudo-steady state mathematical model assumes that the concentration profile of species n is changing very slowly within a narrow time interval because of the low consumption or production rate of species n by the cells. Therefore, the concentration profile is considered to be unchanged for the short time it takes to refill the well and transwell with fresh culture medium.

This mathematical model can be derived from the one developed above by cancelling the time dependent term of the equation 6.1 and the differential equation which describes the time profile of the bulk concentration of species n. The equation which gives the concentration profile is given below:

$$D(\frac{1}{r}\frac{\partial}{\partial r}(r\frac{\partial c}{\partial r}) + \frac{\partial^2 c}{\partial z^2}) - qX \tag{6.4}$$

The boundary condition for the centreline of the well and the sidewalls of the transwell is given by:

$$D\frac{\partial c}{\partial r} = 0 \tag{6.5}$$

The concentration of species n at the top and bottom surface of the construct is set equal to its bulk concentration.

6.2.2 Mathematical model for the simulation of substrate and metabolite diffusion in shaken alginate constructs without cells

A mathematical model with the same assumptions and boundary conditions with the one above was set up to simulate the glucose and lactate diffusion in alginate constructs without cells. The only difference was that there are no cell related assumptions and the term which describes mathematically the production of species *n* in alginate construct has been eliminated as there were no immobilized cells.

The continuity equation for species *n* in shake alginate construct is:

$$\frac{\partial c}{\partial t} = D\left(\frac{1}{r}\frac{\partial}{\partial r}\left(r\frac{\partial c}{\partial r}\right) + \frac{\partial^2 c}{\partial z^2}\right) \tag{6.6}$$

with the following equation as boundary condition for the alginate construct's centreline and for the transwell's sidewalls:

$$D\frac{\partial c}{\partial r} = 0 \tag{6.7}$$

The continuity equation for species *n* in the culture medium is:

$$V(c - c_{t=0}) = -AD\frac{\partial c}{\partial z} \tag{6.8}$$

6.2.3 Mathematical model for the simulation of lactate diffusion in static alginate constructs without cells

The assumptions of the mathematical model are all the same with the assumptions of the mathematical model which simulates the glucose and lactate diffusion in shake-alginate constructs without cells except the one which states that there is no external resistance in mass transfer. It has been replaced with the assumption of having diffusion dominant mass transfer in the culture medium in the transwell and in the supplemented with lactic acid serum in the well.

The continuity equation for species *n* in the static alginate constructs, in the culture medium in the transwell and in the serum supplemented with lactic acid in the well has the following form:

$$\frac{\partial c}{\partial t} = D(\frac{1}{r}\frac{\partial}{\partial r}(r\frac{\partial c}{\partial r}) + \frac{\partial^2 c}{\partial z^2}) \quad (6.9)$$

The boundary conditions for the well's and transwell's sidewalls and centrelines are given by the following equation:

$$D\frac{\partial c}{\partial r} = 0 \quad (6.10)$$

and the boundaries for the culture medium-air interphase, serum-air interphase as well as the bottom of the transwell are given by the following equation:

$$D\frac{\partial c}{\partial z} = 0 \quad (6.11)$$

6.2.4 Model solution and convergence

The above equations were solved by using Comsol Multiphysics 3.3 only (see section 2.6). One half of the system was modelled due to the symmetrical shape of the alginate constructs. The linear time dependent solver was used to simulate the diffusion and production of the species of interest in alginate constructs with and without immobilized cells. The linear stationary solver was used to simulate the concentration profile of the species of interest in the alginate construct after 1.5 days in the incubator.

The linear stationary solver was set up with a relative tolerance of 10^{-3} an absolute tolerance of 10^{-4}, a maximum number of 25 iterations, a minimum step size of 10^{-4} and a tolerance for convergence of 10^{-6}.

The construct, the liquid in the transwell and the liquid in the well was meshed with 408, 1196 and 1692 triangular elements respectively and they were refined to 104448, 306176 and 433152 triangular elements respectively to test the convergence of the solution. The concentration profile was agreed up to 4 significant figures with the one simulated by using the default mesh. The

calculations were always completed to convergence within the number of iterations specified.

The glucose and lactate related parameters with their confidence intervals were calculated by using the inverse method (section 2.7). It is implemented in Comsol Multiphysics wrapped around Matlab. Briefly, the Comsol models were saved as Matlab functions. Their input was the glucose and lactate related parameters and their output the average glucose and lactate concentrations in the well and transwell. The parameters were derived from minimisation of the sum of the squared differences between the experimental and the simulated average glucose and lactate concentration values. The Matlab optimization function "lsqnonlin" gave the values of the parameters and the Matlab Statistical Toolbox function "nparci" gave their confidence intervals. Each parameter evaluation took 1 h on a Pentium IV PC with a 3 GHz processor and 2 Gb memory.

6.3 Results and conclusions

The effective diffusivities of glucose and lactate were calculated in alginate constructs with and without immobilized cells (controls). The microplate with the transwells were shaken at 220 rpm in order to enhance the mass transfer of nutrients to the constructs. The effect of the cell concentration in the values of parameters of interest was studied by forming alginate constructs with $25x10^6$ and $60x10^6$ cells mL^{-1}. Glucose and lactate measurements at various times were undertaken from the medium in the well and transwell by using the Nova Bioprofile analyser. The medium in the well and transwell was weighted before the metabolic analysis in order to take account of evaporation.

It was assumed in the mathematical models which simulated the above experiments that mass transfer in the alginate constructs is governed by diffusion and that there is negligible external mass transfer resistance. These assumptions were validated by comparing the effective diffusivity of lactate in static and shaken alginate constructs without immobilized cells.

The calculated lactate effective diffusivity in static and shaken transwells were 1.43 ± 0.53 and 1.53 ± 0.10x10^{-9} m^2 s^{-1} respectively (Figure 6.5; Figure 6.6). These values are equal within the error of measurement therefore it can be concluded that diffusion is the dominant mean of mass transfer in the alginate constructs whether or not shaken i.e. the external mass transfer resistance is negligible. Additionally, it can be concluded that the rate of diffusion of glucose and lactate in alginate is equal to the rate of diffusion in the culture medium as the effective diffusivities of glucose and lactate in alginate are equal with the diffusivity values in culture medium which have been reported in the literature (Sengers et al, 2005).

No change in the live cell concentration was observed at the 5% significant level during the time period of experiments for the calculation of the glucose and lactate based parameters for the two cultures (p=0.13 for the alginate construct with 25x10^6 cells mL^{-1} and p=0.18 for the alginate construct with 60x10^6 cells mL^{-1}) (Figure 6.2; Figure 6.3). Additionally, there was no loss in viability for the two cultures during the time period of the experiments (p=0.13 for the alginate construct with 25x10^6 cells mL^{-1} and p=0.19 for the alginate construct with 60x10^6 cells mL^{-1}) (Figure 6.2; Figure 6.3).

The glucose effective diffusivity was 0.93 ± 0.12x10^{-9} m^2 s^{-1} in alginate constructs without cells, 0.68 ± 0.18x10^{-9} m^2 s^{-1} in alginate constructs with 25x10^6 cells mL^{-1} and 0.31 ± 0.07x10^{-9} m^2 s^{-1} in alginate constructs with 60x10^6 cells mL^{-1} (Figure 6.4; Figure 6.7; Figure 6.9). The lactate effective diffusivity was 1.53 ± 0.10x10^{-9} m^2 s^{-1} in alginate constructs without cells, 0.88 ± 0.26x10^{-9} m^2 s^{-1} in alginate constructs with 25x10^6 cells mL^{-1} and 0.41 ± 0.09x10^{-9} cells mL^{-1} for the alginate constructs with 60x10^6 cells mL^{-1} (Figure 6.5; Figure 6.8; Figure 6.10).

The values of the glucose and lactate effective diffusivities decrease as the cell concentration in alginate increases. This can be attributed to ECM and cells occupying space within the alginate construct. The higher the cell concentration in the alginate constructs is the less the space available for diffusion will be.

Therefore, the glucose and lactate effective diffusivities have their highest values in alginate constructs without cells.

The glucose consumption rate of the human dermal fibroblasts was 64 ± $2x10^{-18}$ mol cell s^{-1} in the alginate constructs with $60x10^6$ cells mL^{-1} and 77 ± $2x10^{-18}$ mol cell s^{-1} in the alginate constructs with $25x10^6$ cells mL^{-1} (Figure 6.7; Figure 6.9). Concerning the lactate production rate it was 130 ± $5x10^{-18}$ mol cell s^{-1} in the alginate constructs with $25x10^6$ cells mL^{-1} and 150 ± $4x10^{-18}$ mol cell s^{-1} in the alginate constructs with $60x10^6$ cells mL^{-1} (Figure 6.8; Figure 6.10).

The glucose consumption per cell is higher in alginate constructs with $25x10^6$ cells mL^{-1} than in alginate constructs with $70x10^6$ cells mL^{-1}. The lower metabolic activity of the fibroblasts immobilized in alginate at the concentration of $70x10^6$ cells mL^{-1} can be attributed to anaerobic metabolism. The aerobicity of the cell culture can be evaluated by calculating the molar ratio of lactate over glucose. This ratio is approximately 1 for completely aerobic cell metabolism and approximately 2 for completely anaerobic metabolism. It is 1.6 in the case of alginate constructs with $25x10^6$ cells mL^{-1} which indicates aerobic metabolism and 2.2 in the case of $60x10^6$ cells mL^{-1} which indicates anaerobic metabolism.

Similar results have been reported for cardiomyocytes immobilized in PGA constructs cultivated in mixed and static flasks. It was demonstrated that the aerobic metabolism (lactate to glucose molar ratio ≈ 1.5) in the mixed flasks yielded a higher glucose consumption rate per cell than the anaerobic metabolism (lactate to glucose molar ratio >2) in the static flasks (Carrier et al., 1999).

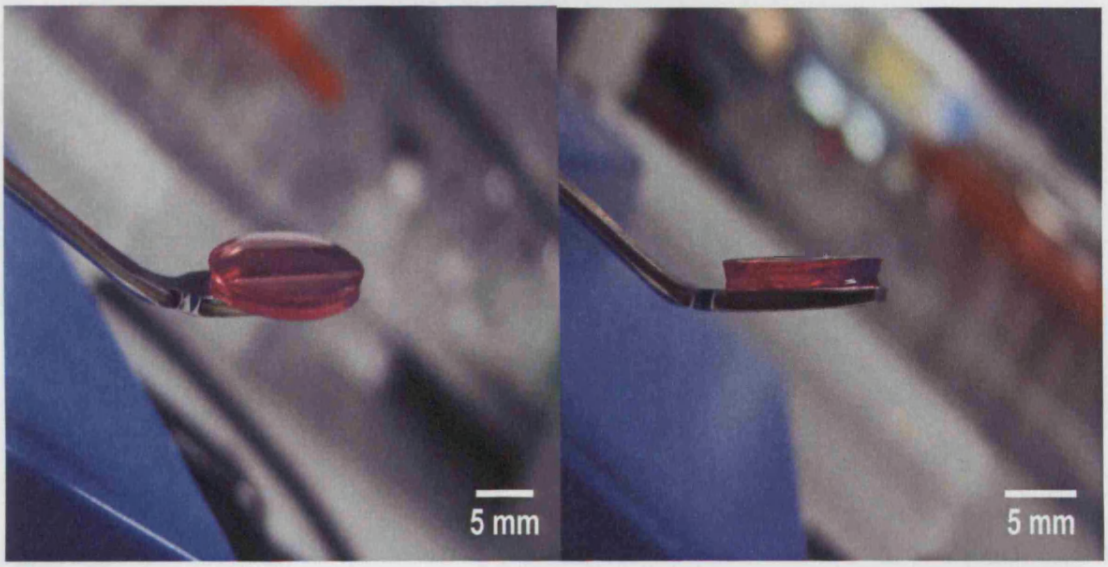

Figure 6.1: Photos of an alginate construct without immobilized cells formed in a transwell and incubated for 1.5 days (37°C, 5% CO_2). The constructs had been used for the measurement of glucose and lactate effective diffusivity in an alginate / cell mix and the glucose consumption and lactate production rates of human dermal fibroblasts. The photos were analysed with the ImageJ software v. 1.37 (National Institute of Health, USA) in order to obtain the dimensions of the constructs. Their volume was 0.15 mL and the diameter of their top and bottom surface was 10.9 and 10.5 mm respectively. The transwells with the alginate constructs were placed in 24-format companion microplates and the immobilized fibroblasts were cultured in IMDM medium (37°C, 5% CO_2). The volume of the culture medium in each transwell was 0.75 mL and in each well 2.3 mL. Nutrient delivery and waste removal from the construct was enhanced by shaking the microplate at 220 rpm in an orbital shaker. Their initial thickness was 1.34 mm stabilizing at 1.64 mm after 2 hours in culture medium (swelling effect). The culture medium in each well and transwell was analysed over time for glucose and lactate. The values of the effective diffusivities and the consumption / production rates of the species of interest in alginate as well as their confidence intervals were provided by a computer program written in Matlab 7.1 and Comsol Multiphysics 3.3 (section 2.6).

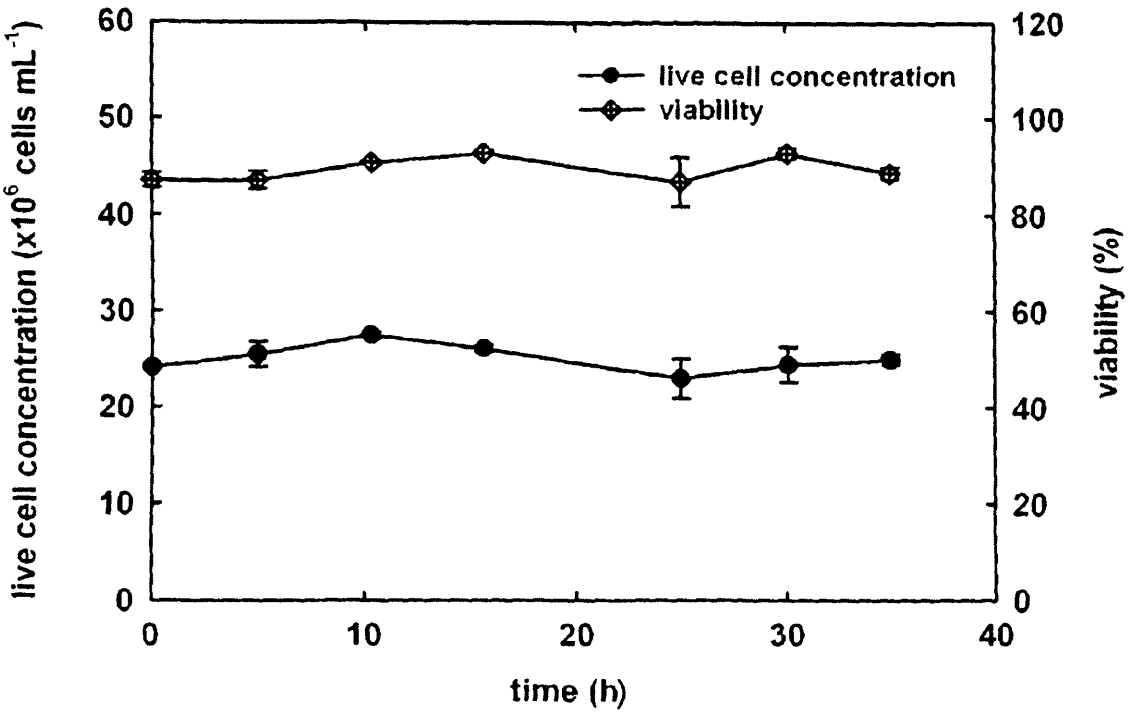

Figure 6.2: Live cell concentration (—●—) and viability (—◈—) profile of human dermal fibroblasts immobilized in alginate at the concentration of $25x10^6$ cells mL^{-1}. The alginate constructs were formed in transwells having a conical frustum shape, a volume of 0.15 mL and a thickness of 1.64 mm each. The volume of IMDM culture medium in each transwell was 0.75 mL and in each well 2.3 mL. Nutrient delivery and waste removal from the construct was enhanced by shaking the microplate at 220 rpm in an orbital shaker. The immobilized cells were refed after 1.5 days incubation at 37°C in 5% CO_2. Three constructs were sacrificed at time intervals for cell counts and viability determination. The data acquisition was achieved by using the Guava EasyCyte cytometer (section 2.3.2). They are represented as average ± standard error of 3 independent measurements. The average cell concentration and viability was 25.1 ± 0.6 cells mL^{-1} and 89.5 ± 1.0% and respectively. No change in the live cell concentration ($p=0.13$) and viability ($p=0.48$) at the 5% significance level was observed during the time period of 35 hours.

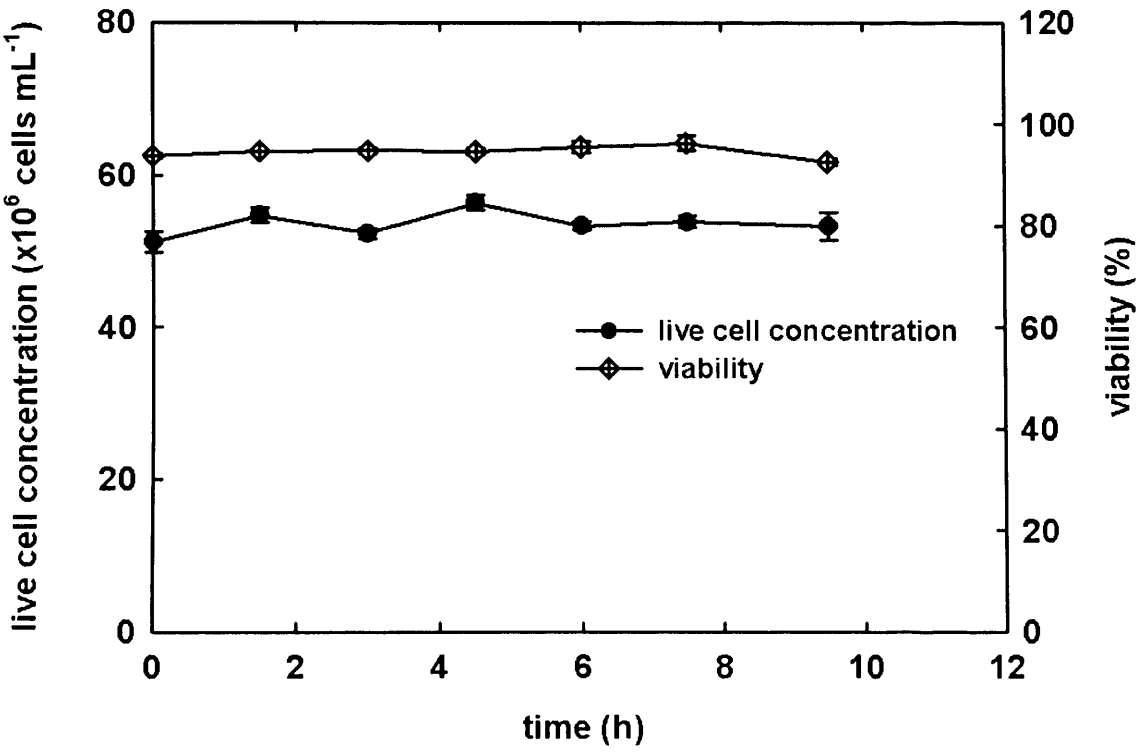

Figure 6.3: Live cell concentration (—●—) and viability (—◈—) profile of human dermal fibroblasts immobilized in alginate at the concentration of $60x10^6$ cells mL^{-1}. The alginate constructs were formed in transwells having a conical frustum shape, a volume of 0.15 mL and a thickness of 1.64 mm each. The volume of IMDM culture medium in each transwell was 0.75 mL and in each well 2.3 mL. Nutrient delivery and waste removal from the construct was enhanced by shaking the microplate at 220 rpm in an orbital shaker. The immobilized cells were refed after 1.5 days incubation at 37°C in 5% CO_2. Three constructs were sacrificed at time intervals for cell counts and viability determination. The data acquisition was achieved by using the Guava EasyCyte cytometer (section 2.3). They are represented as average ± standard error of 3 independent measurements. The average cell concentration and viability was 53.59 ± 0.93 cells mL^{-1} and 94.64 ± 0.60% and respectively. No change in the live cell concentration ($p=0.18$) and viability ($p=0.19$) at the 5% significance level was observed during the time period of 9.5 hours.

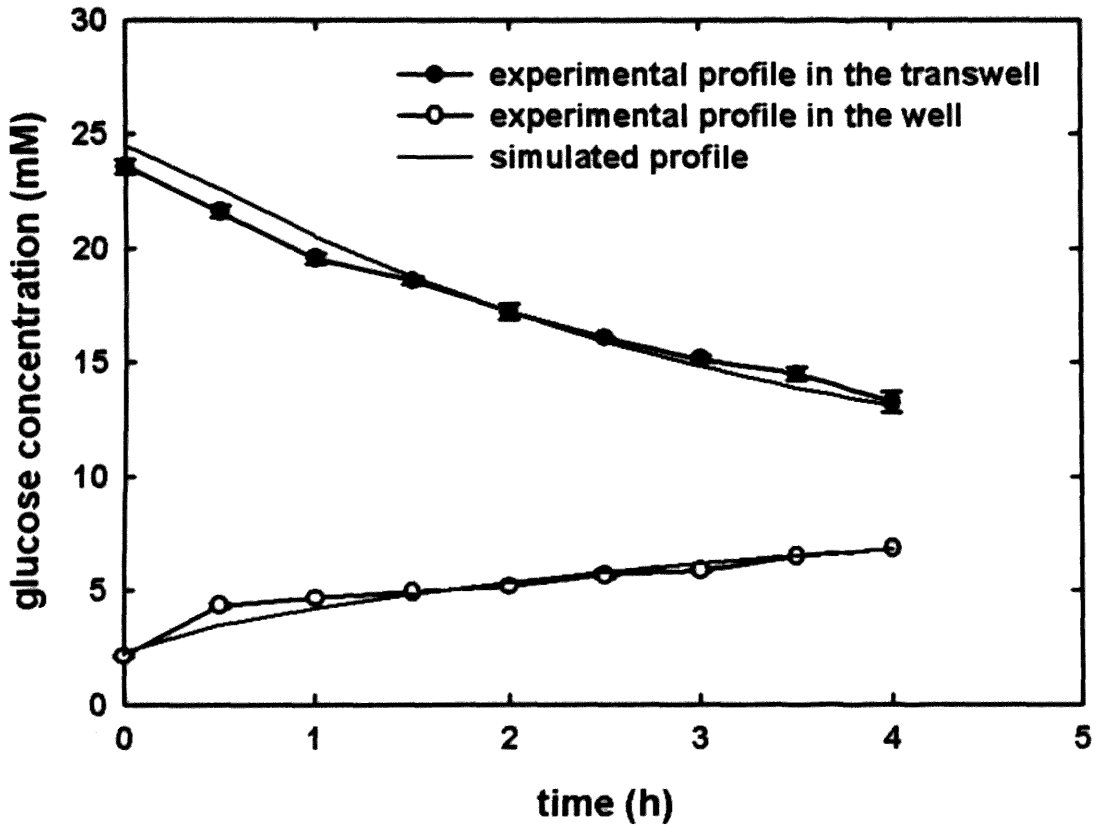

Figure 6.4: Glucose concentration profile for the evaluation of effective glucose diffusivity in alginate constructs without immobilized cells. The alginate constructs were formed in transwells having a conical frustum shape, a volume of 0.15 mL and a thickness of 1.64 mm each. The constructs had been incubated in IMDM medium for 1.5 days before the diffusivity experiment. Serum and IMDM culture medium were used for the diffusivity measurements. They have different glucose concentrations but the same osmolarity, therefore its diffusion through the alginate constructs was attributed only to the difference of its concentration between serum and IMDM medium. The volume of IMDM medium in each transwell was 0.75 mL and the volume of serum in each well was 2.3 mL. The microplate was shaking at 220 rpm in an orbital shaker. Glucose measurements at various instants were undertaken from the serum in the well and the IMDM medium in the transwell by using the Nova Bioprofile analyser. They are represented as average ± standard error of 3 independent measurements. The glucose effective diffusivity was $0.93 \pm 0.10 \times 10^{-9}$ m^2 s^{-1}. The average absolute error of the measurements was 6.3%.

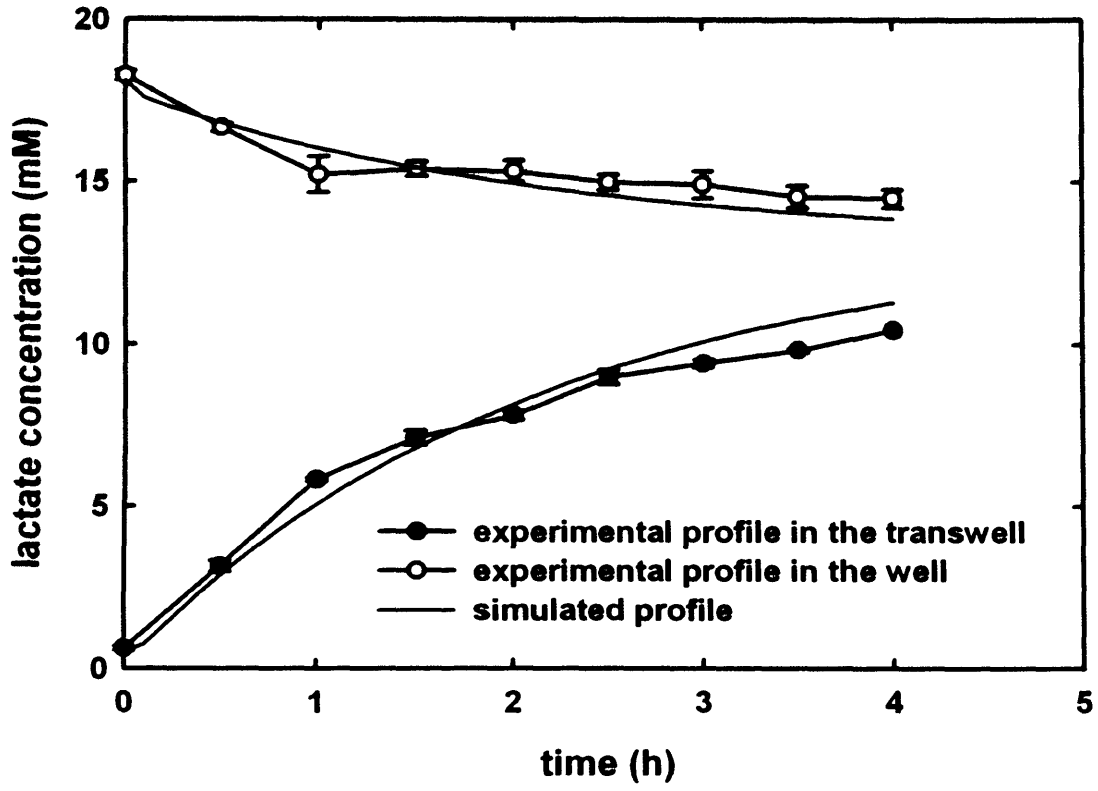

Figure 6.5: Lactate concentration profile for the evaluation of effective lactate diffusivity in alginate constructs without immobilized cells. The alginate constructs were formed in transwells having a conical frustum shape, a volume of 0.15 mL and a thickness of 1.64 mm each. The constructs had been incubated in IMDM medium for 1.5 days before the diffusivity experiment. Serum supplemented with 18 mM lactic acid and IMDM culture medium was used for the diffusivity measurements. They have different lactate concentrations but the same osmolarity, therefore its diffusion through the alginate constructs was attributed only to the difference of its concentration between serum and IMDM medium. The volume of IMDM medium in each transwell was 0.75 mL and the volume of serum in each well was 2.3 mL. The microplate was shaking at 220 rpm in an orbital shaker. Lactate measurements at various instants were undertaken from the serum in the well and the IMDM medium in the transwell by using the Nova Bioprofile analyser. They are represented as average ± standard error of 3 independent measurements. The lactate effective diffusivity was $1.53 \pm 0.10 \times 10^{-9}$ m^2 s^{-1}. The average absolute error of the measurements was 7.1%.

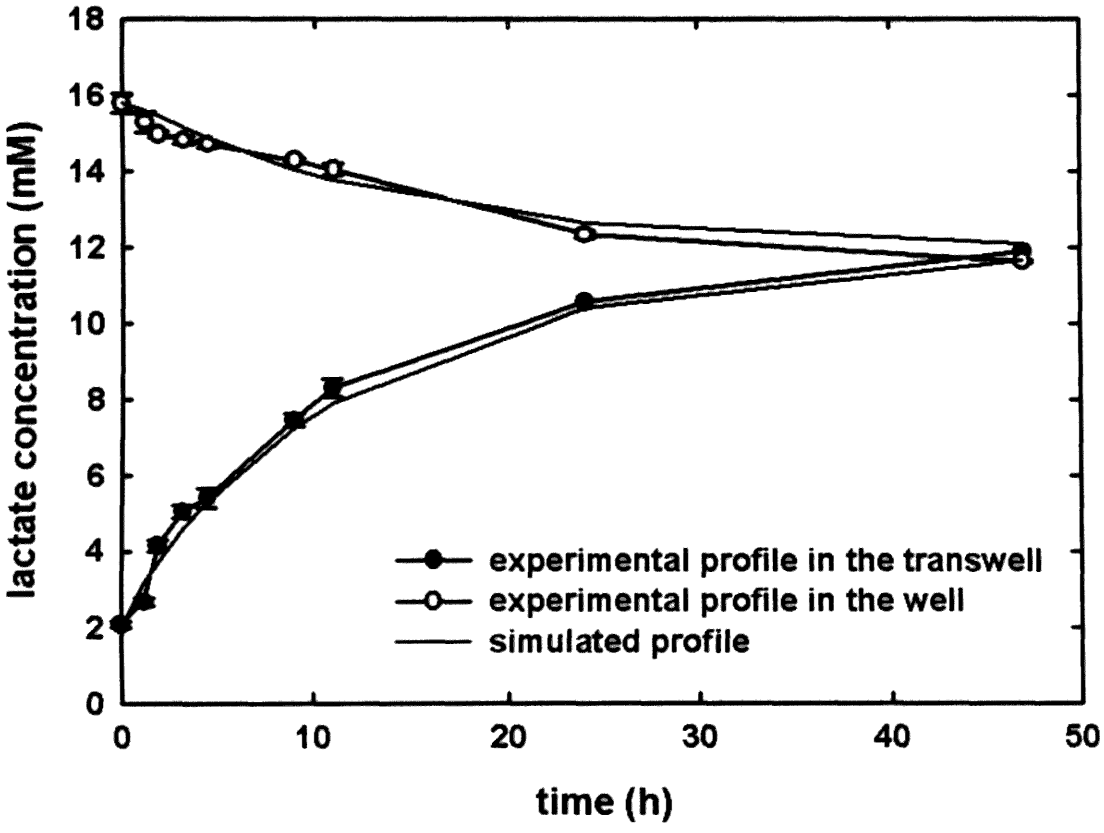

Figure 6.6: Lactate concentration profile for the evaluation of effective lactate diffusivity in static alginate constructs without immobilized cells. The alginate constructs were formed in transwells having a conical frustum shape, a volume of 0.15 mL and a thickness of 1.64 mm each. The constructs had been incubated in IMDM medium for 1.5 days before the diffusivity experiment. Serum supplemented with 18 mM lactic acid and IMDM culture medium was used for the diffusivity measurements. They have different lactate concentrations but the same osmolarity, therefore its diffusion through the alginate constructs was attributed only to the difference of its concentration between serum and IMDM medium. The volume of IMDM medium in each transwell was 0.75 mL and the volume of serum in each well was 2.3 mL. Lactate measurements at various instants were undertaken from the serum in the well and the IMDM medium in the transwell by using the Nova Bioprofile analyser. They are represented as average ± standard error of 3 independent measurements. The lactate effective diffusivity was $1.43 \pm 0.53 \times 10^{-9}$ $m^2 s^{-1}$. The average absolute error of the measurements was 5.0%.

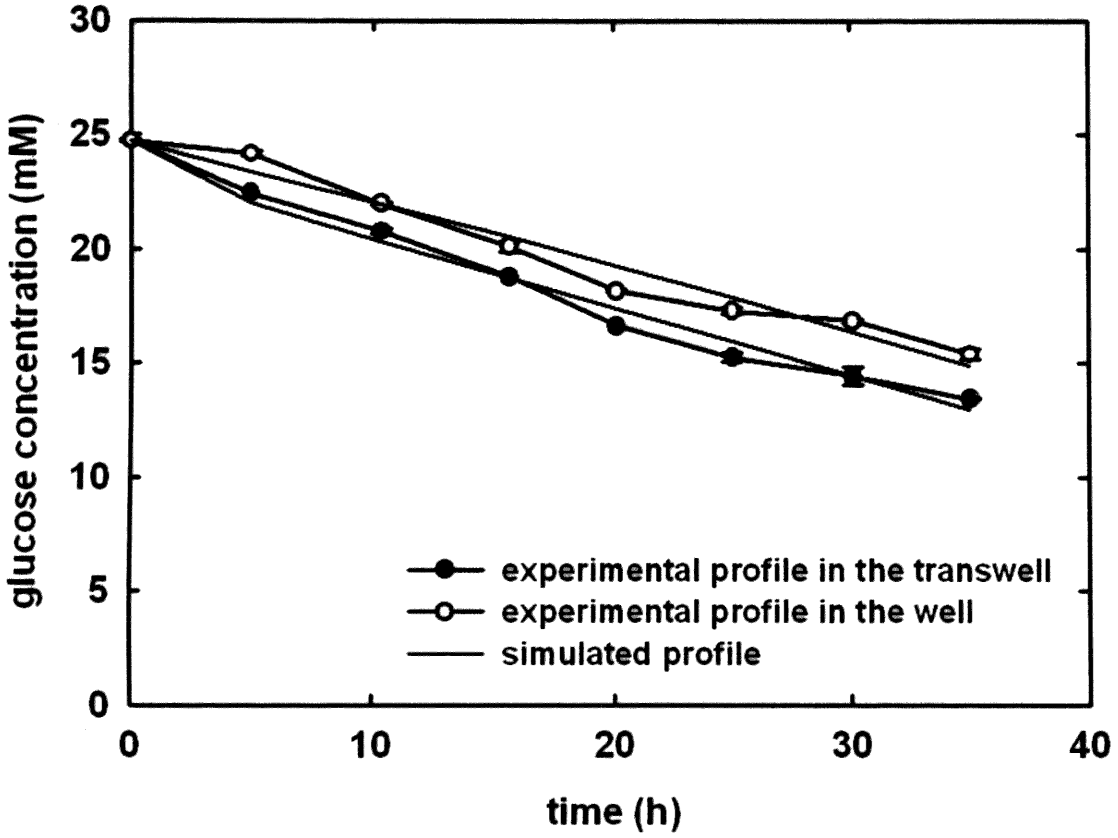

Figure 6.7: Glucose concentration profile of human dermal fibroblasts immobilized in alginate at the concentration of $25x10^6$ cells mL^{-1}. The alginate constructs had been formed in transwells having a conical frustum shape, a volume of 0.15 mL and a thickness of 1.64 mm each. The constructs had been incubated in IMDM medium at 37°C in 5% CO_2 for 2.5 days before the experiment. The volume of IMDM medium in each transwell and well was 0.75 and 2.3 mL respectively. Nutrient delivery and waste removal from the constructs was enhanced by shaking the microplate at 220 rpm in an orbital shaker. Glucose measurements at various instants were undertaken from the medium in the well and transwell by using the Nova Bioprofile analyser. Data are represented as average ± standard error of 3 independent measurements. The glucose effective diffusivity in alginate was $0.68 \pm 0.18x10^{-9}$ m^2 s^{-1} and the glucose consumption rate of the fibroblasts was $77 \pm 2x10^{-18}$ mol $cell^{-1}$ s^{-1}. The average absolute error of measurements was 3.0%.

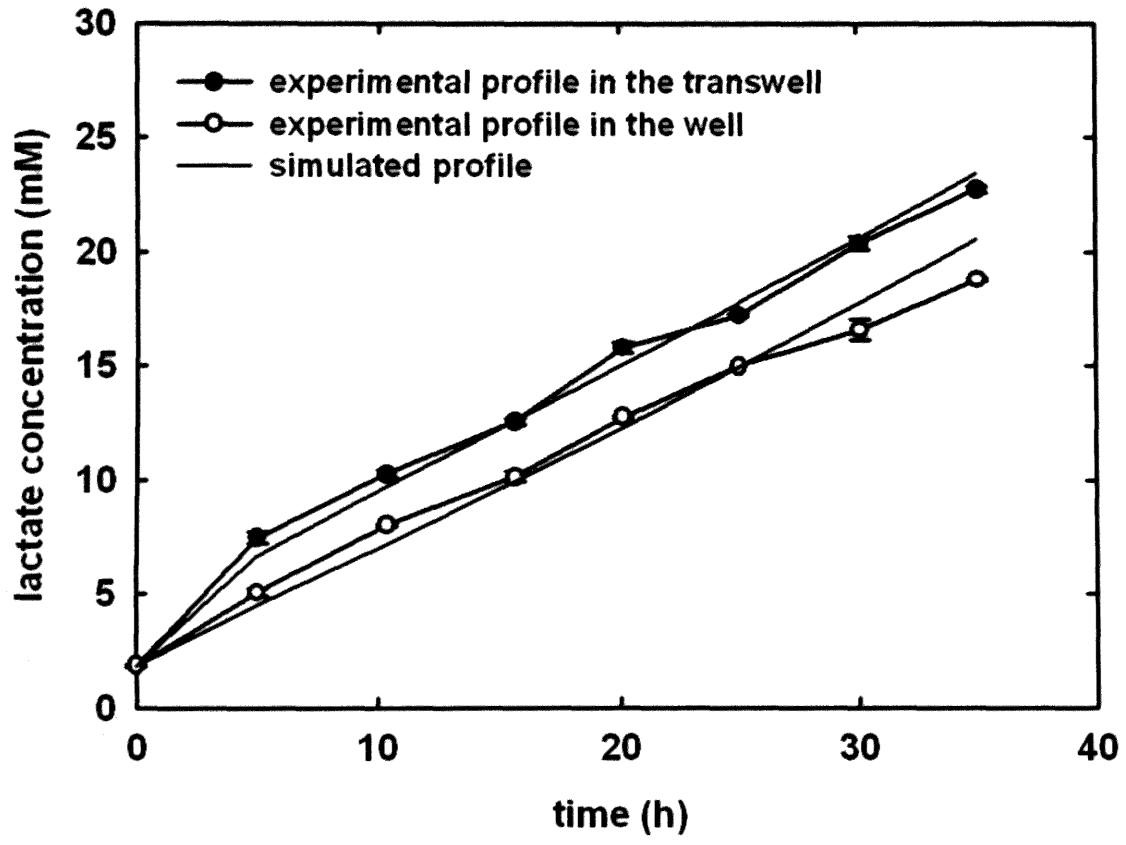

Figure 6.8: Lactate concentration profile of human dermal fibroblasts immobilized in alginate at the concentration of $25x10^6$ cells mL^{-1}. The alginate constructs had been formed in transwells having a conical frustum shape, a volume of 0.15 mL and a thickness of 1.64 mm each. The constructs had been incubated in IMDM medium at 37°C in 5% CO_2 for 2.5 days before the experiment. The volume of IMDM medium in each transwell and well was 0.75 and 2.3 mL respectively. Nutrient delivery and waste removal from the constructs was enhanced by shaking the microplate at 220 rpm in an orbital shaker. Lactate measurements at various instants were undertaken from the medium in the well and transwell by using the Nova Bioprofile analyser. Data are represented as average ± standard error of 3 independent measurements. The lactate effective diffusivity in alginate was $0.88 \pm 0.26x10^{-9}$ m^2 s^{-1} and the lactate production rate of the fibroblasts was $130 \pm 5x10^{-18}$ mol $cell^{-1}$ s^{-1}. The average absolute error of measurements was 7.5%.

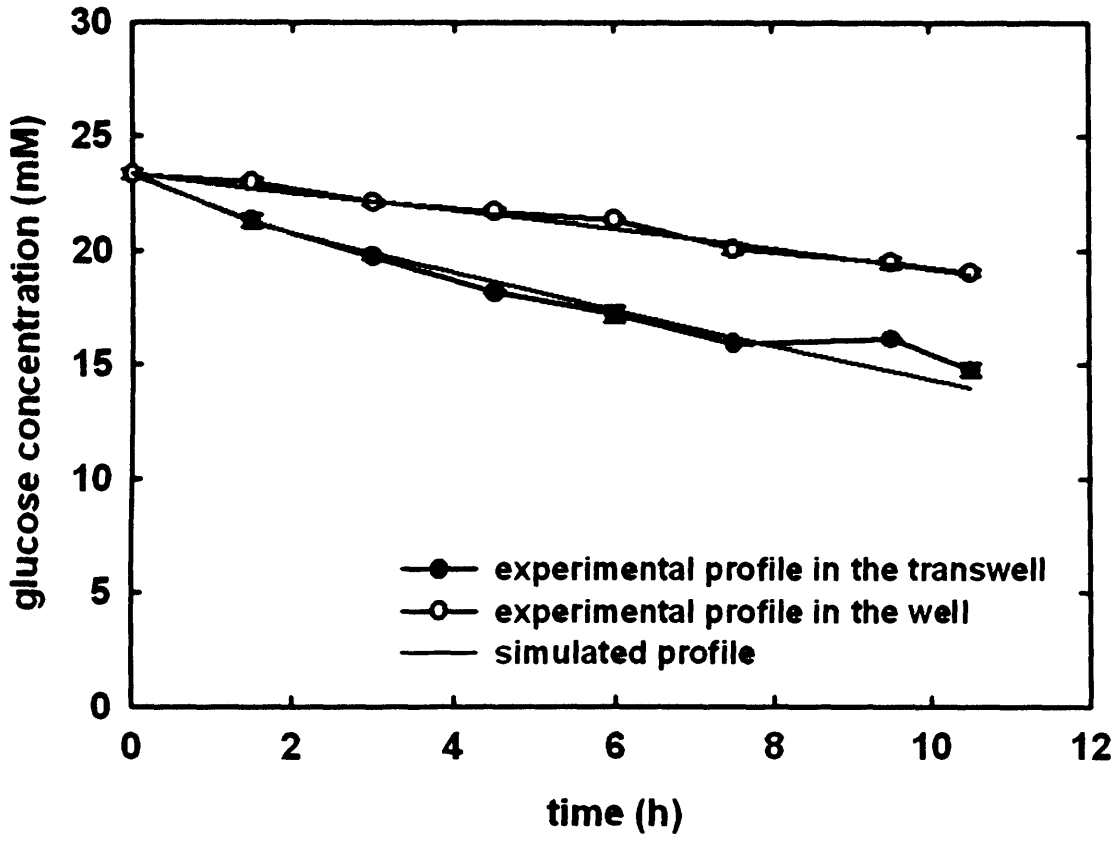

Figure 6.9: Glucose concentration profile of human dermal fibroblasts immobilized in alginate at the concentration of $60x10^6$ cells mL^{-1}. The alginate constructs had been formed in transwells having a conical frustum shape, a volume of 0.15 mL and a thickness of 1.64 mm each. The constructs had been incubated in IMDM medium at 37°C in 5% CO_2 for 2.5 days before the experiment. The volume of IMDM medium in each transwell and well was 0.75 and 2.3 mL respectively. Nutrient delivery and waste removal from the constructs was enhanced by shaking the microplate at 220 rpm in an orbital shaker. Glucose measurements at various instants were undertaken from the medium in the well and transwell by using the Nova Bioprofile analyser. Data are represented as average ± standard error of 3 independent measurements. The glucose effective diffusivity in alginate was $0.31 \pm 0.07x10^{-9}$ m^2 s^{-1} and the glucose consumption rate of the fibroblasts was $64 \pm 3x10^{-18}$ mol $cell^{-1}$ s^{-1}. The average absolute error of measurements was 1.7%

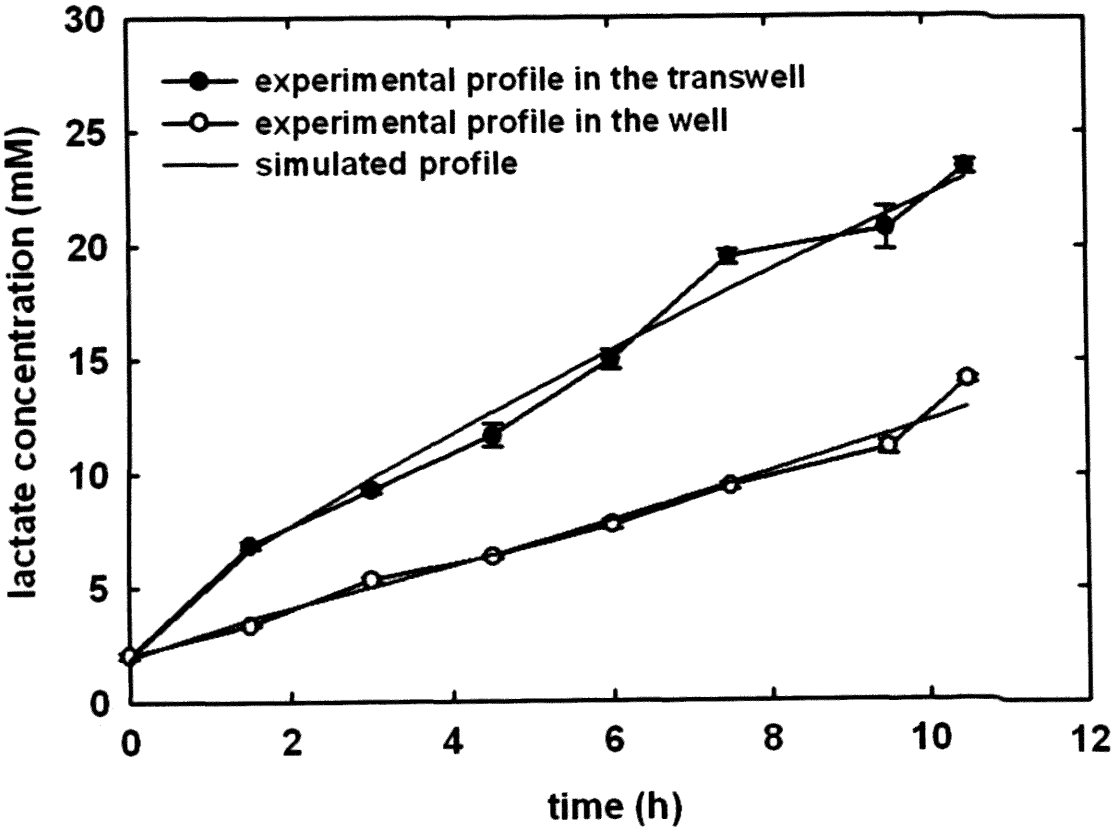

Figure 6.10: Lactate concentration profile of human dermal fibroblasts immobilized in alginate at the concentration of $60x10^6$ cells mL^{-1}. The alginate constructs had been formed in transwells having a conical frustum shape, a volume of 0.15 mL and a thickness of 1.64 mm each. The constructs had been incubated in IMDM medium at 37°C in 5% CO_2 for 1.5 days before the experiment. The volume of IMDM medium in each transwell and well was 0.75 and 2.3 mL respectively. Nutrient delivery and waste removal from the constructs was enhanced by shaking the microplate at 220 rpm in an orbital shaker. Lactate measurements at various instants were undertaken from the medium in the well and transwell by using the Nova Bioprofile analyser. Data are represented as average ± standard error of 3 independent measurements. The lactate effective diffusivity in alginate was $0.41 \pm 0.09x10^{-9}$ m^2 s^{-1} and the lactate production rate of the fibroblasts was $150 \pm 5x10^{-18}$ mol $cell^{-1}$ s^{-1}. The average absolute error of measurements was 6.4%.

Chapter 7

Final conclusions and future work

7.1 Final Conclusions

In this thesis a generic bioreactor design for tissue engineering applications was presented to cover the need for a robust, automated manufacturing process for the production of engineered tissues. A critical issue is the sufficient supply of oxygen and substrates and the efficient removal of metabolites without inhibiting the cell proliferation in the scaffold.

In Chapters 3 and 4 models of transport phenomena were developed in order to predict the fluid flow, and the mass transfer requirements of a bioreactor for the production of artificial tissues. Specifically, in Chapter 3 windows of operation were used to visualize rapidly the variable region in which it is possible to supply oxygen at a sufficient rate to support cell proliferation while maintaining the oxygen level above the prescribed minimum. The effect of each variable on the critical velocity in particular was addressed.

It was shown that they are more sensitive to changes in the tube wall thickness than in the length and effective oxygen diffusivity. It was concluded that the area of the window of operation can be increased either by increasing the feed rate to the reactor or by increasing the recycle rate in the artificial artery. The former will raise the operational cost of the reactor whereas the latter will lead to retention of metabolites inhibiting the metabolism of the cells and consequently increasing the time for the artery to be ready for implantation.

It was demonstrated that the higher the critical flow rate the smaller the difference between the maximum and minimum concentration in the artificial artery will be, assuming no changes in the metabolic behaviour of the cells for the range of the oxygen concentrations studied.

In Chapter 4 the effect of feed and recycle rate on the substrate and metabolite concentration profiles and cell proliferation in the artificial artery was addressed. Simulations showed that the higher the feed rate the sooner the construct will obtain the required cell concentration in order to be ready for implantation. Additionally, it was demonstrated that a high recycle rate enhances the aeration of the artificial artery increasing the concentration of metabolites and decreasing the concentration of the substrates. Therefore, a high recycle rate inhibits cell proliferation and increases consequently the time for the cell population to reach a specific concentration. It was shown that there is sufficient substrate supply and efficient metabolite removal to produce an artificial artery with homogenous cell concentration for the ranges of feed and recycle rates which were studied.

In Chapters 5 and 6 micro-scale experiments were designed as a way to evaluate from measurements, effective diffusivities of substrates and metabolites in matrices as well as substrate consumption and metabolite production rates in matrices with immobilized cells. They have the advantage of generating data sets using a small number of cells in a way which predicts the larger scale. Such a database can be used to define the size of the biopsy, the operating conditions of the bioreactor as well as the time the tissue-engineered construct will be ready for implantation.

Specifically, in Chapter 5 alginate constructs were formed in customized microwells in order to measure indirectly the oxygen effective diffusivity in an alginate gel / cell mix and the oxygen uptake rate of human adult cells. Oxygen concentration was recorded and analysed in a mathematical model which was set up in Matlab 7.1 and Comsol Multiphysics 3.3. Additionally, the cell culture in alginate was evaluated by conducting cell enumeration, viability determination, Ki-67 expression and cell cycle analysis.

No change in the live cell concentration and viability was detected. The pH at the bottom of the construct was relatively constant and acceptable for fibroblast cell growth. It was found that the oxygen demand was higher at the beginning of the incubation of the construct and started decreasing as the cells were entering the low oxygen demanding G0 / G1 phase. The high percentage of

cells in G0 / G1 phase indicated the inability of the fibroblasts to attach to alginate and proliferate.

The values of the parameters were in agreement with values reported in the literature having relatively low confidence intervals (<15%). Additionally, the calculations were verified by changing one of the parameters of the system and the results showed that the mathematical model was reliable as the average absolute relative error between experimental and predicted data was 0.2%

In Chapter 6 alginate constructs with immobilized human dermal fibroblasts were formed in transwells in order to measure indirectly the effective diffusivities of glucose, and lactate as well as the glucose consumption and the lactate production rate. No change in the live cell concentration and viability was observed. The values of the calculated parameters were lying within the range of values which has been reported in the literature having relatively low confidence intervals (<15%). It was demonstrated that glucose and lactate effective diffusivities decrease as the cell concentration in alginate increases which was attributed to formation of extracellular matrix and cells occupying space within the alginate construct.

7.2 Future work

An immediate project arising from this research is to demonstrate how the models developed and substrate / metabolite measurements made in this thesis relate to the actual preparation of engineered tissue. This will require exclusive sterile engineering to prepare a source of cells and alginate for the full scale preparation of a cell alginate matrix and the monitoring of cell growth. Non invasive monitoring of the cell growth is likely to be difficult and hence a sterile sampling system is needed as resource to a series of parallel runs for various times. An economical analysis needed for such a work and creation of a research team is recommended to put such a project in place.

In this thesis the role of mass transfer in the development of engineered tissue was addressed by coupling mathematical models with experimental design. The same strategy can be followed to study other factors which affect the development of tissue engineering.

There is increased evidence that the mechanical stimulation affects the cell behaviour in tissue engineered constructs. However, the mechanism of this stimulation is still elusive. Better understanding of the effect of the mechanical stimulation on cell signalling will be of important consideration in bioreactor design. Studies examining the effect of mechanical factors like cyclic flexure, shear stress, tension and pressure may be conducted in order to understand their role in tissue engineering.

Another challenge in tissue engineering is the understanding of how the microenvironment of the scaffold affects cell function. Several scaffolds can be tested addressing the role of their surface chemistry, their architecture and their degradation rate over time in the control of cell fate.

Biochemical and mechanical signals that regulate cell function under normal and pathological conditions come from extracellular matrix contacts. Therefore, extracellular matrix production and control of its composition in a scaffold can be further studied in how they affect cell function.

The sufficient supply of nutrients and oxygen and the effective removal of the waste products of the cells from the scaffold are limited to only a few micrometers as a result of the slow mass transfer rate the diffusion can provide. Cells in a large-sized engineered tissue will consume nutrients and oxygen in a few hours after implantation. However, the creation of blood arteries will take several weeks. Therefore, the development of controlled release systems delivering molecules over long periods of time which can initiate angiogenesis can be another source of future research.

REFERENCES

Akhyari P., Fedak P.W.M., Weisel R.D., Lee T.J., Verma S., Mickle D.A.G., Li R., 2002. Mechanical stretch regimen enhances the formation of bioengineered autologous cardiac muscle grafts. *Circulation*, **106** (I), pp. I-137-I-142.

Alberts B., Bray D., Lewis J., Raff M., Roberts K., Watson J.D., 1994. *Molecular Biology of the Cell*. 4th ed. New York: Garland Science, 2002.

Alison D.D. Grande-Allen K., 2006. Hyaluronan: a powerful tissue engineering tool. *Tissue Engineering*, **12** (8), pp. 2131-2140.

Asakura T., Karino T. 1990. Flow patterns and spatial distribution of atherosclerotic lesions in human coronary arteries. *Circulation Research*, **66**, pp. 1045-1066.

Atala A., 2002. Experimental and clinical experience with tissue engineering techniques for urethral reconstruction. *Urology Clinics of North America*, **29**, pp. 485–492.

Atala A., Baver S.B., Soker S., Yoo J.J., Retik A.B., 2006. Tissue-engineered autologous bladders for patients needing cystoplasty. *The Lancet*, **367**, pp. 1241-1246.

Atala A., Kim W., Paige K.T., Vacanti C.A., Retik A.B., 1994. Endoscopic treatment of vesicoureteral reflux with a chondrocyte-alginate suspension, *Journal of Urology*, **152**, pp. 641–643.

Aufderheide A.C., Athanasiou K.A., 2004. Mechanical stimulation toward tissue engineering of the knee meniscus. *Annals of Biomedical Engineering*, **32** (8), pp. 1161-1174.

Augst A., Kong H.J., Mooney D.J., 2006. Alginate hydrogels as biomaterials. *Macromolecular Biosciences*, **6**, pp. 623-633.

Bagnaninchi P.O., Yang Y., Zghoul N., Maffouli N., Wang R.K., El Haj A.J., 2007. Chitosan microchannel scaffolds for tendon tissue engineering characterized using optical coherence tomography. *Tissue Engineering*, **13** (2), pp. 323-331.

Bailey J.E., Ollis D.F. 1986. *Biochemical Engineering Fundamentals* 2nd ed. Singapore: McGraw Hill.

Baker R.K., Haendel M.A., Swanson B.J., Shambaugh J.C. Micales B.K., Lyons G.E., 1997. In vitro prselection of gene-trapped embryonic stem cell clones for characterizing novel developmentally regulated genes in the mouse. *Developmental Biology*, **185**, pp. 201-214.

Bancroft G. N., Sikavitsas V. I., van den Dolder Juliette, Sheffield T. L., Ambrose C. G., Jansen J. A., Mikos A. G., 2002. Fluid flow increases mineralized matrix deposition in 3D perfusion culture of marrow stromal osteoblasts in a dose-dependent manner. *Proceedings of the national academy of sciences of the United States of America,* **99**, pp. 12600-12605.

Bancroft G.N., Sikavitsas V.I., Mikos A.G., 2003. Technical note: Design of a flow perfusion bioreactor system for bone tissue-engineering applications. *Tissue Engineering*. **9** (3), pp. 549-554.

Barrilleaux B., Phinney D.G., Prockop D., O'Connor K.C., 2006. Review: Ex vivo engineering of living tissues with adult stem cells. *Tissue Engineering*, **12** (11), pp. 1-13.

Barron V., Lyons E., Stenson-Cox C., McHugh P.E., Pandit A., 2003. Bioreactors for cardiovascular cell and tissue growth: A review. *Annals of Biomedical Engineering*, **33**, pp. 1017-1030.

Bell E., 2000. Tissue engineering in perspective. In: Lanza R., Langer R., Vacanti J., (ed.) *Principles of Tissue Engineering*, 2nd ed. Academic Press, pp. 35-38.

Bell E., Sher S., Hull B., Merrill C., Rosen S., Chamson A., Asselineau D., Dubertret L., Coulomb B., Lapiere C., Nusgens B., Neveux Y., 1983. The reconstitution of living skin. *Journal of Investigative Dermatology*, **81**, pp. 2s-10s.

Bent A.E., Tutrone R.T., McLennan M.T., Lloyd L.K., Kennelly M.J., Badlani G. 2001. Treatment of intrinsic sphincter deficiency using autologous ear chondrocytes as a bulking agent. *Neurology and urodynamics*, **20**, pp. 157-165.

Bilodeau K., Mantovani D., 2006. Bioreactors of tissue engineering: Focus on mechanical constraints. A comparative review. *Tissue Engineering*, **12** (8), pp. 1-17.

Bonassar LJ., Grodzinsky A.J., Frank E.H., Davila S.G., Bhaktav N.R., Trippel S.B., 2001. The effect of dynamic compression on the response of articular cartilage to insulin-like growth factor-I, *Journal of Orthopaedic Research*, **19**, pp. 11-17.

Brezinski M.E., Tearney G.J., Weissman N.J., Boppart S.A., Bouma B.E., Hee M.R., Weyman A.E., Swanson E.A., Southern J.F., Fujimoto J. G., 1997. Assessing atherosclerotic plaque morphology: comparison of optical coherence tomography and high frequency intravascular ultrasound. *Heart*, **77**, pp. 397-403.

Brotherton J.D., Chau P.C., 1995. Protein-free human-human hybridoma cultures in an intercalated-spiral alternate-dead-ended hollow fiber bioreactor. *Biotechnology and Bioengineering*, **47**, pp. 384-400.

Bruder S.P., Jaiswal N., Haynesworth S.E., 1997. Growth kinetics, self-renewal, and the osteogenic potential of purified human mesenchymal stem cells during extensive subcultivation and following cryopreservation. *Journal Cellular Biochemistry*, **64**, pp. 278-294.

Burg K.J.L., Delnomdedieu M., Beiler R.J., Culberson C.R., Greene K.G., Halberstadt C.R., Holder W.D., Loebsack A.B., Roland W.D., Johnson G.A., 2002. Application of magnetic resonance microscopy to tissue engineering: A polylactide model. *Journal of Biomedicine Materials Research*, **61**, pp. 380-390.

Bursac N., Papadaki M., Cohen R.J., Schoen F.J., Eisenberg S,R,, Carrier R.L., Vunjak-Vovakovic G., Freed L.E., 1999. Cardiac muscle tissue engineering: Toward an in vitro model for electrophysiological studies, *American Journal of Physiology*. **46**, pp. H433-H444.

Campbell J.H., Efendy J.L., Campbell G.R., 1999. Novel vascular graft grown within recipient's own peritoneal cavity. *Circulation Research*, **85**, pp. 1173-1178.

Cao F., Lin S., Xie X., Ray P., Patel M., Zhang X., Drukker M, Dylla S.J., Connolly A.I., Chen X., Weissman I.L., Gambhir S., Wu J.C., 2006. *Circulation*, **113**, pp. 1005-1014.

Caplan A.I., 2000. Tissue engineering designs for the future: new logics, old molecules. *Tissue Engineering*, **6** (1), pp. 1-8.

Carrier R., Papadaki M., Bursac N., Langer R., Vunjak-Novakovic G., Freed L., 1999. Cardiac tissue engineering: cell seeding, cultivation parameters, and tissue construct characterization, *Biotechnology and Bioengineering*, **64** (5), pp. 580-589.

Carrier R.L., Rupnick M., Langer R., Schoen F.J., Freed L.E., Vunjak-Novakovic G., 2002. Perfusion improves tissue architecture of engineered cardiac muscle. *Tissue Engineering*, **8**, pp. 175-188.

Cartmell S.H., Porter B.D., García A.J., Guldberg R.E., 2003. Effects of Medium Perfusion Rate on Cell-Seeded Three-Dimensional Bone Constructs *in Vitro*. *Tissue Engineering*, **9** (6), pp. 1197-1203.

Caspi O, Lesman A., Basevitch Y., Gepstein A., Arbel G., Habib I.H.M., Gepstein I., Levenberg S. 2007. Tissue Engineering of Vascularized Cardiac Muscle from Human Embryonic Stem Cells *Circulation Research*, **100** (2), pp. 263-272.

Chan C., Berthiaume F., Nath B.D., Tilles A.W., Toner M., Yarmush M., 2004. Hepatic tissue engineering for adjunct and temporary liver support: critical technologies. *Liver transplantation*, **10** (11), pp. 1331-1342.

Chan R.C., Chau A.H., Karl W.C., Nadkarni S., Khalil A.S., Iftimia N., Shishkov M., Tearney G.J., Kaazempur-Mofrad M.R., Bouma B.E., 2004. OCT-based arterial elastography: robust estimation exploiting tissue biomechanics. *Optics Express*, **12**, pp. 4558-4572.

Chang S.C., Rowley J.A., Tobias G., Genes G., Roy A.K., Mooney D.J., Vacanti C.A., Bonassar J., 2001. Injection molding of chondrocyte / alginate constructs in the shape of facial implants. *Journal of Biomedicine Materials Research*, **55**, pp. 503- 511.

Chow D.C., Wenning L.A., Miller W.M., Papoutsakis E.T., 2001. Modeling pO_2 distributions in the bone marrow hematopoietic compartment. I. Krogh's model. *Biophysical Journal*, **81**, pp. 675-684.

Chresand T.J., Gillies R.J., Dale B.E., 1987. Optimum fiber spacing in a hollow fiber bioreactor. *Biotechnology and Bioengineering*, **32**, pp. 983-992.

Christie A., Butler M., 1994. Glutamine-based dipeptides are utilized in mammalian cell culture by extracellular hydrolysis catalyzed by a specific peptidase. *Journal of Biotechnology*, **37**, pp. 277-290.

Chung C.A., Yang C.W., Chen C.W, 2006. Analysis of cell growth and diffusion in a scaffold for cartilage tissue engineering. *Biotechnology and Bioengineering*, **94** (6), pp. 1138-1146.

Comsol Multiphysics manual, 2005. COMSOL Ltd., Hatfield, United Kingdom.

Constantinidis I., Mukundan N.E., Gamcsik M., Sambanis A., 1997. Towards the development of a bioaqrtificial pancreas: A ^{13}C NMR study on the effect of alginate / poly-L-lysine / alginate entrapment on glucose metabolism by βTC3 mouse insulinoma cells. *Cellular and Molecular Biology*, **43**, pp. 721-729.

Constantinidis I., Sambanis A., 1998. Noninvasive monitoring of tissue-engineered constructs by nuclear magnetic resonance methodologies. *Tissue Engineering*, **4** (1), pp. 9-17.

Cormier J.T., Zur Nieden N.I., Rancroft D.E.,kallos M.S., 2006. Expansion of undifferentiated murine embryonic stem cells as aggregates in suspension culture bioreactors. *Tissue Engineering*, **12** (1), pp. 1-13.

D'Ippolito G., Schiller P.C., Ricordi C., Roos B.A., Howard G.A., 1999. Age-related osteogenic potential of mesenchymal stromal cells from human vertebral bone marrow, *Journal of Bone and Mineral Research*, **14**, pp. 1115–1122.

Dahl S.L.M., Rhim C., Ying C.S., Niklason L.E., 2007. Mechanical properties and compositions of tissue engineered and native arteries. *Annals of Biomedical Engineering*, **35**, pp. 348–355.

Davis M.E., Motion M., Narmoneva D.A., Takahashi T., Hakuno D., Kamm R.D., Zhang S., Lee R.T., 2005. Injectable self-assembling peptide nanofibers create intramyocardial microenvironments for endothelial cells. Circulation, **111**, pp. 442-450.

Davisson T., Kunig S., Chen A., Sah R., Ratcliffe A., 2002. Static and dynamic compression modulate matrix metabolism in tissue engineered cartilage. *Journal of Orthopedic Research*, **20**, pp. 842-848.

Drury J., Mooney D.J., 2003. Hydrogels for tissue engineering: scaffold design variables and applications. *Biomaterials*, **24**, pp. 4337-4351.

Drury J.L., Dennis R.G., Mooney D.J., 2004. The tensile properties of alginate hydrogels. *Biomaterials*, **25**, pp. 3187-3199.

Duflo S., Thibeault S.L, Li W., Shu X.Z., Prestwich G., 2006. Effect of a synthetic extracellular matrix on vocal fold lamina propria gene expression in early wound healing, T*issue Engineering*, **12** (11), pp. 3201-3207.

Dvir T., Benishti N., Shachar M., Cohen S., 2006. A novel perfusion bioreactor providing a homogenous milieu for tissue regeneration. *Tissue Engineering*, **12**, pp. 2843-2852.

Eisenstein M., 2006. Thinking outside the dish. *Nature*, **3** (12), pp. 1035-1043.

Ellis-Behnke, R.G., Liang Y., You S., Tay D.K.C., Zhang S., So K., Scneider G., 2006. Nano neuro knitting: Peptide nanofiber scaffold for brain repair and axon regeneration with functional return of vision. *Proceedings of National Academy of Sciences of United States of America*, **103** (13), pp. 5054-5059.

Engelmayer G.C., Rabkin E., Sutherland F.W.H., Schoen F.J., Mayer J.E., Sacks M.S., 2005. The independent role of cyclic flexure in the early *in vitro* development of an engineered heart valve tissue. *Biomaterials*, **26**, 175-187.

Evans N.D., Gentleman E., Polak J.M., 2006. Scaffolds for stem cells. *Materials Today*, **9** (12), pp. 26-33.

Ezashi T., Das P., Roberts R.M., 2005. Low O_2 tensions and prevention of differentiation of hES cells. *Proceedings of National Academy of Sciences of United States of America*, **102** (13), pp. 4783-4788.

Fedorovich N. E., Albas J., De Wijn J. R., Hennink W E., Verbout A. B. J., Dhert W. J. A., 2007, Hydrogels as extracellular matrices for skeletal tissue engineering: state-of-the art and novel application in organ printing-a review, *Tissue Engineering, in press.*

Foy BD, Lee J, Morgan J, Toner M, Tompkins RG, Yarmush ML., 1993. Optimization of hepatocyte attachment to microcarriers: importance of oxygen. *Biotechology Bioengineering*, **42**, pp. 579-588.

Freed L.E., Marquis J., Nohria A., Mikos A.G., Emmanual J., Langer R., 1993. Neocartilage formation in vitro and in vivo using cells cultured on synthetic biodegradable polymers. Journal of Biomedicine Materials Research, **27**, pp. 11-23.

Freed L.E., Vunjak-Novakovic G., 2000. Tissue engineering bioreactors. In: Lanza R.P., Langer R., Vacanti J. eds. *Principles of Tissue Engineering*, San Diego: Academic Press, pp. 143-156.

Freed L.E., Vunjak-Novakovic G., Langer R., 1993. Cultivation of cell-polymer cartilage implants in bioreactors. *Journal of Cellular Biochemistry,* **51**, pp. 257-264.

Freed L.E., Vunjak-Novakovic, G., Biron, R.J., Eagles, D., Lesnoy, D., Barlow, S.K., Langer, R. 1994. Biodegradable polymer scaffolds for tissue engineering, *Nature Biotechnology*, **12**, pp. 689-693.

Freyer J.P. Sutherland R.M., 1985. A reduction in the *in situ* rates of oxygen and glucose consumption of cells in EMT6/Ro spheroids during growth. *Journal of Celularl Physiology*, **124**: 516-524.

Friedenstein A.J, Pjatetski-Shapiro II, Petrakova K.V., 1966. Osteogenesis in transplants of bone marrow cells. *Journal of Embryology and Experimental Morphology*, **16**, pp. 381-390.

Fuchs J. R., Nasseri B.A., Vacanti J. P. 2001. Tissue Engineering: A 21st Century Solution to Surgical Reconstruction. *Annual Thoracic Surgery*, **72**, pp. 577-591.

Fujimoto J.G., Brezinski M.E., Tearney G.J., Boppart S.A., Bouma B., Hee M.R., Southern J.F., Swanson E.A., 1995. Optical biopsy and imaging using optical coherence tomography. *Nature Medicine*, **1** (9) pp. 970-972.

Gambhir A., Korke R., Lee J., Fu P.C., Europa A., Hu W.S., 2003. Analysis of cellular metabolism of hybridoma cells at distinct physiological states. *Journal of Bioscience and Bioengineering*, **95** (4), pp. 317-327.

Garner J.P., 2004. Tissue Engineering in Surgery. *Surgeon Journal of the Royal Colleges of Surgeons of Edinburgh & Ireland*, **2** (2), pp. 70-78.

Garreta E., Genové E., Borrós S., Semino C.E., 2006. Osteogenic differentiation of mouse embryonic stem cells and mouse embryonic fibroblasts in a three-dimensional self-assembling peptide scaffold. *Tissue Engineering*, **12** (8), pp. 2215-2227.

Gelain F., Bottai D., Vescovi A., Zhang S., 2006. Designer self-assembling peptide nanofiber scaffolds for adult mouse neural stem cell 3-Dimensional cultures. *PLoS one*, **1**, pp. 1-11.

Germain L, Rémy-Zolghadri M., Auger F., 2000. Tissue engineering of the vascular system: From capillaries to larger blood vessels. *Medical and Biological Engineering and Computing*, **38** (2), pp. 232-240.

Glacken M.W., Fleischaker R.J., Sinskey A.J., 1986. Reduction of waste product excretion via nutrient control: Possible strategies for maximizing product and cell yields on serum in cultures of mammalian cells. *Biotechnology and Bioengineering*, **28**, pp. 1376–1389.

Glicklis R., Shapiro L., Agbaria R., Merchuk J.C., Cohen S., 2000. Hepatocyte behaviour within three-dimensional porous alginate scaffolds. *Biotechnology and Bioengineering*, **67** (3), pp. 344-353.

Goix P.J., 2004. *Method and apparatus for detecting microparticles in fluid samples.* United States patent 6710871.

Goodwin T.J., Parker C.R., 2006. *Three-dimensional cell to tissue development process.* United States patent 20060240550.

Gramer M.J., Poeschl D.M., Controy M.J., Hammer B.E., 1999. Effect of harvesting protocol on performance of a hollow fiber bioreactor. *Biotechnology and Bioengineering*, **65**, pp. 334-340.

Grant GT, Morris ER, Rees DA, Smith PJC, Thom D.1973. Biological interactions between polysaccharides and divalent cations: the egg box model. *Federation of European Biochemical Societies Letters*, **32**, pp. 195–198.

Grayson W., Zhao F., Izadpanah R., Bunnell B., Ma T., 2006. Effects of hypoxia on human mesenchymal stem cell expansion and plasticity in 3D constructs. Journal of Cellular Physiology, **207**, pp. 331-339.

Greenwald S.E., Berry C.L. 2000. Improving vascular grafts: the importance of mechanical and haemodynamic properties. *Journal of Pathology*, **190**, pp. 292-299.

Grenier G., Rémy-Zolghadri M., Bergeron F., Guignard R., Baker K., Labbé R., Auger F.A., Germain L., 2006. Mechanical loading modulates the differentiation state of vascular smooth muscle cells. *Tissue Engineering*, **12** (11), 1-12.

Hall A.C., Urban P.G., Gehl K.A., 1991. The effects of hydrostatic pressure on matrix synthesis in articular cartilage. *Journal of Orthopaedic Research*, **9** (1), pp. 1-10.

Halvorsen Y.D., Franklin D., Bond A.L., Hitt D.C., Auchter C., Boskey, A.L., Paschalis E.P., Wilkison W.O., Gimble J.M., 2001. Extracellular matrix mineralization and osteoblast gene expression by human adipose tissue-derived stromal cells. *Tissue Engineering*, **7**, 729–741.

Havehan D.L., Papoutsakis T., Miller W.M., 2000. Physiologically significant effects of pH and oxygen tension on granulopoiesis. *Experimental Haematology*, **20**, pp. 267-275.

Health C. Belfort G. 1987. Immobilization of Suspended Mammalian Cells: Analysis of Hollow Fiber and Microcapsule Bioreactors. *Advances in Biochemical Engineering / Biotechnology*, **34**, pp. 1-31.

Heath C.A., Belfort G., Hammer B.E., Mirer S.D., Pimbley J.M., 1990. Magnetic resoncnance imaging and modelling of low in hollow fiber bioreactors. American Institute of Chemical Engineers Journal, **36** (4), pp. 547-558.

Henderson J.K., Draper J.S., Baillie H.S., Fishel S., Thomson J.A., Moore H., Andrews P.W., 2002. Preimplantation human embryos and embryonic stem cells show comparable expression of stage-specific embryonic antigens. *Stem Cells*, **20**, pp. 329-337.

Hoerstrup S.P., Sodian R., Daebritz S., Wang J., E. Bacha E.A., D. Martin D.P., Moran A.M., Guleserian K.J., Sperling J.S., Kaushal S., Vacanti J.P., Schoen F.J., Mayer J.E., 2000. Functional living trileaflet heart valves grown in vitro. *Circulation*, **102**, pp. SIII-44–SIII-49.

Hoerstrup S.P., Zünda G., Sodian R., Schnell A.M., Grünenfelder J., Turina M.I., 2001. Tissue engineering of small caliber vascular grafts *European Journal of Cardiothoracic Surgery*, **20**,pp. 164-169.

Hollister S.J., 2005. Porous scaffold design for tissue engineering. *Nature Materials*, **4**, pp. 518-524.

Holmes T., Delacalle S, Su X., Rich A., Zhang S., 2000. Extensive neurite outgrowth and active neuronal synapses on peptide scaffold. **97**, pp. 6728-6733.

Huang N.F., Lee R.J., Li S., 2007. Chemical and physical regulation of stem cells and progenitor cells: Potential for cardiovascular tissue engineering. *Tissue Engineering*, in press.

Huynh T., Abraham G., Murray J., Brockback K., Hagen P, Sullivan S., 1999. Remodelling of an acellular collagen graft into a physiologically responsive neovessel. *Nature Biotechnology*, **17**, pp. 1083-1086.

Ishikawa Y., Ito T., 1988. Kinetics of hematopoietic stem cells in a hypoxic culture. *European Journal of Haematology*, **40**, pp. 126 –129.

Jacobs R.E., Cherry S.R., 2001. Complementary emerging techniques: high-resolution PET and MRI. *Current Opinion in Neurobiology*, **11**, pp. 621–629.

Jagodzinski M., Drescher M., Zeichen J., Hankemeier S., Krettek C., Bosch U., van Griensven M., 2004. Effects of cyclic longitudinal mechanical strain and dexamethasone on osteogenic differentiation of human bone marrow stromal cells. *European Cells and Materials*, **7**, pp. 35-41.

Jagodzinski M., Drescher M., Zeichen J., Hankemeir S., Krettek C., Bosch U., Van Griensven M., 2004. *European Cells And Materials*, **7**, pp. 35-41.

Jaiswal R.K., Jaiswal N., Bruder S.P., Mbalaviele G., Marshak D.R., Pittenger M.F., 2000. Adult human mesenchymal stem cell differentiation to the osteogenic or adipogenic lineage is regulated by mitogen-activated protein kinase. *Journal of Biological Chemistry*, **275**, pp. 9645–9652.

Jiang Y., Jahagirdar B.N., Reinhardt R.L., Schwartz R.E., Keene C.D., Ortiz-Gonzalez X.R., Reyes M., Lenvik T, Lund T., Blackstad M., Du J., Aldrich S., Lisberg A., Low W.C., Largaespada D.A., Verfaillie C.M. 2002. Pluropotency of mesenchymal stem cells derived from adult marrow. *Nature*, **418**, pp. 41-49.

Kalyanaraman B., Boyce S., 2007. Assessment of an automated bioreactor to propagate and harvest keratinoncytes of engineered skin substitutes. *Tissue Engineering*, **13** (5), pp. 1-11.

Kehat I., Khimovich L., Caspi O., Gepstein A., Shofti R., Arbel G., Huber I., Satin J., Itskovitz-Eldor J., Gepstein L., 2004. Electrochemical integration of cardiomyocytes derived from human embryonic stem cells. *Nature Biotechnology*, **22** (10), pp. 1282-1289.

Khademhosseini A., Langer R., Borestein J., Vacanti J.P., 2006. Microscale technologies for tissue engineering and biology. *Proceedings of National Academy of Sciences of United States of America*, **103** (8), pp. 2480-2487.

Kim B., Nikolovski J., Bonadio J., Mooney D.J., 1999. Cyclic mechanical strain regulates the development of engineered smooth muscle tissue. *Nature*, **17**, pp. 979-983.

Kisiday J., Jin M., Kurz B., Hung H., Semino C., Zhang S., Grodzinsky A.J., 2002. Self-assembly peptide hydrogel fosters chrondrocyte extracellular matrix production and cell division: Implications for cartilage tissue repair. *Proceedings of the National Academy of Sciences of the United States of America*, **99** (15), pp. 9996-10001.

Ko H., Tan W., Stack R, Boppart S.A., 2006. Optical coherence elastography of engineered and developing tissue. *Tissue Engineering*, **12** (1), pp. 63-73.

Kopen G.C., Prockop D.J., Phinney D.G., 1999. Marrow stromal cells migrate throughout forebrain and cerebellum, and they differentiate into astrocytes after injection into neonatal brains. *Proceedings of the National Academy of Sciences of the United States of America*, **96**, pp. 10711 -10716.

Kulig K.M, Vacanti J.P., 2004. Hepatic tissue engineering. *Transplant immunology*, **12**, pp. 303-310.

Kuznetsov S.A., Friedenstein A.J., Robey P.G., 1997. Factors required for bone marrow stromal fibroblast colony formation *in vitro*. *British Journal of Haematology*, **97**, pp. 561-570.

L'Heureux N., Dusserre N., Konig G., Victor B., Keire P., Wight T. N., Chronos N.A.F., Yles A.E., Gregory C.R., Hoyt G., Robbins R.C., McAllister T.N., 2006. Human tissue-engineered blood vessels for adult arterial revascularization. *Nature*, **12**(3), pp. 361-365.

Laflamme M.A., Murry C.E., 2005. Regenerating the heart. *Nature Biotechnology*, **23** (7), pp. 845-856.

Lalan S., Pomerantseva I., Vacanti J. P. 2001. Tissue Engineering and Its Potential Impact on Surgery. *World Journal of Surgery*, **25**, pp. 1458-1466.

Langer R., Vacanti J.P., 1993. Tissue engineering. *Science*, **260**, pp. 920-926.

Lee G.M., Jeffrey J. Gray J.J., Palsson B.O., 1991. Effect of trisodium citrate treatment on hybridoma cell viability. *Biotechnology Techniques*, **5** (4), pp. 295-298.

LeRoux M.A., Guilak F., Setton L.A., 1999. Compressive and shear properties of alginate gel: Effects of sodium ions and alginate concentration. *Journal of Biomedicine Materials Research,* **47**, pp. 46-53.

Levenberg S, Golub JS, Amit M, Itskovitz-Eldor J, Langer R., 2002. Endothelial cells derived from human embryonic stem cells. *Proceedings of the National Academy of Sciences of the United States of America*, **99**, pp. 4391-4396.

Levenberg S., Huang N.F., Lavik E., Rogers A.B., Itskovitz-Eldor J., Langer R., 2003. Differentiation of human embryonic stem cells on three-dimensional polymer scaffolds. *Proceedings of the National Academy of Sciences of the United States of America*, **100** (22), pp. 12741-12746.

Lewis M.C., MacArthur B.D., Malda J., Pettet G., Please C.P., 2005, Heterogeneous proliferation within engineered cartilaginous tissue: the role of oxygen tension. *Biotechnology and Bioengineering*, **91** (5), pp. 607-615.

Lu H.H, Cooper Jr. J.A., Manuel S, Freeman J.W, Attawia M.A, Ko F.K, Laurencin C.T. 2005. Anterior cruciate ligament regeneration using braided biodegradable scaffolds: in vitro optimization studies. *Biomaterials*, **26**, pp. 4805-16.

Ma C.Y.J., Kumar R., Xu X.Y., Mantalaris A., 2007. A combined fluid dynamics, mass transport and cell growth model for a three-dimensional perfused bioreactor for tissue engineering of haematopoietic cells. *Biochemical Engineering Journal*, **35**, pp. 1-11.

Macnair R., Underwood M.J., Angwelini G.D., 1998. Biomaterials and cardiovascular devices. *Proceedings of the Institution of Mechanical Engineers, Part H: Journal of Engineering in Medicine*, **212** (6), pp 465-471.

Malda J., Klein T.J., Upton Z., 2007. The roles of hypoxia in the *in vitro* engineering of tissues. *Tissue Engineering*, in press.

Malda J., Rouwkema J., Martens D.E., le Conte E.P., Kooy F.K., Tramper J., van Blitterswijk C.A., Riesle J., 2004. Oxygen gradients in tissue-engineered PEGT/PBT cartilaginous constructs: Measurement and modelling. *Biotechnology and Bioengineering*, **86**, pp. 9-18.

Malda J., Van den Brink P., Meewse P., Grojec M., Martens D.E., Tramper J., Riesle J., Van Blitterswijk C.A. 2004. Effect of oxygen tension on adult articular chondrocytes in microcarrier bioreactor culture. *Tissue Engineering*, **10** (7/8), pp. 987-994.

Maranga L., Goochee C.F., 2005. Metabolism of PER.C6TM Cells Cultivated Under Fed-Batch Conditions at Low Glucose and Glutamine Levels. *Biotechnology and Bioengineering*, **94**, pp. 139-150.

Martin I., Wendt D., Heberer M., 2004. The role of bioreactors in tissue engineering. *Trends in Biotechnology*, **22** (2), pp. 80-86.

Martin Y., Vermette P. 2005. Bioreactors for tissue mass culture: Design, characterization, and recent advances. *Biomaterials*, **26**, pp. 7481-7503.

Martinsen A., Skjåk-Braek G., Smidsrød O., 1989. Alginate as immobilization material: I. Correlation between chemical and physical properties of alginate gel beads. *Biotechnology and Bioengineering*, **33**, pp. 79-89.

Mason C., Markusen J.F., Town M.A., Dunnill P., Wang R.K., 2004. The potential of optical coherence tomography in engineering of the living tissue. *Physics in Medical and Biology*, **49**, pp. 1097-1115.

Mason C., Town M.A., 2002. *Method for forming hardened sheets and tubes.* World Intellectual Property Organisation patent W.O./ 2002/077336.

Mauck R., Nicoll S., Seyhan S.L., Ateshian G.A., Hung C.T., 2003. Synergistic action of growth factors and dynamic loading for articular cartilage tissue engineering. *Tissue Engineering*, **9** (4), pp. 597-611.

Mauney J.R., Volloch V., Kaplan D., 2005. Role of adult mesenvhymal stem cells in bone tissue-engineering applications: Current status and future prospects. *Tissue Engineering*, **11** (5/6), pp. 787-802.

McCulloch A.D., Harris A.B., Sarraf C.E., Eastwood M., 2004. New multi-cue bioreactor for tissue engineering of tubular cardiovascular samples under physiological conditions. *Tissue Engineering*, **10** (3/4) pp. 565-573.

McGuigan A.P., Sefton M.V., 2007. Design criteria for modular tissue-engineered construct. *Tissue Engineering*, **13** (5), pp. 1079-1089.

Mironov V., Kasyanov V., McAllister K., Oliver S., Sistino J., Markwald R., 2003. Perfusion bioreactor for vascular tissue engineering with capabilities for longitudinal stretch. *The Journal of Craniofacial Surgery*, **14** (3), pp. 340-347.

Mitchell S.L. Niklason L.E., 2003. Requirements for growing tissue-engineered vascular grafts. *Cardiovascular Pathology*, **12**, pp. 59-64.

Mitsui K., Tokuzawa Y., Itoh H., Segawa K., Murakami M., Takahashi, K., Maruyama M., Maeda M., Yamanaka S. 2003. The homeoprotein Nanog is required for maintenance of pluripotency in mouse epiblast and ES cells, *Cell*, **113** (5), pp. 631–642.

Morgan J, Waldock A, Jeffery G, Cowey A. 1998. Retinal nerve fibre layer polarimetry: histological and clinical comparison. *British Journal of Ophthalmology*, **82** (6), pp. 684–690.

Mostafa S.S., Miller W.M., Papoutsakis E.T., 2000. Oxygen tension influences the differentiation, maturation and apoptosis of human megakaryocytes. *British Journal of Haematology*, **111**, pp. 879-889.

Murphy C.L., Sambanis A., 2001. Effect of oxygen tension and alginate encapsulation on restoration of the differentiated phenotype of passaged chrondrocytes. *Tissue Engineering*, **7** (6), pp. 791-803.

Muschler G.F., Nakamoto C., Griffith L.G., 2004. Engineering principles of clinical cell-based tissue engineering. The journal of bone and joint surgery, **86a** (7), pp. 1541-1558.

Narita Y., Hata K., Kagami H., Usui A., Ueda M., Ueda Y., 2004. Novel pulse duplicating bioreactor system for tissue-engineered vascular construct. *Tissue Engineering*, **10** (7/8), pp. 1224-1233.

Nasseri B.A., Ogawa K., Vacanti J.P., 2001. Tissue Engineering: An evolving 21st - century science to provide biologic replacement for reconstruction and transplantation. *Surgery*, **130**, pp. 781-785.

Naughton GK, 2002. From lab bench to market: critical issues in tissue engineering. *Annals of New York Academy Sciences*, **961**, pp. 372–385.

Navran S. 2006. Rotating bioreactors for manufacturing. *Genetic Engineering & biotechnology News*, **26** (18).

Neves A.A., Medcalf N., Smith M., Brindle K.M., 2006. Evaluation of engineered meniscal cartilage constructs based on different scaffold geometries using magnetic resonance imaging and spectroscopy. Tissue Engineering, **12** (1), pp. 53-62.

Niklason L.E., Gao J., Abbot W. M., Hirschi K. K., Houser S., Marini R., Langer R., 1999. Functional Arteries Grown in Vitro. *Science*, **284**, pp. 489-493.

Nova Bioprofile 400 reference manual, 2002. Nova Biomedical, Flintshire, United Kingdom.

O'Callaghan C.J., Williams B., 2000. Mechanical strain-induced extracellular matrix production by human vascular smooth muscle cells. Hypertension, **36**, pp. 319-324.

O'Halloran Cardinal K., Bonnema G.T., Hofer H., 2006. Tissue-engineered vascular grafts as in vitro blood vessel mimics for the evaluation of endothelialisation of intravascular devices. *Tissue Engineering,* **12**, pp. 3431-3438.

Oswald J., Boxberger S., Jorgensen B., Feldmann S., Ehninger G., Bornhauser M., Werner C., 2004. Mesenchymal stem cells can be differentiated into endothelial cells in vitro. *Stem Cells*, **22**, pp. 377-384.

Ozturk S. S., Palsson B. O., 1990. Chemical Decomposition of Glutamine in Cell Culture Media: Effect of Media Type, pH, and Serum Concentration. *Biotechnology Progress*, **6,** pp.121-128.

Paige K.T., Cima L.G., Yaremchuk M.J., Vacanti J.P., Vacanti C.A., 1995. Injectable cartilage. *Plastic and Reconstructive Surgery*, **96**, pp. 1390-1398.

Palsson B., Bhatia S. N., 2004. *Tissue Engineering*, 1st ed. London: CRC Press.

Palsson B., Hubbel J. A., Plonsey R., Bronzino J. D. 2003. *Tissue Engineering: Principles and applications in engineering series*, 1st ed. London: CRC Press.

Park H., Cannizzaro C., Vunjak-Novakovic G., Langer R., Vacanti C.A., Farokhzad O.C., 2007. Nanofabrication and microfabrication of functional materials for tissue engineering. *Tissue Engineering*, **13** (4), pp. 1-11.

Patel S.D., Papoutsakis E.T., Winter J.N., Miller W.M., 2000. The Lactate Issue Revisited: Novel Feeding Protocols To Examine Inhibition of Cell Proliferation and Glucose Metabolism in Hematopoietic Cell Cultures. *Biotechnology Progress*, **16**, pp. 885-892.

Pazzano D., Mercier K.A., Moran J.M., Fong S.S., D. D., DiBiasio D.D., Rulfs J.X., Kohles S.S., Bonassar L.J., 2000. Comparison of chondrogensis in static and perfused bioreactor culture. *Biotechnology Progress*, **16**, pp. 893-896.

Peng C., Palsson B.O., 1996. Determination of Specific Oxygen Uptake Rates in Human Hematopoietic Cultures and Implications for Bioreactor Design. *Annals of Biomedical Engineering*, **24**, pp. 373-381.

Perry R. H. and Green D. 1984. *Perry's Chemical Engineers' Handbook*, 6th ed. London: McGraw Hill.

Pfeuffer J., Flögel U., Dieter Leibfritz D., 1998. Monitoring of cell volume and water exchange time in perfused cells by diffusion-weighted 1H NMR spectroscopy. *NMR in Biomedicine*, **11**, pp. 11-18.

Phinney D.G., Kopen G., Righter W., Webster S., Tremain N., Prockop D.J., 1999. Donor variation in the growth properties and osteogenic potential of human marrow stromal cells. *Journal of Cellular Biochemistry*, **75**, pp. 424-436.
Phi-Wilson J.T., Rackham D.F., Sheehan K.M., 2002. *Cell viability assay reagent*, Unites States patent 6403378.

Piret J.M., Cooney C.L., 1990. Immobilized mammalian cell cultivation in hollow fiber bioreactors. *Biotechnology Advances*, **8**, pp. 763–783.

Piret J.M., Cooney C.L., 1990. Mammalian cell and protein distributions in ultrafiltration hollow fiber bioreactors. *Biotechnology and Bioengineering*, **36**, pp. 902-910.

Piret J.M., Cooney C.L., 1991. modelof oxygen transport limitation in hollow fiber bioreactors. *Biotechnology and Bioengineering*, **37**, pp. 80-82.

Pittenger M.F., Mackay A.M., Beck S.C., Jaiswal R.K., Douglas R., Mosca J.D., Moorman M.A., Simonetti D.W., Craig S., Marshak D.R., 1999. Multilineage potential of adult human mesenchymal stem cells. *Science*, **284**, pp. 143-147.

Planchamp C., Vu T.L., Mayer J.M., Reist M., Testa B., 2003. Hepatocyte hollow-fibre bioreactors: design, set up, validation and applications. *Pharmacy and Pharmacology*, **55**, pp. 1181-1198.

Pörter R., Nagel-Hayer S., Goepfert C., Adamietz P., Meenen N.M., 2005. Bioreactor design for tissue engineering. *Journal of Bioscience and Bioengineering*, **100** (3), pp. 235-245.

Powell C.A., Smiley B.L., Mills J., Vandenburgh H.H., 2002. Mechanical stimulation improves tissue-engineered human skeletal muscle. *American Journal of Physiology-Cell Physiology*, **283**, pp. C1557-C1565.

Presens Fibox-3 Instruction manual, 2004. PreSens - Precision Sensing GmbH, Regensburg, Germany.

Presens pH-1 mini Instruction manual, 2004. PreSens - Precision Sensing GmbH, Regensburg, Germany.

Prockop D.J., 1997. Marrow stromal cells as stem cells for nonhematopoietic tissues. *Science*, **276**, pp. 71-74.

Radisic M., Malda J., Epping E., Geng W., Langer R., Vunjak-Novakovic G., 2005. Oxygen gradients correlate with cell density and cell viability in engineered cardiac tissue. *Biotechnology and Bioengineering*, **93** (2), pp. 332-343.

Ramirez O.T., Mutharasan R., 1990. Cell cycle and growth phase-dependent variations in size distribution, antibody productivity, and oxygen demand in hybridoma cultures. *Biotechnology and Bioengineering*, **36**, pp. 839-848.

Ratcliffe A., 2000. Tissue engineering of vascular grafts. *Matrix Biology*, **19**, pp. 353-357.

Reddy J.N., 1993. *Introduction to the Finite Element Method.* 2nd ed. London: McGraw-Hill.

Riha G.M., Lin P.H., Lumsden A.B., Yao Q., Chen C., 2005. Application of stem cells for vascular tissue engineering. *Tissue Engineering*, **11** (9/10), pp. 1535-1552.

Robertson C.R., Kim I.H., 1985. Dual aerobic hollow fiber bioreactor for cultivation of Streptomyces aureofaciens. *Biotechnology and Bioengineering*, **27**, pp. 1012-1020.

Rogowska J., Patel N.A., Fujimoto J.G., Brezinski M.E., 2004. Optical coherence tomographic elastography technique for measuring deformation and strain of atherosclerotic tissues. *Heart*, **90**, pp. 556-562.

Rosenberg N., Martinez A., Sawyer PN., Wesolowsky SA, Postlethwait RW, Dillon ML., 1966. Tanned collagen arterial prosthesis of bovine carotid origin in man. *Annual Surgery*; **164**: pp. 247-256.

Roufosse C.A., Direkze N.C., Otto W.R., Wright N.A., 2004. Circulating mesenchymal stem cells. *The International Journal of Biochemistry and Cell Biology*, **36**, pp. 585-597.

Rowley J. A., Mooney D. J., 2002. Alginate type and RGD density control myoblast phenotype. *Journal of Biomedical Materials Research*, **60**, pp. 217-223.

Rowley J.A., Madlambayan G. and Mooney D.J. 1999. Alginate Hydrogels as Synthetic Extracellular Matrix Materials. *Biomaterials*, **20**, pp. 45-53.

Sabra W., Zeng A.P., Deckwer W.D., 2001. Bacterial alginate:physiology, product quality and process aspects. *Applied Microbiology and Biotechnology*, **56,** pp. 315-325.

Schmedlen R. H., Elbjeirami W. M., Gobin A. S., West J. L. 2003. Tissue engineered small-diameter vascular grafts. *Clinics of Plastic Surgery*, **30**, pp. 507-517.

Schmitt J.M. 1998. OCT elastography: imaging microscopic deformation and strain of tissue. *Optical Express*, **3** (6), pp. 199-211.

Schneider M, Marison W., von Stockar U., 1996. The importance of ammonia in mammalian cell culture. *Journal of Biotechnology*, **46**, pp. 161-185.

Scholzen T., Gerdes J., 2000. The Ki-67 protein: From the known and the Unknown. *Journal of Cellular Physiology*, **182**, pp. 311-322.

Schonberg J. A. Belfort G. 1987. Enhanced Nutrient Transport in Hollow Fiber Perfusion Bioreactors: A Theoretical Analysis. *Biotechnology Progress*, **3** (2), pp. 80-89.

Seliktar D., Nerem R.M., Galis Z.S., 2003. Mechanical strain-stimulated remodelling of tissue-engineered blood vessel constructs. *Tissue Engineering*, **9** (4), pp. 657-666.

Semino C.E., Merok J.R., Crane G.G., Panagiotakos G., Zhang S., 2003. Functional differentiation of hepatocyte-like spheroid structures from putative liver progenitor cells in three-dimensional peptide scaffolds. *Differentiation*, **71**, pp. 262-270.

Sengers B.G.,van Donkelaar C.C.,Oomens C.W.J.,Baaijens F.P.T., 2005. Computational Study of Culture Conditions and Nutrient Supply in Cartilage Tissue Engineering. *Biotechnology Progress*, **21**, pp. 1252-1261.

Shin H., Jo S., Mikos A.G., 2003. Biomimetic materials for tissue engineering. *Biomaterials*, **24**, pp. 4353-4364.

Shin'oka T., Shum-Tim D., Ma P. X., Tanel R. E., Isogai N., Langer R., Vacanti J. P., Mayer J. E. 1998. Creation of viable pulmonary artery Autografts through tissue engineering. *Journal of Thoracic Cardiovascalar Surgury*, **115**, pp. 536-546.

Simmons C.A., Matlis S., Thornton A.J., Chen S., Wang C., Mooney D.J., 2003. Cyclic strain enhances matrix mineralization by adult human mesenchymal stem cells via the extracellular signal-regulated kinase (ERK1/2) signalling pathway. *Journal of Biomechanics*, **36**, pp. 1087-1096.

Smidsrød O. Skjåk-Braek G. 1990. Alginate as immobilization matrix for cells. *Tibtech*, **8**, pp. 71-78.

Smidsrod, O., Haug A., 1972a. Dependence upon the gel sol state of the ion-exchange properties of alginate. *Acta Chemica Scandinavica*. **26**, 2063-2074.

Sodian R., Lemke T., Fritsche C., Hoerstrup S.P., Fu P., Potapov E.V., Hausmann H., Hetzer R., 2002. Tissue Engineering, **8** (5), pp. 863-870.
Solan A. Prabhakar V., Niklason L. 2001. Engineered Vessels: Importance of the Extracellular Matrix. Transplantation Proceedings **33**, pp. 66-68.

Stabler C., Wilks K., Sambanis A., Constantinidis I., 2001. The effects of alginate composition on encapsulated βTC3 cells. *Biomaterials*, **22**, pp. 1301-1310.

Steinbrech D.S., Longaker M.T., Mehrara B.J., Saadeh P.B., Chin G.S., Gerrets R.P., Chau D.C., Rowe N.M., Gittes G.K., 1999. Fibroblast response to hypoxia: The relationship between angiogenesis and matrix regulation. *Journal of Surgical Research*, **84**, pp. 127-133.

Sumanasinghe R.D., Bernacki S.H., Loboa E.G., 2006. Osteogenic differentiation of human mesenchymal stem cells in collagen matrices: Effect of uniaxial cyclic tensile strain on bone morphogenetic protein (BMP-2) mRNA expression. *Tissue Engineering*, **12** (12), pp. 1-7.

Swijnenburg R, Tanaka M., Vogel H., Baker J., Kofidis T., Gunawan F., Lebl D.R., Caffarelli A.D., de Bruin J. Fedoseyeva E.V., Robbins R.C., 2005. Embryonic stem cell immunogenicity increases upon differentiation after transplantation into ischemic myocardium. *Circulation*, **112** (I), pp. I-166-I-172.

Tan W., Sndemir-Urkmez A., Fahrner L.J., Jamison R., Leckband D., Boppart S.A., 2004. Structural and functional optical imaging of three-dimensional engineered tissue development. *Tissue Engineering*, **10** (11/12), pp. 1747-1756.

Teebken O.E., Haverich A. 2002. Tissue Engineering of Small Diameter Vascular Grafts. European *Journal of Vascular and Endovascular Surgery*, **23**, pp. 475-485.

Temenoff J.S., Mikos A.G., 2000. Review: tissue engineering for regeneration of articular cartilage. *Biomaterials*, **21**, pp. 431-440.

Thomson J.A., Itskovitz-Eldor J., Shapiro S.S., Waknitz m.A., Swiergiel J.J, Marshall V.S., Jones J.M., 1998. Embryonic stem cell lines derived from human blastocysts. *Science*, **282**, pp. 1145-1147.

Török É, Pollok J.M., Ma P.X., Vogel C., Dandri M, Petersen J., Burda M.R., Kaufmann P.M., Kluth D., Rogiers X., 2001. Hepatic tissue engineering on 3-dimensional biodegradable polymers within a pulsatile flow bioreactor. *Digestive Surgery*, **18**, pp. 196-203.

Treml H., Woelki S., Kohler H. H. 2003. Theory of capillary formation in alginate gels. *Chemical Physics*, **293**, pp. 343-353.

Vacanti C.A, Langer R, Schloo B, Vacanti J.P, 1991. Synthetic polymers seeded with chondrocytes provide a template for new cartilage formation. *Plastic Reconstractive Surgury*, **88**, pp. 753–759.

Vunjak-Novakovic G., Martin I., Obradovic B., Treppo S., Grodzinsky A.J., Langer R., Freed L.E., 1999, Bioreactor cultivation conditions modulate the composition and mechanical properties of tissue engineered cartilage, *Journal of Orthopaedic Research*, **17**, pp. 130-138.

Vunjak-Novakovic G., Radisic M., Obradovic B., 2006. Cardiac tissue engineering: effects of bioreactor flow environment on tissue constructs. *Journal of Chemical Technology & Biotechnology*, **81**, (4), pp. 485-490.

Weinberg C.B., Bell E., 1986. A blood vessel model constructed from collagen and cultured vascular cells. *Science*, **231**, pp. 397-400.

Welty J. R., Wicks C. E., Wilson R. E., Rorrer G. 2001. *Fundamentals of Momentum, Heat, and Mass Transfer*, 4th ed. John Wiley &Sons, Inc.

Wight T.N., Kinsella M.G., Keating A., Singer J.W., 1986. Proteoglycans in human long-term bone marrow cultures: Biochemical and ultrastructural analyses. *Blood*, **6**, pp. 1333-1343.

Wobus A.M., Boheler K.R., 2005. Embryonic stem cells: Prospects for development biology and cell therapy. *Physiological Reviews*, **85**, pp. 635-678.

Wood M., Yang Y., Thomas P.B.M., El Haj A.J., 2006. Using dihydropyridine-release strategies to enhance load effects in engineered human bone constructs. *Tissue Engineering*, **12** (9), pp. 1-9.

Woodley J.M., Titschener-Hooker N.J., 1996. The use of windows of operation as a bioprocess tool. *Bioprocess Engineering*, **14**, pp. 263-268.

Xie L, Wang D.I. 1993. Fed-Batch Cultivation of Animal Cells Using Different Medium Design Concepts and Feeding Strategies. *Biotechnology and Bioengineering*, **43**, pp. 1175-1189.

Xu C., Inokuma M.S., Denham J., Golds K., Kundu P., Gold J.D., Carpenter M.K., 2001. Feeder-free growth of undifferentiated human embryonic stem cells. *Nature Biotechnology*, 19 (10), pp. 971-974.

Xu X., Wang R. K., El Haj A., 2003. Investigation of changes in optical attenuation of bone and neuronal cells in organ culture or three-dimensional constructs in vitro with optical coherence tomography: relevance to cytochrome oxidase monitoring. *European Biophysics Journal*, **32**, pp. 355–362.

Yannas I., 2004. Synthesis of tissues and organs. *ChemBioChem*, **5**, pp. 26-39.

Yannas I.V., Burke J.F., 1980. Design of an Artificial Skin. I. Basic Design Principles. *Journal of Biomedical Materials Research*, **14**, pp. 65-81.

Ye H., Das D.B., Triffit J.T., Cui Z., 2006. Modelling nutrient transport in hollow fibre membrane bioreactors for growing three-dimensional bone tissue. Journal of Membrane Science, **272**, pp. 169-178.

Yokoi H., Kinoshita T., Zhang S. 2005. Dynamic reassembly of peptide RADA16 nanofiber scaffold. *Proceedings of the National Academy of Sciences of the United States of America*, **102** (24), pp. 8414-8419.

Zarins C. K., Giddens D. P., Bharadvaj B. K., Sottiurai V. S., Mabon R. F., Glagov S. 1983. *Carotid bifurcation atherosclerosis: quantitative correlation of plaque localization with flow velocity profiles and wall shear stress. Circulation Research*, **53**, pp. 502-514.

Zeng A.P., Hu W.S., Deckwer W.D., 1998. Variation of stoichiometric ratios and their correlation for monitoring and control of animal cell cultures. *Biotechnology Progress*, **14**, pp. 434–441.

Zhang S., 2003. Fabrication of novel biomaterials through molecular self-assembly. *Nature Biotechnology*, **21** (10), pp. 1171-1178.

Zhang S., Holmes T.C., Dipersio M., Hynes R.O., Su X., Rich A., 1995. Self-complementary oligopeptide matrices support mammalian cell attachment. *Biomaterials*, **16**, pp. 1385-1393.

Zhang S., Todd C., Holmes T.C., DiPersio C.M., Richard O. Hynes R.O., Xing Su X., Rich A. 2005. Self-complementary oligopeptide matrices support mammalian cell attachment. Biomaterials, **16**, pp. 1385-1393.

Zhao F., Chella R., Ma T., 2007. Effects of shear stress on 3-D human mesenchymal stem cell construct development in a perfusion bioreactor system: experiments and hydrodynamic modelling. *Biotechnology and Bioengineering*, **96** (3), pp. 584-595.

Zhao F., Pathi P., Grayson W., Xing Q., Locke B. R., Ma T. 2005. Effects of Oxygen Transport on 3-D Human Mesenchymal Stem Cell Metabolic Activity in Perfusion and Static Cultures: Experiments and Mathematical Model. *Biotechnology Progress*, **21** (4), 1269 -1280.

Zhou S., Cui Z., Urban J.P.G., 2004. Factors influencing the oxygen concentration gradient from the synovial surface of articular cartilage to the cartilage-bone interface. *Arthritis and Rheumatism*, **50** (12), pp. 3915-3924.

Zhou Y. H. Titchener-Hooker N. J., 1999. Visualizing integrating bioprocess designs through "Windows of Operation". *Biotechnology and Bioengineering*, **65**, pp. 550-557.

Ziengler T., Nerem R., 1994. Tissue engineering a blood vessel: Regulation of vascular biology by mechanical stress. *Journal of Cellular Biochemistry*, **56**, pp. 204-209.

Zimmerman W.B.J., 2006. *Multiphysics modelling with finite element methods.* London: World Scientific Publishing Co. Pte. Ltd.

NOMENCLATURE

Chapter 3

R_1	lumen radius, in m
R_2	outer radius, in m
L	axial length, in m
$C_{initial}$	initial cell concentration, in cells mL-1
X_{max}	cell concentration of native coronary artery, in cells mL-1
X_{eng}	cell concentration of engineered coronary artery, in cells mL-1
q_{ox}	specific oxygen uptake rate, in mol cell-1 s-1
K_{ox}	oxygen half-saturation constant, in mM
X	cell concentration, in cells mL^{-1}
m	specific maintenance rate, mM $cell^{-1}$ s^{-1}
μ	specific proliferation rate, in h^{-1}
μ_{MAX}	maximum specific proliferation rate, in h^{-1}
c_{oxygen}^{lumen}	concentration of component *n* in the lumen, mM
$c_{oxygen}^{alginate}$	concentration of component *n* in the lumen, mM
D_{oxygen}^{lumen}	diffusivity of component *n* in the lumen, in $m^2 s^{-1}$
$D_{oxygen}^{alginate}$	diffusivity of component *n* in the lumen, in $m^2 s^{-1}$
c	concentration, in mM
r	radial coordinate, in m
θ	angular coordinate, in m
z	axial coordinate, in m
$v_{r,}$	radial velocity, in m s^{-1}
v_{Θ}	angular velocity, in m s^{-1}
v_Z	axial velocity, in m s^{-1}
D	diffusion constant, in $m^2 s^{-1}$
q	production rate, mM s^{-1}

Chapter 4

R_1	lumen radius, in m
R_2	outer radius, in m
L	axial length, in m
$C_{initial}$	initial cell concentration, in cells mL^{-1}
X_{max}	cell concentration of native coronary artery, in cells mL^{-1}
X_{eng}	cell concentration of engineered coronary artery, in cells mL^{-1}
Q_{max}	specific oxygen uptake rate, in mol cells mL^{-1}
K_{ox}	oxygen half-saturation constant, in mM
C_{gluc0}	glucose concentration in fresh medium, in mM
C_{glut0}	glutamine concentration in fresh medium, in mM
$Y_{glu/ox}$	yield of glucose from oxygen, in mol mol^{-1}
$Y_{glu/gln}$	yield of glucose from glutamine, in mol mol^{-1}
$Y_{lac/glu}$	yield of lactate from glucose, in mol mol^{-1}
$Y_{gln/amm}$	yield of glutamine from ammonia, in mol mol^{-1}
K_{glu}	glucose half-saturation constant, in mM
K_{lac}	lactate inhibition constant, in mM
K_{gln}	glutamine half-saturation constant, in mM
K_{amm}	ammonia inhibition constant, in mM
K_{ox}	oxygen half-saturation constant, in mM
$K_{glutdec}$	glutamine chemical decomposition rate constant, in s^{-1}
D_{gluc}^{lumen}	glucose diffusivity in the lumen, in $m^2 s^{-1}$
D_{lact}^{lumen}	lactate diffusivity in the lumen, in $m^2 s^{-1}$
D_{glut}^{lumen}	glutamine diffusivity in the lumen, in $m^2 s^{-1}$
D_{amm}^{lumen}	ammonia diffusivity in the lumen, in $m^2 s^{-1}$
D_{ox}^{lumen}	oxygen diffusivity in the lumen, in $m^2 s^{-1}$
F	feed rate, in mL h^{-1}
W	waste rate, in mL h^{-1}
R	recycle rate, in mL h^{-1}
V	input rate to the artificial artery, in mL h^{-1}
$c_{F,n}$	feed concentration to the artificial artery, in mM

$c_{R,n,}$ recycle concentration to the artificial artery, in mM

$c_{A,n}$ inlet concentration to the artificial artery, in mM

$c_{W,n}$ waste concentration, in mM

c concentration, in mM

r radial coordinate, in m

θ angular coordinate, in m

z axial coordinate, in m

$v_{r,}$ radial velocity, in m s^{-1}

v_{Θ} angular velocity, in m s^{-1}

v_Z axial velocity, in m s^{-1}

D diffusion constant, in $m^2 s^{-1}$

q production rate, mM s^{-1}

c_n^{lumen} concentration of component n in the lumen, mM

$c_n^{alginate}$ concentration of component n in the lumen, mM

D_n^{lumen} diffusivity of component n in the lumen, in $m^2 s^{-1}$

$D_n^{alginate}$ diffusivity of component n in the lumen, in $m^2 s^{-1}$

X cell concentration, in cells mL^{-1}

m specific maintenance rate, mM $cell^{-1}$ s^{-1}

μ specific proliferation rate, in h^{-1}

μ_{MAX} maximum specific proliferation rate, in h^{-1}

k_n, k_{n+1} half saturation constants of the substrates n and $n+1$, in mM

K_p, K_{p+1} inhibition constants of the metabolites p and $p+1$, in mM

Chapter 5

D_1, oxygen diffusivity in culture medium, in $m^2 s^{-1}$

c^I oxygen concentration in culture medium, in mM

c^{II} oxygen concentration in the alginate matrix, in mM

X cell concentration, cells mL^{-1}

D_2 oxygen diffusivity the alginate matrix, in $m^2 s^{-1}$

q_{MAX}	maximum uptake rate, mol cell^{-1} s^{-1}
K_m	Monod constant, mM

Chapter 6

r	radial coordinate, in m
D	diffusivity in alginate consrtuct, in m^2 s^{-1}
c	concentration in culture medium, in mM
X	cell concentration, cells mL^{-1}
q	production rate, mol cell^{-1} s^{-1}
V	volume of culture medium, in mL
A	area of the top or bottom surface of the alginate construct, in mm^2